THE ROLES OF PROTEIN N-MYRISTOYLATION IN CELL MORPHOGENESIS IN *Aspergillus nidulans*

A Dissertation

by

SOO CHAN LEE

Submitted to the Office of Graduate Studies of
Texas A&M University
in partial fulfillment of the requirements for the degree of

DOCTOR OF PHILOSOPHY

December 2007

Major Subject: Plant Pathology

THE ROLES OF PROTEIN N-MYRISTOYLATION IN CELL MORPHOGENESIS IN *Aspergillus nidulans*

A Dissertation

by

SOO CHAN LEE

Submitted to the Office of Graduate Studies of
Texas A&M University
in partial fulfillment of the requirements for the degree of

DOCTOR OF PHILOSOPHY

Approved by:

Chair of Committee,	Brian D. Shaw
Committee Members,	Daniel J. Ebbole
	Herman B. Scholthof
	Deborah Bell-Pedersen
Head of Department,	Dennis C. Gross

December 2007

Major Subject: Plant Pathology

ABSTRACT

The Roles of Protein N-myristoylation in Cell Morphogenesis

in *Aspergillus nidulans*. (December 2007)

Soo Chan Lee, B.S.; M.S., Kyung Hee University, Seoul, South Korea

Chair of Advisory Committee: Dr. Brian D. Shaw

Polarized hyphal growth dominates the life cycle of filamentous fungi and is essential to disease progression for many fungal pathogens. Despite its importance, much of the basic biology controlling the process remains to be elucidated. Protein N-myristoylation is one process important to hyphal growth for which the direct mechanism for this connection is not understood. N-myristoylation is mediated by N-myristoyltransferase (NMT), which links 14-carbon myristate to target proteins. In *Aspergillus nidulans*, a mutation in the NMT gene (*swoF1*) results in abnormal morphogenesis during spore germination and the establishment of hyphal polarity. I hypothesize that a protein or proteins downstream of NMT are important for polarized hyphal growth.

Using a forward genetic approach, I obtained six suppressors of *swoF1*. I found that three were proteasome-related and a mutation in genes encoding 26S proteasome subunits by-passed the polarity defects of *swoF1*. Interestingly, N-myristoylation negatively regulated the activity of the 26S proteasome. This result was confirmed by treating with the proteasome inhibitor MG132. This is the first finding of a connection between N-myristoylation and proteasome function during polarized growth.

To identify targets by reverse genetic analysis, I found that 41 proteins (of more that 10,000 encoded by the organism) were predicted to be myristoylated *in silico*. Three were ADP ribosylation factors (ARF), proteins known to be involved in vesicle formation and trafficking in other systems. I chose ArfA (AN1126.3), ArfB (AN5020.3), and ArlA (AN5912.3) for further characterization of polarization in this study. ArfA::GFP discretely localized to endomembrane likely to be Golgi bodies. ArfB::GFP localized to septa and plasma membrane. N-myristoylation determined the localization of both ArfA and ArfB. Disruption of the *arfB* gene resulted in loss of polarity establishment and endocytosis. Together these results suggest that endocytosis plays an important role in maintaining hyphal polarized growth and in shaping the cell apex.

DEDICATION

To my parents, Jong Tae Lee and Gum Ju Goh, to my parents-in-law, Jong Bum Huh and Hyung Ja Park, and to my wife Eun Young for their love and belief in me

ACKNOWLEDGMENTS

I would like to express my sincere gratitude and appreciation to my academic advisor, Dr. Brian Shaw, for his continuous guidance, encouragement, and support in the past four years. I thank him for giving me a chance to work with him, giving me intellectual insight into mycology, providing a friendly environment for research and for giving me opportunities to communicate with peers at professional conferences. My work would not be possible without him.

I am indebted to my committee members, Dr. Dan Ebbole, Dr. Herman Scholthof, and Dr. Deborah Bell-Pedersen for their time and insightful advice on my research, Dr. Rustem Omarov for his kind guidance and fruitful discussions concerning protein biochemistry, Dr. Paul de Figueiredo for his kind comments on my research manuscript and Dr. Larry Dangott for his collaboration in MALDI/TOF mass spectroscopy.

I also would like to give my thanks to my current and former lab mates, Srijana Upadhyay, Dawoon Chung, Melissa Long, Gustavo Rebello, Justin McCharen, and Lindsey Harris for their interest in my research, technical assistance, and friendship. I could not have completed my research without them.

I sincerely appreciate the Department of Plant Pathology and Microbiology at Texas A&M University for generous support for me to conduct my research. Appreciation is extended to the Robert Nicholson Endowed Fellowship for providing me a stipend, health insurance, and tuition for the last two semesters of my study.

I am indebted to my brothers and sisters and their families in South Korea for their support and encouragement. They deserve far more credit than I can give.

My final deepest gratitude goes to my wife, Eun Young Huh, whose love, patience, encouragement, and devotion has always been with me during my long journey in pursuit of my PhD degree. My study at TAMU would not have succeeded without her.

TABLE OF CONTENTS

Page

CHAPTER Page

LIST OF FIGURES

FIGURE Page

LIST OF TABLES

CHAPTER I

INTRODUCTION

Polarized cell expansion is a developmental mode observed in many biological systems including pollen tube formation of plants, neuronal cell development of animals, and hyphal growth of filamentous fungi (Bartnicki-Garcia and Lippman, 1969; Bradke and Dotti, 1997; Taylor *et al.*, 1992). Filamentous fungi serve as an attractive model for this developmental pattern since they display an extensive polarized growth phase during the majority of their life cycle. For these organisms, conidia (asexual spores) initially establish polarity by sending a germ tube during germination. Polarization of the cell is maintained as hyphae elongate at their apex to make a complex mycelium. Many plant and human fungal pathogens infect and cause disease by penetrating their host by invasive hyphal growth. A thorough understanding of the mechanisms of polarized growth remains to be elucidated for filamentous fungi. Therefore, understanding the genetics and cell biology of polarized hyphal growth of filamentous fungi is of fundamental importance and will assist in development of anti-fungal agents.

YEAST PARADIGM OF POLARIZED GROWTH

In budding yeast (*Saccharomyces cerevisiae*) the most obvious parallel to polarized hyphal growth is the process of bud site selection and polarization during

---

This dissertation follows the style of *Molecular Microbiology*.

daughter cell budding. Polarization in yeast cells can be divided into three steps: bud site selection, establishment of an axis of polarity, and polarity maintenance (including polarized cytoskeleton assembly) (Pruyne and Bretscher, 2000a, b; Pruyne *et al.*, 2004). For bud site selection, yeast has two different cortical marker protein complexes for the haploid axial budding and the diploid bipolar budding. Bud3p, Bud4p, and Ax12p act as cortical markers for axial budding (Fujita *et al.*, 1994), and in diploid bipolar budding, Bud8p, Bud4p, and Rax2p are involved (Zahner *et al.*, 1996). Mutants in haploid and diploid cortical markers are characterized by a failure to select the correct bud site (Fujita *et al.*, 1994; Zahner *et al.*, 1996). Downstream of these cortical markers Cdc42p, a rho-family GTPase, was found to be a central protein to cell polarity (Adams *et al.*, 1990; Pruyne *et al.*, 2004). The Cdc42 mutant was unable to select a correct bud site (Adams *et al.*, 1990). Its biological partner is Cdc24p, a GTP Exchanging Factor (GEF) which activates Cdc42 to participate in bud site selection. The Cdc24p mutant is unable to form a chitin ring at the bud neck resulting in the loss of bud emergence (Chenevert *et al.*, 1994). The Bem1p protein scaffolds these two GTPase circuit proteins to form a triple protein complex, Cdc42p/Cdc24p/Bem1p that is essential to establish polarity (Pruyne and Bretscher, 2000a; Pruyne *et al.*, 2004). The polarisome is a protein complex downstream of Cdc42p/Cdc24p/Bem1p, which was found to organize the actin cytoskeleton to the polarized growth site (Jaquenoud and Peter, 2000). The polarisome consists of Pea2p, Spa2p, Sph1p, Bud6p, and Bni1p that co-localize at the site of polarized grow (Fujiwara *et al.*, 1998; Pruyne and Bretscher, 2000a; Sheu *et al.*, 1998). The primary function of the polarisome is to nucleate actin filament polarization to the

bud site primarily through interaction with Bni1p (Sagot *et al.*, 2002)**.** This polarized cytoskeleton then functions as the track upon which secretory vesicles deliver their cargo to the growth site. In yeast, polarized secretion has been suggested to be important in the polarized growth (Pruyne and Bretscher, 2000b). The secretory vesicle delivery system brings a subset of new proteins, lipids and cell wall synthesis substrates to the growth site (Chuang and Schekman, 1996; Govindan *et al.*, 1995). A rab-family GTPase, Sec4p, is involved in assembly of Golgi derived exocytotic vesicles. Sec4p is localized to bud sites in polarized cells (Schott *et al.*, 1999; Walch-Solimena *et al.*, 1997). Considering the spitzenkörper of filamentous fungi (see below) and exocytosis of yeast together, polarization of vesicle trafficking to incipient growth sites is likely to be important for hyphal growth of filamentous fungi.

POLARIZED GROWTH IN FILAMENTOUS FUNGI

Interestingly, filamentous fungi have been found not to share many aspects of the polarized growth paradigm established for *S. cerevisiae*. First, orthologs of the cortical landmarks are not conserved in the filamentous fungi that have been sequenced and annotated (Harris and Momany, 2004). Secondly, although the Cdc42 signaling module is required for polarized morphogenesis in mammalian systems as well as in yeast, Cdc42p is not critical in polarized hyphal growth in filamentous fungi (Boyce *et al.*, 2001; Scheffer *et al.*, 2005; Seiler and Plamann, 2003). Additionally the role of the polarisome in hyphal growth is unclear in filamentous fungi. In *Candida albicans*, a dimorphic fungus, components of the polarisome during yeast-like growth are different

from the components of the polarity determining organelle termed the spitzenkörper (see below), during invasive hyphal growth (Crampin *et al.*, 2005). Thus, although the yeast system provides a powerful genetic model to understand the fungal polarized growth, it remains inadequate to describe hyphal growth as found in filamentous fungi.

WHAT IS KNOWN ABOUT POLARIZED GROWTH IN FILAMENTOUS FUNGI

Spitzenkörper

The spitzenkörper (apical body) is a structure unique to filamentous fungi, which is located at growing apices and is thought to control apical growth (Girbardt, 1957; Harris *et al.*, 2005). Microscopic analyses clarified that the spitzenkörper is located at the polarized growth sites *e. g.* hyphal tips and lateral branching sites. Since its discovery, extensive research has focused on the role of spitzenkörper in polarized hyphal growth. Electron microscopic analyses showed the spitzenkörper is an assembly of vesicles, which consists of two different types of vesicles, apical vesicles (79 to 90 nm in diameter) and microvesicles (30 to 40 nm in diameter). Microvesicles are now thought to be chitosomes since they are morphologically identical to fractionated vesicles that can reconstitute chitin synthesis *in vitro* (Bracker *et al.*, 1976). The spitzenkörper corresponds with a postulated vesicle supply center (VSC) thought to be necessary to explain hyphal tip growth (Grove and Bracker, 1970; Harris *et al.*, 2005). Bartnicki-Garcia has used mathematic modeling to suggest that the spitzenkörper is a vesicle

distribution center for polarized hyphal growth (reviewed in (Bartnicki-Garcia, 2002)). This has driven the hypothesis that polarized secretion through the spitzenkörper plays a key role in hyphal growth.

Endocytosis in polarized growth

Endocytosis functions in nutrional uptake and in recycling of plasma membrane and its associated components. This is a multistep process, and it includes: assembly of effectors at the plasma membrane, deformation of membranes, vesicle budding and disassembly. These processes have been reviewed recently (Kaksonen *et al.*, 2003; Walther *et al.*, 2006).

Relative to exocytosis, endocytosis has been considered less important in polarized morphogenesis of filamentous fungi. For example, the vesicle supply center model has focused exclusively on exocytosis (Bartnicki-Garcia, 2002). Recently, data has begun to point to a critical role in endocytosis in regulating cell shape during polarized development. For example, chitin synthases are recycled on plasma membrane through endocytosis in *S. cerevisiae* (Ziman *et al.*, 1996). Moreover a mathematical model has been proposed that supports the idea that endocytosis mediates cell polarity in the yeast (Marco *et al.*, 2007). Indeed, an endocytotic marker dye, FM4-64, is now used routinely in filamentous fungi to label first the plasma membrane and later the spitzenkörper (Fischer-Parton *et al.*, 2000; Penalva, 2005). The fact that the spitzenkorper, an organelle traditionally thought to function exclusively in exocytosis, is labeled by an endocytotic marker dye suggests the need for a re-examination of the

accepted function for the spitzenkorper. Recent work in the Shaw lab has pointed to a direct role for the endocytotic protein fimbrin in maintaining cell shape during hyphal growth (Updhayay, Lee and Shaw, in preparation). In this document (Chapter III), additional evidence is presented which suggests a role for endocytosis in hyphal growth.

Actin, microtubule, and motor proteins

Although yeast and filamentous fungi appear to maintain certain parts of the polarization machinery that are unique, both systems require the actin cytoskeleton for polarization. Deletion of actin in filamentous fungi is lethal. There is, however, one viable actin mutant, *act*^{1} (Cys 374 Phe) in *Neurospora crassa*. The mutant displays altered distribution of actin in hyphal tips and defects in tip-growing and branching (Virag and Griffiths, 2004). Microfilament networks were visualized by electron microscopy within the core area of the spitzenkörper, suggesting that the spitzenkörper is likely an organizing center for microfilament formation (Bourett and Howard, 1991; Harris *et al.*, 2005). Treatment with cytochalasin, which blocks microfilament formation leads to swollen hyphal tips in *A. nidulans* (Harris *et al.*, 1994; Torralba *et al.*, 1998). Actin localizes to septation sites, where it forms contractile actin rings. *A. nidulans* SepA is a formin (an ortholog of Bni1 of yeast) which regulates actin polymerization. *sepA* mutants have phenotypes associated with hyphal polarized growth and septum formation (Sharpless and Harris, 2002) suggesting actin organization is critical for polarity.

In addition to microfilaments, actin also forms cortical patches. These patches are highly dynamic structures that are thought to be sites of endocytosis in yeast (Kaksonen

et al., 2003). In *A. nidulans*, actin patches are found predominantly at the hyphal tip and at septation sites. A mutation in fimbrin, an actin binding protein which localizes to actin patches, resulted in polarization related phenotypes (Upadhyay and Shaw, in preparation). The fimbrin mutant also exhibited a delay in FM4-64 staining, consistent with a defect in endocytosis.

Two actin-based motor protein myosins are well-studied in filamentous fungi. The class I myosin including MyoA of *A. nidulans* and Myo5 of *C. albicans* were found to be required for the establishment of hyphal polarity (McGoldrick *et al.*, 1995; Oberholzer *et al.*, 2002). The class V myosins include Myo5 in *Ustilago maydis* and Myo2 in *C. albicans*, which are also involved in hyphal growth (Schott *et al.*, 1999).

Microtubules are formed parallel to the long axis of hyphal growth direction in filamentous fungi (Hoch and Staples, 1983; Howard, 1981). These microtubules are thought to take part in the delivery of exocytotic vesicles from sub-apical areas to the growing apex (Harris, 2006). In *N. crassa* and *A. nidulans*, the spitzenkörper is destablized by treatment of the microtubule depolymerization chemical, benomyl, and in kinesin and dynein (microtubule motor proteins) mutants (Konzack *et al.*, 2005; Riquelme *et al.*, 2000). This disturbance of the spitzenkörper resulted in the disruption of the polarized hyphal growth.

Signaling and protein kinases

Calcium signaling from phosphoinositide 1,4,5-triphosphate (IP3) to phospholipase C is thought to be required for the polarized hyphal growth (Silverman-

Gavrila and Lew, 2003). Calcium is concentrated in the hyphal apex (Shaw and Hoch, 2001; Silverman-Gavrila and Lew, 2003). Disruption of the calcium gradient resulted in the loss of hyphal polarity and multiple germ-tube emergence during spore germination (Schmid and Harold, 1988). In *A. nidulans*, a Ras GTPase cascade was found to be critical for germination (Osherov and May, 2000). In *N. crassa*, the involvement of a Rho GTPase in polarized growth was verified, in which mutations inhibiting Cdc24 (Rho GEF) activity caused destabilization of the axis of polarity (Seiler and Plamann, 2003).

In yeast, p21-activated kinases (PAK) (i.e., Ste20 and Cla4) are important for bud site selection. These PAKs are activated by Cdc42. However, in *Magnaporthe grisea*, Ste20 and Cla4 are not required for polarized hyphal growth (Li *et al.*, 2004), further illustrating the difference between yeast and filamentous fungi. In filamentous fungi, cyclic AMP-dependent protein kinase (i.e., PKA) is likely to be more important. For example in *N. crassa*, a mutation in the regulatory subunit of PKA fails to form an axis of polarity (Bruno *et al.*, 1996). In addition, a *N. crassa* serine/threonine protein kinase, Cot-1 is required for the proper localization of cytoskeleton and vesicle trafficking machinery to the polarized growth site (Yarden *et al.*, 1992). CotA of *A. nidulans*, an ortholog of Cot-1, is also involved in polarized growth (Zarrin *et al.*, 2005).

Protein mannosylation

Protein mannosylation is required for hyphal polarization in *A. nidulans*. The characteristics of mutations in SwoA, a protein mannosyl transferase, and SwoN, a

GDP-mannose pyrophosphrylase, result in a loss of polarity during spore polarization and hyphal polarization respectively (Shaw and Momany, 2002), (unpublished data, from the Shaw lab). Our current model is that protein mannosylation is required for maturation of the cell wall. In mannosylation mutants the wall is elastic resulting in cells that are unable to rigidly adhere to the hyphal morphogenesis program.

PROTEIN N-MYRISTOYLATION IN POLARIZED GROWTH

N-myristoyl transferase (NMT) is essential for hyphal polarity maintenance in *A. nidulans* (Shaw *et al.*, 2002). The temperature sensitive *swoF1* mutant displayed an abnormal swelling immediately after germ tube emergency resulting from loss of polarity whereas wild-type is able to maintain the polarity of the hyphal growth without swellings.

N-myristoylation is a form of protein lipidation. Examples of protein lipidation include protein (iso) prenylation, protein palmitoylation, glycosylphosphatidylinositol (GPI) lipid anchoring, and protein N-myristoylation (Bhatnagar and Gordon, 1997; Casey, 1995). Protein myristoylation is an irreversible modification, in which 14 carbon myristate is covalently attached to the N-terminal glycine of target proteins. After cleavage of the leading methionine, an amide linkage between myristate and the second residual glycine is followed (Johnson *et al.*, 1994a). In this reaction, NMT transfers myristate from myristoyl-CoA and attaches the myristate to the N-terminal glycine residue of proteins. The covalent linkage of myristate to the N-terminus of the target protein provides increased hydrophobicity allowing the subset of target proteins to

localize to cell membranes (Johnson *et al.*, 1994a; Rudnick *et al.*, 1993). The myristoylated proteins also take part in hydrophobic protein-protein interactions (Rudnick *et al.*, 1993).

N-myristoylation has been studied in many eukaryotic systems. For example, in fungal pathogens, including *Cryptococcus neoformans* and *Aspergillus fumigatus,* N-myristoylation is essential for viability (Lodge *et al.*, 1994; Maurer-Stroh *et al.*, 2002). Viral proteins must be myristoylated to function, for example the Pr55gag protein of *Human Immunodeficiency Virus 1*, the capsid protein VP4 of *Poliovirus*, and the pre6S protein of *Hepatitis B virus*, must be myristoylated to function (Chow *et al.*, 1987; Göttlinger *et al.*, 1989; Veronese *et al.*, 1988). Furthermore, N-myristoylated proteins have been found to be involved in carcinogenesis in various tissues (Felsted *et al.*, 1995), for example, pp60c-src kinase in colon cancer (Bolen *et al.*, 1987). In the gene-for-gene system, AvrPto, type III secreted avirulence factor by plant pathogenic bacteria, must be myristoylated in the host plant cell to localize to cell membrane and interact with Pto in the host (Nimchuk *et al.*, 2000). N-myristoylation is also important for cell polarization. For example in *S. cerevisiae*, myristoylation of Arf3p is critical to select the bud site (Huang *et al.*, 2003).

TARGETS OF N-MYRISTOYLATION TRANSFERASE

In *S. cerevisiae*, verified myristoylated proteins include heterotrimeric G alpha subunit proteins (Mumby *et al.*, 1990), a calcineurin beta subunit (Kennedy *et al.*, 1996), an ATPase of the 19S proteasome particle (Kimura *et al.*, 2003), as well as the ADP

ribosylation factors (ARF). The ARF protein family is a group of Ras related small GTPase, involved in vesicle assembly and trafficking (Stearns *et al.*, 1990). This is of particular interest since the ARF protein family is critical for vesicle assembly. This protein family may provide the link between the *swoF1* myristoylation mutant in *A. nidulans* and hyphal polarized growth (see below)

HYPOTHESIS

Since the *swoF1* temperature sensitive NMT mutant displays abnormal polarized growth at restrictive temperature in *Aspergillus nidulans* (Shaw *et al.*, 2002), I formulated the hypothesis that **one or more proteins downstream of NMT are important for polarized hyphal growth.** Based on the assumption that elements downstream of NMT are important for hyphal polarity we formulated the following hypotheses: **1) NMT mutant suppressors will reveal downstream regulators connecting N-myristoylation and cellular processes involved in polarized growth. 2) Disruption of a subset of myristoylated targets will reveal novel myristoylated proteins directly involved in hyphal polarization.** To probe these hypotheses I pursued the following objectives: Objective 1 –Characterization of suppressor mutants of *swoF1*

In this forward genetic approach I generated suppressor mutants of the *swoF1* myristoylation mutant working under the hypothesis that I would identify either a) targets of myristoylation or b) downstream effectors of these targets. In this study, I

found that 26S proteasome activity is involved in polarized hyphal growth and NMT regulates the activity of the 26S proteasome. (See chapter II)

Objective 2 – Investigate the role of ARF family proteins in fungal growth and how N-myristoylation plays a role in their function in *A. nidulans*.

In this reverse genetic approach, I targeted a group of proteins that have been shown to be myristoylated in other systems and to be involved in vesicle assembly and trafficking. In this study, I found that ArfB is important for polarity establishment and maintenance in *A. nidulans* and linked endocytosis to hyphal polarity (See chapter II). I also found that ArfA is involved in polarized growth (See appendix B), and that N-myristoylation defines the localization of the ARF proteins. (See chapter II; and appendix B).

CHAPTER II

A NOVEL INTERACTION BETWEEN N-MYRISTOYLATION AND THE 26S PROTEASOME DURING CELL MORPHOGENESIS*

SUMMARY

N-myristoylation is a protein lipidation event in which myristate is covalently linked to the N-terminal glycine of target proteins. In *Aspergillus nidulans*, the N-myristoylation deficient *swoF1* mutant was previously shown to lose cell polarity during the early morphogenic event of germ tube emergence. To further investigate this defect, we mutagenized *swoF1* and recovered six partial suppressors designated *ssf* (**s**uppressor of **s***wo***F***1*). The secondary mutations enabled *swoF1* to partially by-pass its growth defect. We characterized a frame-shift mutation in *ssfA1,* which encodes an alpha subunit of the 20S core particle of the 26S proteasome. Fewer ubiquitinated proteins accumulated in the *swoF1* mutant compared to wild-type. In contrast, the *swoF1;ssfA1* mutant accumulated higher levels of ubiquitinated proteins than wild-type. The *swoF1* mutant was by-passed in the presence of the proteasome inhibitor, MG132.

---

* This chapter is reprinted with permission from "A novel interaction between N-myristoylation and the 26S proteasome during cell morphogenesis" by Lee, S. C., and B. D. Shaw. 2007. Molecular Microbiology. 63: 1039-1053.

These results demonstrate that the *swoF1* phenotype was caused, at least in part, by an increased activity of 26S proteasome-dependent proteolysis and suppression occurred by attenuating the 26S proteasome activity. This is the first report linking N-myristoylation and ubiquitin-proteasome dependent proteolysis during morphogenesis.

INTRODUCTION

Lipidation is an important protein maturation process in eukaryotic cells including modifications such as: protein (iso) prenylation, protein palmitoylation, glycosylphosphatidylinositol (GPI) lipid anchoring, and protein N-myristoylation (Bhatnagar and Gordon, 1997; Casey, 1995). Protein N-myristoylation is an irreversible co-translational modification, in which 14 carbon myristate is covalently linked to the N-terminal glycine of target proteins. The leading methionine is cleaved and the residual glycine at the second position makes an amide linkage with myristate (Johnson *et al.*, 1994a). This reaction is mediated by the highly conserved protein N-myristoyl transferase (NMT). NMT transfers myristate from myristoyl-CoA to the N-terminus of target proteins. The covalent linkage of myristate provides increased hydrophobicity allowing the target proteins to localize to cell membranes (Johnson *et al.*, 1994a; Rudnick *et al.*, 1993) and to take part in hydrophobic protein-protein interactions (Rudnick *et al.*, 1993).

N-myristoylation plays important roles in a variety of biological systems. In *Saccharomyces cerevisiae*, disruption of the sole NMT gene results in lethality (Duronio *et al.*, 1989). Verified targets of NMT in yeast include signaling components such as

heterotrimeric G alpha subunits (Mumby *et al.*, 1990)**,** the calcineurin Beta subunit (Kennedy *et al.*, 1996) as well as the ARF GTPase proteins that are involved in vesicle assembly and trafficking (Stearns *et al.*, 1990). In *Cryptococcus neoformans,* the cause of cryptococcal infections in humans, NMT is essential for viability and pathogenicity (Lodge *et al.*, 1994). Viruses also utilize their host NMT. Examples of viral proteins that must be myristoylated to function include the Pr55gag protein of *Human immunodeficiency virus 1* (Bryant and Ratner, 1990), a capsid protein VP4 of *Poliovirus* (Marc *et al.*, 1989), and the pre6S protein of *Hepatitis B virus* (Ma *et al.*, 2003). Furthermore, differential expression and altered function of N-myristoylated oncoproteins, for example $pp60^{c\text{-}src}$ protein kinase in human colon carcinoma (Bolen *et al.*, 1987), have been found to be involved in carcinogenesis (Felsted *et al.*, 1995). N-myristoylation is also involved in the gene-for-gene pathogen recognition system in plants. For example, AvrPto, a type III secreted avirulence factor produced by plant pathogenic bacteria, must be myristoylated in the host plant cell to localize to host cell membranes and interact with the Pto protein of the host (Nimchuk *et al.*, 2000).

In the model filamentous fungus *Aspergillus nidulans*, N-myristoylation plays an important role in development. The temperature sensitive *swoF1* mutant, containing the D369Y point mutation, failed to maintain growth at the apex of its germ tube during cell elongation and the *swoF* gene was found to encode an NMT (Shaw *et al.*, 2002). The connection between N-myristoylation and cell morphogenesis remains to be determined mechanistically.

In this paper, the characterizations of second site mutations that partially bypass the *swoF* NMT growth defect are detailed. We report that a mutation in a 20S proteasome subunit by-passes the cell polarization phenotypes associated with the *swoF1* mutation. The proteasome is responsible for the lytic degradation of transcription factors, cyclins, misfolded proteins, and parasitic proteins among others (Driscoll and Goldberg, 1990; Hiller *et al.*, 1996; Pines and Lindon, 2005). The 26S proteasome complex consists of two components, a 20S and two 19S particles. The 19S particle or regulatory particle (RP) is composed of 14 different proteins, six of which have an ATPase domain associated with function (Rubin *et al.*, 1998). In the 20S proteasome, or core particle (CP), two inner beta rings and two outer alpha rings are stacked to form a barrel shaped structure. Each alpha and beta ring consists of seven subunits. The 19S RP is the 'cap' at each end of the 20S CP that recognizes the ubiquitinated proteins and unfolds them for introduction to the 20S CP. The alpha rings take part in the interaction between 19S RP and 20S CP and the beta ring contains the proteolytic activity (Driscoll and Goldberg, 1990; Finley *et al.*, 1998; Groll *et al.*, 2000; Smalle and Vierstra, 2004). In this study, we describe increased activity of the 26S proteasome in the *swoF1* NMT mutant. We also report our analysis of the mode of suppression of the NMT mutant by a mutation in the 20S core proteasome particle. Our data support the hypothesis that an N-myristoylated protein mediates cell morphogenesis by regulating proteasome activity.

RESULTS

Generation of *swoF1* suppressor mutation

The temperature sensitive s*woF1* mutation in *A. nidulans* results in loss of hyphal polarity soon after germ tube emergence resulting in a characteristic dumbbell-like cell morphology (Figure 2.1A). The *swoF* gene was previously shown to encode an N-myristoyl transferase (NMT) (Shaw *et al.*, 2002). To study the downstream effects of NMT in cell morphogenesis, we mutagenized the *swoF1* strain, AXL19 (Table 2.1) using UV light (Wavelength = 253.7 nm) and screened for mutants that suppress the hyphal polarity defect. Due to its polarity defect, the *swoF1* mutant is unable to form a visible mycelial colony at restrictive temperature (42 ºC) (Shaw *et al.*, 2002) (Figure 2.1B and C). Six phenotypic suppressor mutants that could form a colony at 42 ºC (Figure 2.1B and C) were recovered out of approximately 40,000 spores plated. Colony diameter was small in comparison to wild-type, indicating that the second site mutations partially suppressed *swoF1*. This is not surprising since myristate amended medium also only partially restored growth if *swoF1* (see discussion) (Shaw *et al.*, 2002). The suppressor strains were designated *swoF1; ssf* (**s**uppressor of ***s**wo**F**1*).

The *swoF1;ssf* mutants were able to maintain growth along their long axis of polarity during spore germination without apical swellings (Figure 2.1A). In contrast to wild-type, their growth was limited to less than 100 µm long hyphae even after prolonged incubation. Wild-type *A. nidulans* hyphae are subdivided by septa delineating cell compartments which typically contain three to four nuclei each (Castiglioni Pasgon *et al.*, 2001; Harris *et al.*, 1994). The *swoF1* mutant, however, has eight to sixteen nuclei

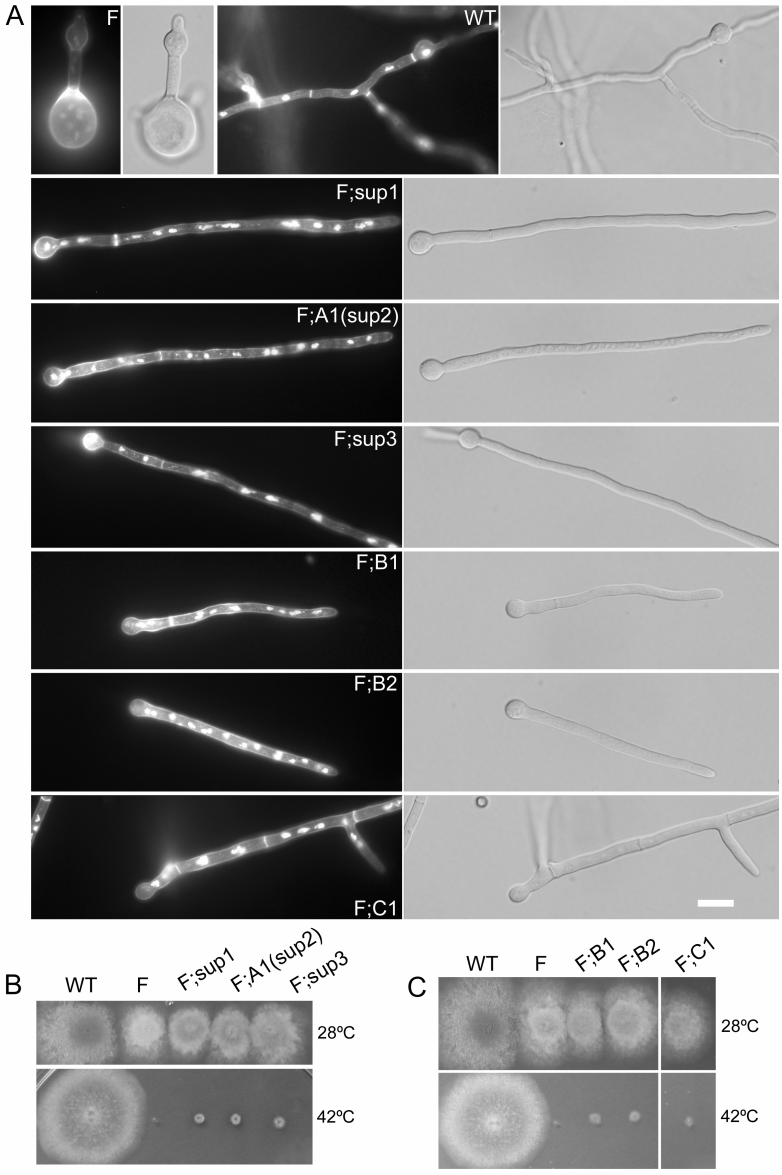

Figure 2.1 Growth and morphology of wild-type, the *swoF1* mutant, and suppressor mutants (*swoF1;ssf*). (A) Fluorescence and Nomarski Differential Interference Contrast (DIC) images of wild-type, *swoF1*, and *swoF1;ssf*'s at 42 ºC. The *swoF1* mutant reverted to isotropic growth at its apex resulting in abnormally swollen cells. Each *swoF1;ssf* can maintain polarized growth along their long axis of polarity leading to germ tubes at least 100 µm long. No swellings were observed. Hoechst 33258 staining for nuclei revealed that each cell compartment of the *swoF1;ssf*'s and *swoF1* contained multiple nuclei indicating that cell cycle arrest did not occur. (B and C) At 28 ºC (upper), all strains grew as wild-type. At 42 ºC (bottom), the *swoF1* mutant is not able to form a mycelial colony. Each suppressor mutant forms a visible mycelial colony at 42 ºC.

Abbreviations used WT: wild-type, F: *swoF1*, *sup1*: *ssfsup1*, *sup3*: *ssfsup3*, A1(*sup2*): *ssfA1*(*sup2*), B1: *ssfB1*, B2: *ssfB2*, C1: *ssfC1*. Objective NA = 1.4 with oil. Scale = 10 µm.

Table 2.1 Strains used in this study

Strains	Genotypes	Sources
A4	*veA1*	FGSC
A773	*pyrG89;pyroA4;wA3;veA1*	FGSC
A234	*pabaA1;yA2;veA1*	FGSC
AXL19	*swoF1;pyrG89;veA1*	(Shaw *et al.*, 2002)
AXL18	*swoF1;pyrG89;wA3;veA1*	(Shaw *et al.*, 2002)
ASL84	*swoF1;argB2;wA3;veA1*	This study
ASF1	*swoF1;ssfsup1;pyrG89;veA1*	This study
ASF2	*swoF1;ssfA;pyrG89;veA1*	This study
ASF3	*swoF1;ssfC1;pyrG89;veA1*	This study
ASF4	*swoF1;ssfsup3;pyrG89;veA1*	This study
ASL5	*swoF1;ssfB1;pyrG89;veA1*	This study
ASF6	*swoF1;ssfB2;pyrG89;veA1*	This study
ASL16	*ssfsup1;pyrG89;yA2;veA1*	This study
ASL21	*ssfA1(ssfsup2);pyrG89;veA1*	This study
ASL24	*ssfA1(ssfsup2);pabaA1;yA2;veA1*	This study
ASL31	*ssfC1;pabaA1;yA2;veA1*	This study
ASL42	*ssfsup3;pyrG89;wA3;veA1*	This study
AMH3	*pyrG89;argB2;wA;veA1;alcA::swoF1::3xHA;argB2*	This study
AMH5	*pyrG89;argB2;wA;veA1;alcA::swoF1::3xHA;argB2*	This study
PW1	*argB1;methG1;veA1*	FGSC

at its swollen apex indicating that mitotic division of the nuclei continued despite cessation of polarized growth. Similarly all *swoF1;ssf* mutants also have cell compartments containing more nuclei than does wild-type (Figure 2.1A).

Germlings of the *swoF1* mutant recovered wild-type germination patterns when incubated at 42 ºC for 24 hrs then transferred to permissive temperature (28 ºC) (Shaw *et al.*, 2002). If incubation at 42ºC was extended to 48 hrs, however, the *swoF1* mutant was not viable when down-shifted to 28 ºC indicating a conditional lethality upon prolonged temperature challenge (Figure 2.2). All six *swoF1;ssf* mutants recovered wild-type growth patterns when they were shifted to 28 ºC after being challenged at 42 ºC for 48 hrs. Interestingly, one strain designated *swoF1;ssfC1* (see below and Table 2.1) continued sub-apical isotropic growth of the conidium but also recovered wild-type growth at the cell apex . This intercalary growth is rarely seen in wild-type *A. nidulans*.

Genetic analyses of the single suppressor mutants

The *swoF1;ssf* mutants were crossed with A773 ($swoF^{+}$;ssf^{+}, Table 2.1) to produce single *ssf* mutants released from *swoF1*. By identifying a novel phenotype in comparison to the known phenotypes of wild-type, *swoF1*, and *swoF1;ssf*, we identified each single *ssf* mutant among the progeny. To classify the six single *ssf* mutants into genetic linkage groups, we crossed the *ssf* mutants in each pairwise combination (Table 2.2). No wild-type progeny were observed from the cross between *ssfB1* and *ssfB2* strains (n=200)

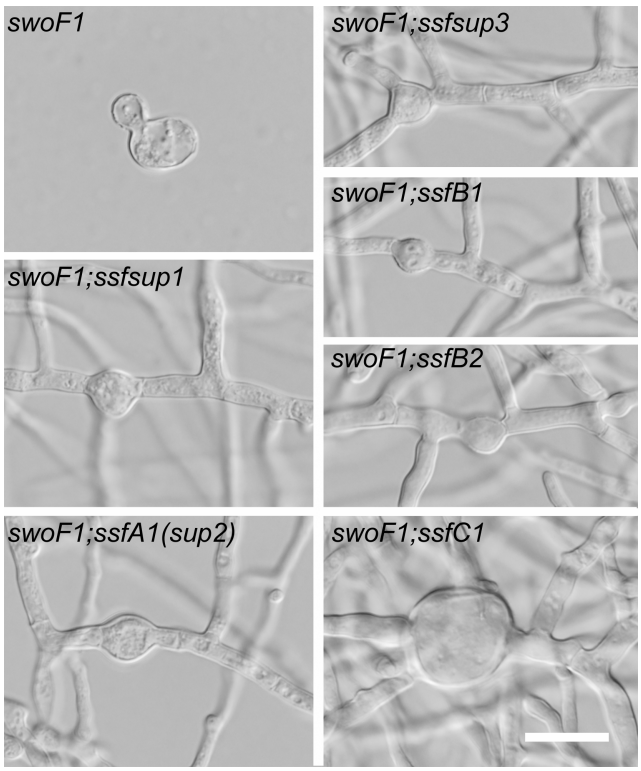

Figure 2.2 Nomarski Differential Interference Contrast images of *swoF1* and *swoF1;ssf* mutants after temperature down-shift. The *swoF1* mutant can not recover growth after temperature shift to permissive temperature (28 ºC) after 48 hr incubation at restrictive temperature (42 ºC). Each *swoF1;ssf* proliferated after temperature downshift. *swoF1;ssfC1* produced giant-swollen conidia after temperature downshift resulting from continued isotropic growth of this cell. Objective NA = 1.4 with oil. Scale = 10 µm.

Table 2.2 Pairwise sexual crosses between single *ssf* mutants

	ssfsup1	*ssfA1(ssfsup2)*	*ssfsup3*	*ssfB1*	*ssfB2*
ssfsup1					
ssfA1(ssfsup2)	ST				
ssfsup3	ST	ST			
ssfB1	WT	WT	WT		
ssfB2	WT	WT	WT	MT	
ssfC1	WT	WT	WT	WT	WT

ST: the crosses are sexually sterile.

WT: wild-type progeny were recovered from sexual crosses along with each mutant combination.

MT: only mutant progeny were recovered from sexual cross.

indicating that they are allelic or tightly linked, while wild-type progeny were recovered when either *ssfB* mutant was crossed with any of the other four mutants (Table 2.2). The *ssfC1* mutant produced wild-type progeny when crossed to any of the other five mutants, indicating that the *ssfC* gene is unlinked to any other gene in this study.

These three mutants and their corresponding genes have therefore been given the formal names *ssfB* and *ssfC* based on *A. nidulans* nomenclature standards previously proposed (Clutterbuck and Arst, 1995). Interestingly, the other three *ssf* mutants could not undergo sexual development in any pairwise combination with each other, whereas they could cross with wild-type and with the other suppressor mutants (Table 2.2). These three mutants have been designated by the informal names *ssfsup1, ssfsup2,* and *ssfsup3*. The *ssfsup2* mutant was renamed *ssfA1* after identifying its lesion (see below). Because we did not identify the mutated gene in either the *ssfsup1* or the *ssfsup3* mutants, we have chosen to use the names *ssfsup1* to *ssfsup3*. Characterization of the *ssfB* and *ssfC* mutants was not pursued further in this study, though none appear to be involved in proteasome function (Lee and Shaw, unpublished). At 42 ºC the mutants designated *ssfsup1, ssfA1* (*ssfsup2*), and *ssfsup3* (referred to as a group hereafter as the '*ssfsup* mutants') each displayed reduced colony size, sporulated poorly and produced an unidentified red pigment on solid minimal media (Figure 2.3A and the figure on page 28). The '*ssfsup* mutants' produced germ tubes restricted to less than 200 µm in length (Figure 2.3B) even after prolonged incubation longer than 48 hrs. At 28 ºC *ssfsup* conidia germinated as wild-type (data not shown), but formed colonies that were distinguishable from wild-type based on colony size and or conidiation levels (Figure

2.3A). Therefore, even at permisive temperature, the mutation(s) in the *ssfsup* strains was also detrimental to growth and colony formation. Random ascospore progeny from crosses between ASL21 (*ssfsup2* (*ssfA1*)) and A234 (wild-type at *ssfsup* loci) (n=100) and between ASL42 (*ssfsup3*) and A234 (n=170) segregated 48:52 (*ssfsup2*: wild-type) and 77:93 (*ssfsup3*: wild-type). χ^2 analysis (p<0.05), using Yates correction factor with one degree of freedom, indicated that there is no significant difference from a 1:1 segregation ratio in either cross. In a cross between ASL16 (*ssfsup1*) and A234 (n=150), segregation ratio was 63:87 (*ssfsup1*: wild-type) which deviated from a 1:1 segregation ratio. This may indicate that the mutation resulting in *ssfsup1* may have also resulted in a chromosomal translocation or other mutational event (see discussion). Heterozygous diploids of each *ssfsup*$^-$/*ssfsup*$^+$ produced colonies comparable in size and morphology to wild-type on solid media and germlings that were indistinguishable from wild-type. The diploid strains produced some red pigment on solid media, however, and did not conidiate well (data not shown). Because the heterozygotes have intermediate phenotypes between wild-type and each *ssfsup*, we have designated the *ssfsup* mutations as codominant (Miller and Hollander, 1995; Miller, 1997). This characteristic allowed for screening for complementation with a genomic library based on colony morphology and size.

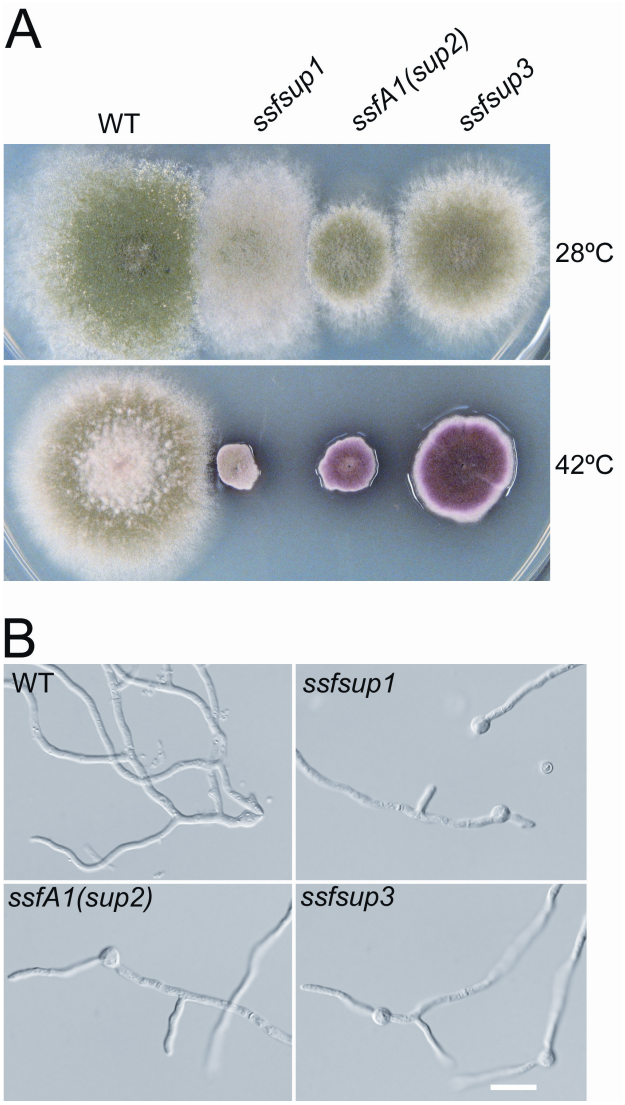

Figure 2.3 Morphology of single *ssfsup* mutants. (A) Compared to wild-type, the ssfsup mutants produce small compact colonies and produced an unknown red pigment (see Figure 2.5) at 42 ºC. At 28 ºC, the ssfsup mutants develop as wild-type. (B) Nomarski DIC images of wild-type germlings showing primary and secondary germ tubes and lateral branches. The ssfsup mutants produced germlings with shorter germ tubes and fewer lateral branches. All germlings incubated at 42 ºC for 24 hrs. Objective NA = 1.4 with oil. Scale = 10 µm. Abbreviations used WT: wild-type.

Sexual development of *ssfsup1, ssfA1* (*ssfsup2*), and *ssfsup3*

The *ssfsup1, ssfA1* (*ssfsup2*), and *ssfsup3* mutants were unable to complete sexual development in any pairwise combination with each other but all three mutants were fertile in crosses to the other *ssf* mutants as well as to wild-type (Table 2.2). No cleistothecia were formed in the cross between ASL21 (*ssfA1* (*ssfsup2*)) and ASL42 (*ssfsup3*) (Figure 2.4A). Small, immature cleistothecia were found in a self cross between two *ssfsup2* mutants (Figure 2.4B and C). These cleistothecia contained no viable ascospores. In the cross between ASL21 (*ssfA1* (*ssfsup2*)) and wild-type (Figure 2.4D) and between ASL21 and ASL31 (*ssfC1*) (Figure 2.4E), mature cleistothecia containing fertile ascospores were formed. Interestingly, in all cross plates mature Hülle cells were formed (Figure 2.4F and G). Hülle cells are associated with cleistothecia specifically in the sexual development stage in some *Aspergillus* species (e.g. *A. nidulans*) (Malloch, 1985).

In all cross plates where cleistothecia were not formed or did not reach maturity a red/brown pigment was formed (Figures 2.4 and 2.5). The identity of the pigments was not determined. All sexual crosses were performed at room temperature (approximately 22 ºC) indicating that these mutants were temperature insensitive for sexual developmental defects.

Complementation of *ssfsup* mutants with two proteasome alpha subunit genes

Since the *ssfsup+*/*ssfsup-* diploids had wild-type colony size, the *ssfsup* mutants were recessive for colony morphology defects. Therefore, we screened for

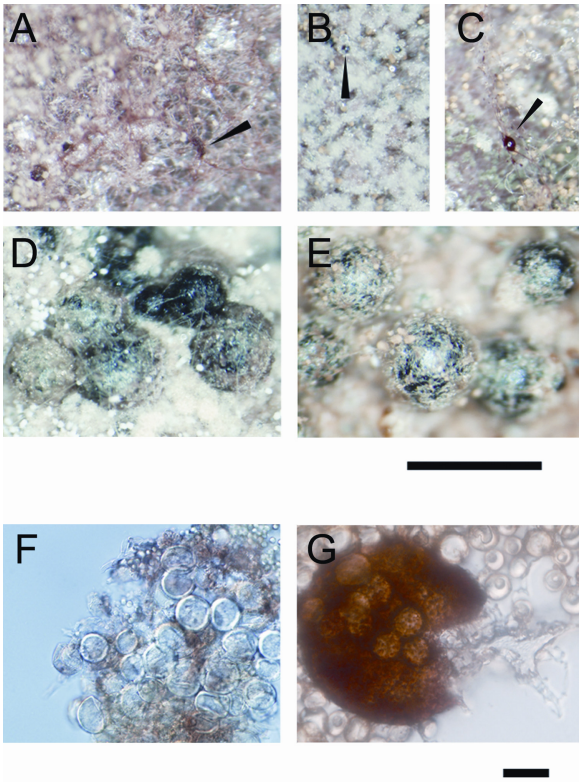

Figure 2.4 Sexual development of the single *ssfsup* mutants. (A) In a cross between ASL21 (*ssfA1* (*ssfsup2*)) and ASL42 (*ssfsup3*), mature cleistothecia were not formed. (B) In a cross between ASL21 (*ssfA1* (*ssfsup2*)) and ASL24 (*ssfA1* (*ssfsup2*)) strains, immature cleistothecia (arrow) were formed. (C) Droplets of reddish pigment (arrow) in the cross between two *ssfA1* mutants were formed. (D and E) Mature cleistothecia were formed in crosses between ASL21 (*ssfA1* (*ssfsup2*)) and wild-type (D) and between ASL21 (*ssfA1* (*ssfsup2*)) and ASL31 (*ssfC1*) (E). (F) A region corresponding to that indicated by the arrow in (A) examined under higher magnification. Hülle cells but no cleistothecia were formed in the cross between ASL21 (*ssfA1* (*ssfsup2*)) and ASL42 (*ssfsup3*). (G) A region corresponding to that indicated by the arrow in (B) examined under higher magnification. Hülle cells were formed and aborted cleistothecia did not bear ascospores. Objective NA = 0.95 for (F) and (G). Scale = 1 mm for (A-E) and 25 µm for (F and G).

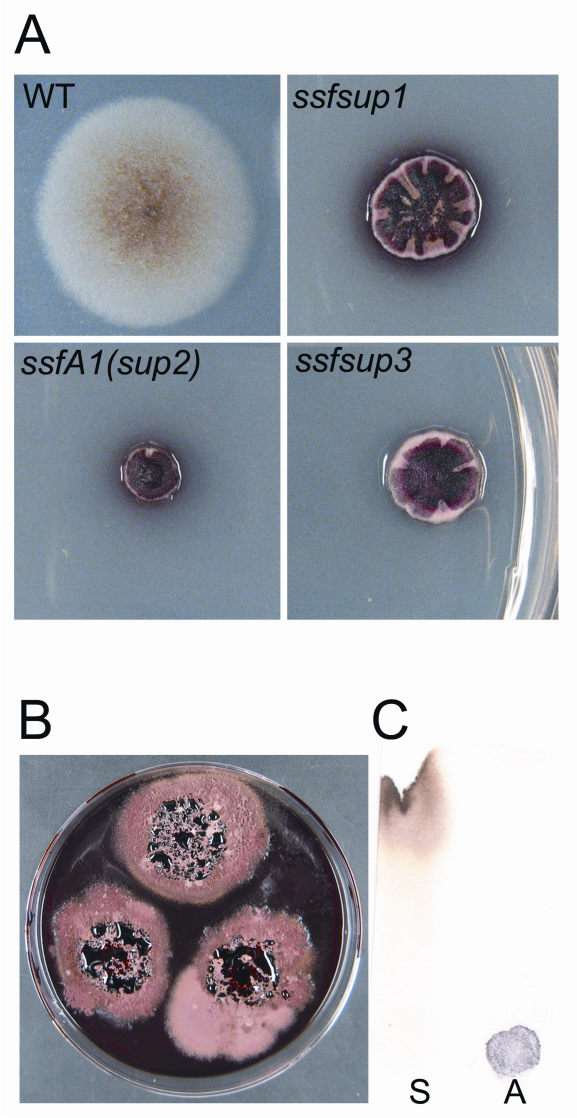

Figure 2.5 Pigments from *ssfsup1*, *ssfA1* (*ssfsup2*), and *ssfsup3* and paper chromatography of the sexual pigment of *ssfsup* mutants and ascoquinone A. (A) Colonies on solid minimal media were washed with sterile deionized H_2O to remove mycelia and conidia revealing that the *ssfsup* mutants produced an unknown red pigment. (B) A cross plate between *ssfA1* (*ssfsup2*) and *ssfsup3*. During failed sexual reproduction, the proteasome mutant strains produced unknown brown pigments. (C) Paper chromatography of the pigment from cross plate (S) and ascoquinone A (A) from ascospores revealed the pigment was not ascoquinone A, a red pigment produced during sexual development. To prepare ascoquinone A from ascospores, cleistothecia were disrupted with a pellet pestle in 100 µl of deionized distilled H_2O in microcentrifuge tubes. Those two pigments were not identified.

complementation by assaying for restoration of wild-type colony size at restrictive temperature (42 ºC). A genomic library constructed in the pRG3AMA1 autonomously replicating plasmid (described in Experimental Procedures) was transformed into strain ASL42 (*ssfsup3*). 3,100 transformants were screened and we found a single colony with colony growth diameter approaching that of wild-type at 42 ºC. The complementing plasmid was rescued and designated pRG-comD1 (Table 2.3). The 3' and 5' ends of the genomic DNA in pRG-comD1 were sequenced. By comparing the acquired sequence against the *A. nidulans* genome database using Blast algorhythms (Altschul *et al.*, 1997), we found that the plasmid contains a genomic fragment from 96,558-103,762 bp of contig 1.27 as designated in the Broad Institute genomic database for *A. nidulans* data release 4. Transposon insertion (Shaw *et al.*, 2002; Shaw and Upadhyay, 2005) within the predicted gene AN1757.3 eliminated the complementing activity of the plasmid (Figure 2.6A). Plasmid pAN1757 (Table 2.3) containing the AN1757.3 gene cloned into pRG3AMA1 (see Experimental Procedures) complemented ASL42 (*ssfsup3*) by restoring growth of the colony to a diameter comparable to wild-type (Figure 2.6B). The AN1757.3 gene is predicted to be 953 bp long, containing three introns at positions 25-87 bp, 273-333 bp, and 753-813 bp. The predicted AN1757.3 protein contains 255 amino acids and is an ortholog (65 % identity) of Pre9p from *S. cerevisiae* which is an alpha subunit of the 20S proteasome (Hochstrasser, 1996). We also transformed ASL21 (*ssfA1* (*ssfsup2*)) with the same genomic library. After screening 1,700 transformants, we identified one transformant with a colony morphology that was intermediate between wild-type and *ssfA1* (*ssfsup2*). The complementing plasmid, pRG-comB1 (Table 2.3),

Table 2.3 Plasmids used in this study

Plasmid	Characteristics	Sources
pRG3AMA1	Multicopy autonomous plasmid; *pyr-4*	(Osherov *et al.*, 2000; Osherov and May, 2000)
pRG3-comB1	pRG3AMA1 with 96,558-103,762bp fragment at *A. nidulans* contig 1.27	This study
pRG3-comD1	pRG3AMA1with122,236-115,518bp fragment at *A. nidulans* contig 1.139	This study
pAN1757	pRG3AMA1 with AN1757.3 gene (*ssfA*)	This study
pAN8054	pRGAMA1 with AN8054.3 gene	This study
pMT-3xHA	*alcA::ccdB::3xHA;argB;bla*	(Toews *et al.*, 2004)
pSL-3xHA	*alcA::ccdB::3xHA;pyr-4;bla*	This study
pENTR	Entry vector for Gateway cloning	Invitrogen
pmswoF-entry	pENTR with *swoF1*	This study
pmswoF-3xHA	*alcA::swoF1::3xHA;pyr-4;bla*	This study
pGEM-T easy	TA cloning vector	Promega
pGEM-pyr4	*pyr-4* in pGEM-T easy vector	This study

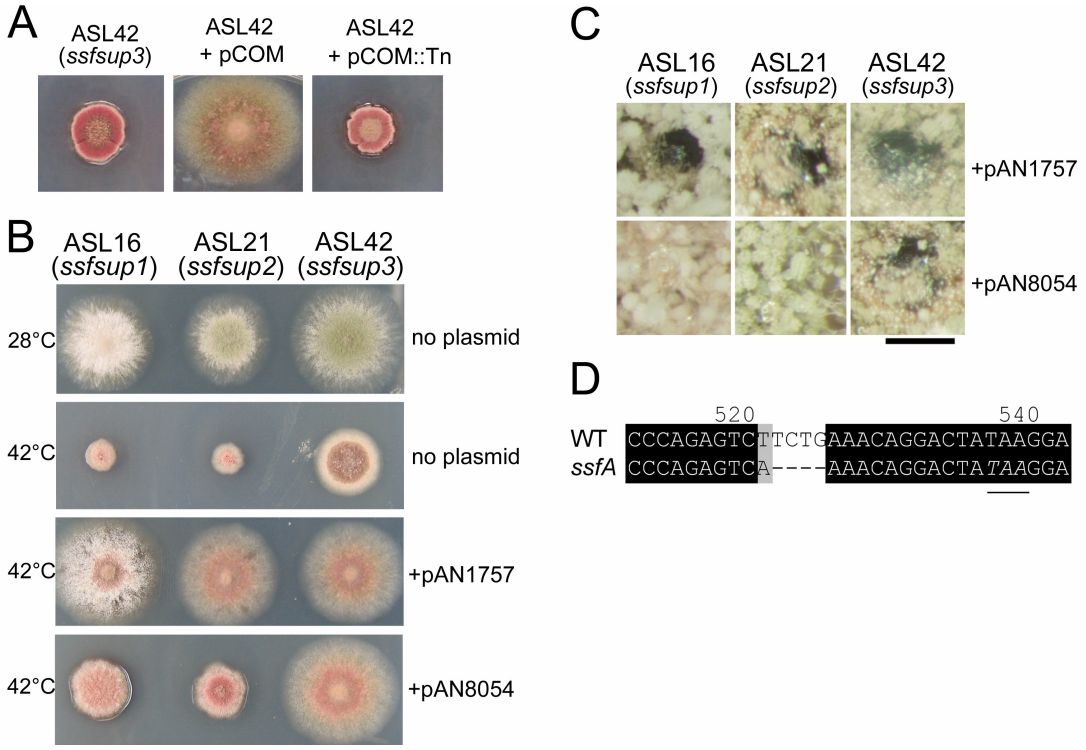

Figure 2.6 Complementation of ASL16 (*ssfsup1*), ASL21 (*ssfA1* (*ssfsup2*)), and ASL42 (*ssfsup3*) with two proteasome subunit genes and the mutant lesion of *ssfA1* from ASL21. (A) ASL42 harboring pRG-com1 restored growth of the colony to be indistinguishable from wild-type. A transposon insertion into AN1757.3 gene disrupted the complementing activity. (B) All *ssfsup* mutants recovered growth of the colony to be indistinguishable from wild-type when carrying the plasmid pAN1757. Strains ASL16 and ASL21 carrying pAN8054 produced smaller diameter mycelial colonies and their sporulation was rescued. Strain ASL42 carrying plasmid pAN8054 grew to wild-type colony diameter. (C) ASL16, ASL21, and ASL42 carrying pAN1757 or pAN8054 were each self-crossed. When carrying pAN1757 each formed fertile cleistothecia. Only ASL42 formed fertile cleistothecia when carrying pAN8054. Scale = 0.5 mm. (D) The AN1757.3 gene from ASL21 was sequenced from 512 bp upstream of start to 542 bp downstream of stop. The mutant lesion was identified as a deletion of four bases and an exchange of one base (grey) causing a frame-shift leading to premature termination at the underlined codon. Abbreviations used pCOM: pRG-comD1, pCOM::Tn: pRG-com1 with a transposon in AN1757.3 gene, WT: wild-type.

was recovered and the genomic DNA sequence was obtained for the genomic insert as described above. This genomic DNA fragment includes the sequence from 122,236-115,518 bp of *A. nidulans* contig 1.139. Because it encodes another 20S proteasome alpha subunit, the AN8054.3 gene was selected and subcloned (see Experimental procedures) into pRG3AMA1 to produce the plasmid pAN8054 (Table 2.3). We transformed pAN8054 into ASL21 and ten independent transformants displayed partial restoration of their colony phenotype (Figure 2.6B). The AN8054.3 gene is predicted to be 1073 bp long and has three introns at position 31-52 bp, 212-284 bp, and 674-740 bp. The predicted AN8054.3 protein contains 269 amino acids with 66 % identity to Pre6p from *S. cerevisiae*, another alpha subunit of 20S proteasome (Hochstrasser, 1996). Because each of the three *ssfsup* mutants 1) suppress the *swoF1* mutation, 2) result in similar growth defects of colonies, 3) share similar sexually sterile phenotypes and 4) were complemented by proteasome alpha sub-unit encoding genes, we hypothesized that all three are involved in proteasome function. We next tested the ability to cross complement among the three *ssfsup*'s with the plasmids pAN1757 and pAN8054. Complementation in colony formation and sexual sterility of the *ssfsup* mutants by both plasmids was examined. Plasmid pAN1757 (containing the Pre9 ortholog) complemented the colony formation defect and the sexual development defect of all three *ssfsup* mutants (Figure 2.6B and 2.6C). Plasmid pAN8054 (containing the Pre6 ortholog) partially restored growth of the colony of ASL16 (*ssfsup1*) and ASL21 (*ssfA1* (*ssfsup2*)) and fully restored growth of the colony of ASL42 (*ssfsup3*). Plasmid

pAN8054, restored sexual development of ASL42 (*ssfsup3*) but not that of ASL16 (*ssfsup1*) and ASL21 (*ssfA1* (*ssfsup2*)).

Next we sequenced the AN1757.3 gene from 384bp upstream of the start codon to 87bp downstream of the stop codon and the AN8054.3 gene from 484bp of the start codon to 100bp downstream of the stop codon from the strains ASL16, ASL21 and ASL42. We found a sequence alteration from wild-type at the AN1757.3 locus in strain ASL21 (*ssfA1* (*ssfsup2*)) (Figure 2.6D). This mutation consists of a four base pair deletion and one base pair exchange which causes a frame-shift leading to a premature termination codon (underlined *TAA* in the Figure 2.6D) resulting in a predicted 71 amino acid truncation at the C-terminus of the protein. Therefore we designate the AN1757.3 gene as *ssfA* and the mutant allele contained in strain ASL21 (*ssfsup2*) was designated *ssfA1*. Unexpectedly, no mutation was found at the AN1757.3 (*ssfA*) locus or the AN8054.3 locus in either ASL16 (*ssfsup1*) or ASL42 (*ssfsup3*).

To confirm that the mutation in the *ssfA* gene is responsible for suppression of the *swoF1* mutation, we back-crossed two different F1 progeny and two different F2 progeny of *ssfA1* to AXL18 (*swoF1*). From all crosses, progeny of wild-type, *ssfA1*, *swoF1*, and *swoF1;ssfA1* segregated 1:1:1:1 (Table 2.4) indicating that the mutant phenotype of *ssfA1* strains resulted from the mutation in the AN1757.3 gene and resulted in the suppression.

Table 2.4 Segregation of progeny from the cross between *ssfA1* segregants and AXL18 (*swoF1*)

	WT	*ssfA1*	*swoF1*	*swoF1;ssfA1*	The number of tested progeny
ASL24* x AXL18	40	37	42	46	165
ASL25* x AXL18	49	52	45	45	191
ASL211** x AXL18	42	38	38	38	156
ASL212** x AXL18	43	36	38	42	159

* Progeny from a cross between ASF2 and A234 (Table 2.1)

** Progeny from a cross between ASL21 and PW1

The χ^2 analysis (p<0.05), using Yates correction factor with three degrees of freedom, indicated that there is no significant difference from a 1:1:1:1 segregation ratio in four crosses.

The *swoF1* mutant accumulates lower levels of ubiquitinated protein

To investigate further how the proteasome mutation suppress the mutation in *swoF1*, we used the web-based algorhythm MyrPredictor (http://mendel.imp.ac.at /myristate/SUPLpredictor.htm) (Maurer-Stroh *et al.*, 2002) to identify possible myristoylation targets. Of the approximately 10,000 proteins predicted to be encoded by *A. nidulans*, AN2213.3 is among only 41 proteins predicted to be myristoylated (Table 2.5). AN2213.3 is an ortholog of Rpt2p in *S. cerevisiae* (71 % identity) which is a 19S proteasome subunit that has ATPase activity (Lucero *et al.*, 1995). The Rpt2 protein from *S. cerevisiae* also has a myristoylation motif at its N-terminus (Maurer-Stroh *et al.*, 2002) and its myristoylation was biochemically confirmed (Kimura *et al.*, 2003). Protein myristoylation is involved in membrane positioning of the proteins and hydrophobic protein-protein interaction (Rudnick *et al.*, 1993). Since in *Schizosaccharomyces pombe* the proteasome is localized primarily in the nucleus and to a lesser extent to the cytosol (Wilkinson *et al.*, 1998), N-myristoylation may be involved in a hydrophobic protein-protein interaction between Rpt2p ortholog, a 19S subunit protein and the hydrophobic inner barrel of the 20S particle. In a myristoylation mutant such as *swoF1*, the non-myristoylated-Rpt2p of the 19S particle may interact with the 20s particle less efficiently than does myristoylated Rpt2p. Since Rpt2p is required to control substrate entry and gate the channel of the 20S core particle (Kohler *et al.*, 2001), the different interaction patterns would result in a differential ratio of ubiquitinated proteins targeted for degradation. If this was true, ubiquitinated protein levels in the *swoF1* mutant and the suppressor mutants would be different from wild-type. To test this hypothesis we

Table 2.5 The *A. nidulans* predicted myristoylome. *

A. nidulans	*S. cerevisiae* homolog	N-terminal 20 amino acids	Function of Homologs
AN3090.3	Gpa2/Gpa1	MGCMSSKQLEAGDDKEAIQR	G alpha subunit
AN3793.3	Ppz1/Ppz2	MGQSHSKGNSGAGDSLQSYP	Calcineurin-like phosphoesterase
AN7461.3	Hst2	MGNESSTLVDEKTPPSVLEA	NAD(+)-dependent protein deacetylases
AN5020.3	Arf2/Arf3	MGGSVSKIMGKIFGTKEMRI	ADP-ribosylation factor, ArfB
AN5608.3	NONE	MGSNISYQCSDCEVQLPGAK	Acetylcholinesterase
AN5609.3	Ume6	MGQSSGANNDPAPRPRRARV	Transcription factor
AN5780.3	NONE	MGSSFSVQTKANRRRSNRLS	Unknown function
AN9311.3	NONE	MGQTASVPKPGTQIQVIGAG	Unknown
AN1126.3	Arf2/Arf1	MGLAISKLFDRLWGKKEMRI	ADP-ribosylation factor, ArfA
AN1173.3	NONE	MGCCFSVSREPHDSNGQTPT	Unknown
AN8391.3	Pdr1	MGSQSSGDLTLSQPRRHIIK	Pleiotropic drug response element
AN1682.3	NONE	MGSSASKPARSAAQASRRQY	Unknown filamentous fungi specific
AN0903.3	NONE	MGNCHSAQDHQHTVPAQRKS	Unknown function
AN6399.3	Kic1	MGSSYSVPALEEKSPRGETE	Protein kinase
AN10815.3	Yor246c	MGAQFSQFFPPHPTFTSENL	Dehydregenase
AN9060.3	Jjj1	MGQGHSTAEAGTGVSSERKD	DnaJ-like domain
AN10990.3	NONE	MGSQSTAVNTHPHVPKAGVW	Dihydrodipicolinate synthetase family
AN6633.3	NONE	MGAVFSCIRDLFRSIGACIM	Unknown filamentous fungi specific
AN6137.3	NONE	MGSSNGKAVESSDRVVVTPG	Unknown filamentous fungi specific
AN1420.3	Sip5	MGNSQTKETRPSHSQSSRRS	Glucose repression via Snf1
AN4156.3	Aro8	MGSIGTGSGVDLSHHINRKS	Aromatic amino acid aminotransferase
AN6570.3	Sip2	MGNNPSKGPVGDGPSPVVSG	Glucose repression via Snf1
AN11595.3	NONE	MGNTSDSSSAGGYTGRRHAD	*A. nidulans* specific predicted protein
AN3866.3	Cha1	MGSIGFATATTTQMTSTGSQ	Pyridoxal-phosphate dependent enzyme
AN5152.3	Chs7	MGSTQFGNFDDFCRDSTLPV	Regulating Chs3p export from the ER
AN0651.3	Gpa1/Gpa2	MGCGMSTEDKEGKARNEEIE	G alpha subunit
AN10233.3	Gnd1/Gnd2	MGSMMAFAFSEIGLDVSIWD	Phosphogluconate dehydrogenase
AN1762.3	NONE	MGVCSSCLGGGRRDSTDPES	Unknown filamentous fungi specific
AN4069.3	Ess1	MGKGNAKNSGGGDKKSKAKA	PPIC-type Ppiase domain
AN3193.3	NONE	MGTDLTQPPDGLIGGYKGDN	NADH dehydrogenase
AN1529.3**	NONE	GQKSSNPVMGRQSRPPSSST	*A. nidulans* specific predicted protein
AN5912.3	Arl1	MGGSLSRLWSLFWSKKEIRI	ADP-ribosylation factor like, ArlC
AN10760.3	NONE	MGQYSSTQREHRHQFPTESP	Zinc finger, C3HC4 type (RING finger)
AN4618.3	Reb1	MGQGSSQPAGLAQSGESDDE	Myb-like DNA binding domain
AN3227.3	NONE	MGSLWSSPSLLPSQQDNETE	Monooxygenase domain
AN1016.3	Gpa2	MGSCFSSESAGDVEQKKRSQ	G protein alpha subunit
AN4415.3	Cyt2	MGAGASTPVSPPPSTPAATC	Cytochrome c1 heme lyase
AN8690.3	Yfr011c	MGAGSSKPEASAGSKHIFES	Unknown
AN1995.3	Muc1	MGLVSSASSHLISPSPLPTL	GPI-anchored cell surface glycoprotein
AN2213.3	Rpt2	MGNQQSNIGGGHDGKDDKDK	19S protease subunit
AN1365.3	Ymr077c	MGNTNSSHKISSQDRAILDM	ESCRT-III complex subunit

* N-terminal and internal myristoylation motif of 10,701 predicted proteins from Broad Institute Data for *A. nidulans* release 4 were examined with fungal specific parameter by using web-based software (http://mendel.imp.ac.at/myristate/SUPLpredictor.htm).
**AN1529.3 has an internal myristoylation motif.

measured the total ubiquitinated protein levels in wild-type, *swoF1*, *swoF1;ssfA1,* and *ssfA1* by western blotting using anti-ubiquitin monoclonal antibody (Santa Cruz Biotechnology, Inc., Santa Cruz, CA, USA). This antibody recognizes ubiquitin, mono- and poly-ubiquitinated proteins. Because of the short half-life of ubiquitinated proteins, (for example the half-life of a cyclin is 90 seconds *in vitro* (Glotzer *et al.*, 1991; Pines and Lindon, 2005)) relatively low levels of ubiquitinated proteins were detected in wild-type cells. Surprisingly, in the *swoF1* mutant, significantly lower levels of ubiquitinated proteins were detected compared to wild-type (lane WT vs. lane F in Figure 2.7A). Whereas the *swoF1*;*ssfA1* mutant accumulated higher levels of ubiquitinated proteins than did wild-type (lane WT vs. lane F;A in Figure 2.7A). The single *ssfA1* mutant also accumulated more ubiquitinated protein compared to wild-type and *swoF1* (lane A in Figure 2.7A). To verify equal loading the same membrane used for western blot analysis was stained with protogold (Figure 2.7A). A replica gel was also stained with Coomassie blue. In the Coomassie stained gel, the total protein of the *swoF1* mutant displayed a smeared banding pattern characteristic of degraded protein (Figure 2.7B). Three independent protein preparations and western blots were performed to confirm the result. These data are consistent with the interpretation that the *swoF1* mutant has increased proteasome activity.

Mutant SwoF1^{D369Y} protein is not the target of the 26S proteasome

Previously, it was suggested that the SwoF1^{D369Y} mutation, responsible for the *swoF1* phenotype, may result in misfolding and destabilization of the protein

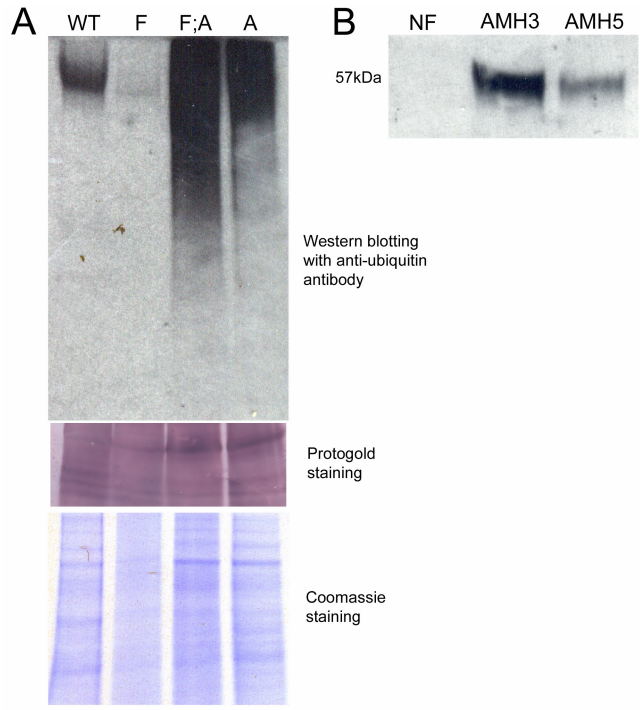

Figure 2.7 Ubiquitinated proteins from wild-type, *swoF1*, *swoF1;ssfA1*, and *ssfA1* and stability of the SwoF1^{D369Y}::3xHA. (A) Western blotting against ubiquitin demonstrates the concentration of ubiquitinated proteins was depleted in the *swoF1* mutant compared to wild-type (upper). The *swoF1;ssfA1* mutant was enriched for ubiquitinated proteins and the *ssfA1* mutant also accumulated more ubiquitinated protein than did wild-type. The same membrane used for western blot analysis was stained with protogold to verify equal loading of protein. In lane F of a Coomassie blue stained companion gel smeared protein bands were observed indicating the proteins in the *swoF1* mutant are unstable. (B) Stability of SwoF1^{D369Y}::3xHA. Protein from wild-type and two SwoF1^{D369Y}::3xHA transformants is shown. Strains AMH3 and AMH5 both expressed a protein a ~57 kDa which corresponds to the expected size of SwoF1^{D369Y}::3xHA band. Abbreviations used WT: wild-type, F: AXL19 (*swoF1*), F;A: ASF2 (*swoF1;ssfA1*), A: *ssfA1*, NF:ASL84 (*swoF1*, non transformant)

(Shaw *et al.*, 2002).

Our finding that a proteasome mutation suppresses the *swoF1* myristoylation defect, led us to consider that the *swoF1* polarity defect was the result of degradation of misfolded SwoF1^{D369} protein. To test this hypothesis we assayed the stability of the mutant protein by constructing a SwoF1^{D369Y}::3xHA (hemagglutinin epitope) fusion that was inserted ectopically into ASL84 (*swoF1*) (Table 2.1). These transformant strains harbor a mutant *swoF1* allele behind the native *swoF* promoter and the mutant *swoF1::3xHA* fusion under control of the *alcA* promoter which is repressed in the presence of glucose and is highly inducible in the presence of ethanol (Flipphi *et al.*, 2002). To assess the stability of the mutant protein we performed western blotting with an anti 3xHA monoclonal antibody (Santa Cruz Biotechnology, Inc., Santa Cruz, CA, USA) against total protein extracted from wild-type (A4), AMH3 (*alcA(p)::swoF1::3xHA*) and AMH5 (*alcA(p)::swoF1::3xHA*) grown at 42 ºC in the presence of ethanol and glycerol (Figure 2.7B). SwoF1^{D369Y}::3xHA was recovered from the strains AMH3 and AMH5, indicating that the misfolded SwoF1 protein does persist in the presence of functioning proteasome. Therefore, the mechanism of suppression of *swoF1* by the *ssfA1* proteasome mutant is not through stabilization of SwoF1^{D369Y} by inactivation of the proteasome.

The proteasome inhibitor, MG132 restores *swoF1* growth

Because the *swoF1* mutant showed an increased activity of the proteasome, we hypothesized that MG132, which selectively inhibits proteasome activity (Lee and Goldberg, 1996), would by-pass the *swoF1* polarity defect. To test this, we incubated the *swoF1* mutant and wild-type in the presence of MG132 at 42 ºC. After 24 hr incubation with MG132 (25 and 50 µM in 0.5% DMSO), there was no measurable difference from controls (data not shown). After 48 hr incubation, however, the *swoF1* mutant established a germ tube at least 60 µm in length that maintained its axis of polarity in the media containing MG132 (Figure 2.8). This germ tube could emerge from the conidium (Figure 2.8E) or the swollen primary germ tube (Figure 2.8F). Growth of wild-type was not visibly affected by MG132 at tested concentrations (Figure 2.8C and D). It is likely that inefficient uptake of the drug is responsible for the delayed response of *swoF1* and the lack of response in wild-type. Controls incubated in 0.5 % DMSO but no MG132 were not affected in their growth (Figure 2.8A and B). It is likely that *in vivo* inhibition of the proteasome is incomplete due to inefficient uptake of the compound (see discussion). Therefore, it is possible that actively growing wild-type could compensate better than the *swoF1* mutant for lost proteasome activity and therefore show no phenotype in the presence of MG132.

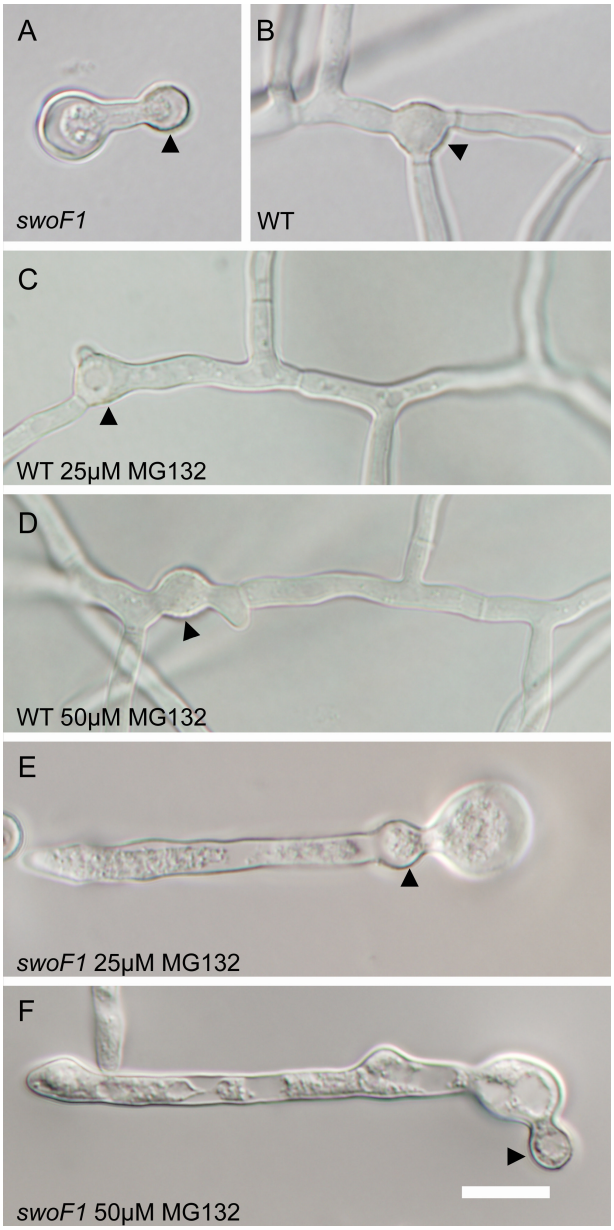

Figure 2.8 Effect of MG132 on the *swoF1* mutant during early morphogenesis. (A and B) 0.5 % DMSO (used to dissolve MG132) did not affect the growth of the *swoF1* mutant or wild-type. (C and D) In the presence of 25 and 50 µM of MG132 and 0.5% DMSO, wild-type growth was not affected. (E and F) The *swoF1* mutant re-established its axis of polarity during germ tube elongation. Conidia of *swoF1* grew isotropically but also established a polarized germ tube from the conidium (E) or from the swollen primary germ tube (F). Arrows indicate conidia. Objective NA=1.4 with oil. Scale=10 µm.

DISCUSSION

The temperature sensitive mutant *swoF1* of *A. nidulans* was isolated due to its defect in maintaining hyphal polarity during conidium germination (Shaw *et al.*, 2002). The germ tube failed to maintain its axis of polarity during growth and reverted to isotropic swelling at its apex (Figure 2.1). The *swoF* gene was found to encode an N-myristoyl transferase (NMT), an enzyme responsible for the co-translation lipidation of the N-terminus of a small subset of proteins (Shaw *et al.*, 2002). This study was undertaken to gain a greater understanding the role of protein N-myristoylation in cell morphogenesis. In a previous study of suppressors of *S. cerevisiae nmt1-181*, mainly components upstream of NMT were identified, for example genes involved fatty acid synthesis (Johnson *et al.*, 1994b). In this study, we identify the 26S proteasome as a component downstream of NMT. Johnson and colleagues found growth rate of the suppressor mutants in *S. cerevisiae* was similar to that of the *nmt1-181* mutants grown in myristic acid amended medium. Similarly, the partial suppression of *swoF1* in *A. nidulans* in this study resulted in growth rates comparable to that of the *swoF1* mutant grown in myristic acid amended medium (Shaw *et al.*, 2002).

A mechanism for the connection between myristoylation and the proteasome

We identified the *ssfA1* mutation in a gene encoding the ortholog of Pre9p from *S. cerevisiae*, a 20S proteasome alpha subunit. The possible mechanism of suppression of the *swoF1* mutant phenotype was examined using Myr Predictor. Within the *A. nidulans* predicted myristoylome (Table 2.5), AN2213.3 provides the most plausible connection

between myristoylation and the proteasome. Interestingly, Rpt2p of *S. cerevisiae,* an ortholog of *A. nidulans* AN2213.3, also has a conserved myristoylation motif at its N-terminus (Maurer-Stroh *et al.*, 2002). In yeast, N-myristoylation of Rpt2p was experimentally verified (Kimura *et al.*, 2003). However, the relation between N-myristoylation of Rpt2p and the proteasome activity was not discussed. Rpt2p plays a role in the recognition of ubiquitinated protein and in the interaction between the 19S and 20S particles (Eisenhaber *et al.*, 2003; Kohler *et al.*, 2001; Lucero *et al.*, 1995; Rubin *et al.*, 1998). N-myristoylation of Rpt2p may act to gate the 20S particle by enhancing the interaction between the 19S particle and the 20S particle. Despite the conserved myristoylation motif, the functional connection between N-myristoylation and the 26S proteasome has not been investigated.

In western blot analysis, we observed reduced accumulation of ubiquitinated proteins in the *swoF1* mutant compared to those in wild-type. In contrast in *swoF1*;*ssfA1* double mutants, an increase in the amount of ubiquitinated proteins was observed (Figure 2.7A). Since the antibody for this experiment recognizes mono- and poly-ubiqutin chains as well as poly-ubiquitinated proteins, the lower ubiquitin signal in the *swoF1* mutant (Figure 2.7A) resulted from the enhanced degradation of ubiquitinated proteins caused by increased activity of 26S proteasome dependent proteolysis. This demonstrates that suppression may have occurred through inhibition of the proteasome and therefore greater accumulation of ubiquitinated proteins. It is possible, however, that enhanced ubiquitination of abundant proteins in the *swoF1;ssfA1* and *ssfA1* strains resulted in the accumulation of ubiquitinated proteins without changing proteasome

activity, for example by increasing ubiquitin ligase activity. Our data eliminate this possibility, since the proteasome inhibitor MG132 bypasses the growth defect of both strains (Figure 2.8). It is surprising that disruption of N-myristoylation results in greater activity of the 26S proteasome. This result suggests that N-myristoylation attenuates proteasome activity in wild-type. To our knowledge this is the first report identifying a mechanism for the connection between N-myristoylation and 26S proteasome activity.

In the presence of the proteasome inhibitor, MG132, hyphal polarity was re-established resulting in germ tubes that extended approximately 60 µm in length after 48 hr incubation (Figure 2.8). This observation supports the hypothesis that the increased activity of the 26S proteasome resulted in the isotropic swelling at hyphal apices phenotype of the *swoF1* mutant. In contrast to the *swoF1;ssfA1* phenotype (Figure 2.1), *swoF1* hyphal growth in the presence of MG132 continued to display hyphal swellings resulting from subapical isotropic growth in addition to polarized hyphal growth (Figure 2.8E and F). Inefficient uptake of MG132 might have resulted in minimal inhibition of the proteasome. Since the mutant is growing slowly it contains less cytoplasm and by default fewer copies of active proteasome. Therefore even small amounts of inhibitor result in profound effects. In the wild-type, with more growth, more cytoplasm and therefore more copies of active proteasome shared throughout the continuous cytoplasm of organism, inefficient uptake of the inhibitor is more likely to leave active proteasome present in each germling. In *S. cerevisiae*, a delta(24)-sterol C-methyltransferase mutant was shown to enhance MG132 uptake by permeablizing the membrane (Lee and Goldberg, 1996). This mutant is not available at this time in *A. nidulans* to test whether

enhanced uptake of MG132 would further suppress *swoF1* or detectably alter wild-type growth.

Other possible mechanisms of suppression

The 26S proteasome is responsible for the degradation of transcription factors, cyclins, and misfolded proteins among other targets (Driscoll and Goldberg, 1990; Hiller *et al.*, 1996). It is possible that a short half-life of transcription factors in the *swoF1* mutant restricted expression of proteins required for maintaining cell polarity. It is, however, unlikely that cell cycle alterations through cyclin degradation caused the growth defect since the *swoF1* mutant continued nuclear division despite loss of polarity (Figure 2.1C). Another possibility is that the SwoF1^{D369Y} protein is misfolded and is therefore a target for degradation by the 26S proteasome since the proteasome is responsible for the removal of misfolded proteins (Hiller *et al.*, 1996). We found that SwoF1^{D369Y}::3xHA persisted in the *swoF1* mutant background (Figure 2.8B) indicating that targeted degradation of SwoF1^{D369} is not the cause of the *swoF1* growth defect. Total proteins from the *swoF1* mutant were smeared on an SDS-gel (Figure 2.7A), however, suggesting that many proteins were unstable.

Similarity of *ssfsup* mutants to COP9 mutants

The *ssfsup* mutant phenotypes including sexual sterility and production of a red pigment on solid media (Figure 2.5A) are similar to those of the constitutive

photomorphogenesis complex 9 (COP9) mutants (Busch *et al.*, 2003). Like the *ssfsup* mutants, the COP9 signalosome mutants have been found to be involved in sexual development of *A. nidulans* and they produce an unidentified red pigment (Busch *et al.*, 2003; Schwechheimer, 2004). In other studies, the COP9 signalosome has been found to be interchangeable with the 19S proteasome by binding the 20S proteasome particle (Huang *et al.*, 2005; Serino and Deng, 2003). It is possible that the *ssfA1* (ortholog of Pre9 in *S. cerevisiae*) proteasome mutant may fail to interact with the COP9 signalosome and therefore display similar sexual development defects. Our data support the hypothesis that ubiquitin-proteasome dependent proteolysis is required for sexual development (Krappmann *et al.*, 2006).

Multi-copy suppression among proteasome alpha subunits

Our complementation data (Figure 2.6) indicate that AN8054.3 is a multi-copy suppressor of *ssfA1* since pAN8054 contains the AMA1 sequence which results in autonomous maintenance of 10-30 copies per nucleus (Gems *et al.*, 1991). The predicted proteins SsfA (AN1757.3) and AN8054.3 are orthologs of Pre9p and Pre6p of *S. cerevisiae* respectively. In *S. cerevisiae,* deletion of *pre9* is compensated by the overexpression of *pre6* (Velichutina, 2004). But neither *ssfA* nor the AN8054.3 gene from *ssfsup1* and *ssfsup3* carried a mutation. It is possible the overexpression of SsfA and AN8054.3 multi-copy suppressed the mutation in another proteasome alpha subunit yet to be identified in the *ssfsup1* and *ssfsup3* strains. This result raises the possibility that other subunits in the 20S proteasome can be interchangeable with each other in

addition to the substitution of Pre9p by Pre6p already documented in *S. cerevisiae* (Velichutina, 2004). Additionally, though it was complemented with the same proteasome subunit genes, the *ssfsup1* mutant displayed an unusual segregation pattern. This may be due to a translocation or other rearrangement that occurred in this strain during UV mutagenesis (Käfer, 1965).

Our data support the model outlined in Figure 2.9. In the *swoF1* NMT, mutant an increased activity of the proteasome resulted in the observed polarity defects. In wild-type, N-myristoylation regulates cell morphogenesis at least in part through attenuating the 26S proteasome (Figure 2.9A and B). The mechanism of this interaction remains to be revealed. Though the proteasome mutations suppressed and MG132 by-passed the *swoF1* mutant, the suppression was not complete. This is most likely due to complications induced by disruption of proteasome activity. In addition, 26S proteasome dependent protein degradation is not the only event downstream of NMT. In fact, the list of possible myristoylation targets contains 41 proteins of diverse function (Table 2.5). We have recovered additionally suppressor mutants, *ssfB* and *ssfC* (Figure 2.1B, C, and D), which have not been further characterized. Neither is complemented by the proteasome alpha subunits discussed in this study. Also, neither the *ssfB* or *ssfC* mutants accumulated ubiquitinated proteins at levels different from wild-type (data not shown). Future work is needed also to investigate if myristoylation of the Rpt2p ortholog, AN2213.3, affects the activity and localization of the 26S proteasome and how *ssfB* and *ssfC* are involved in N-myristoylation and cell morphogenesis.

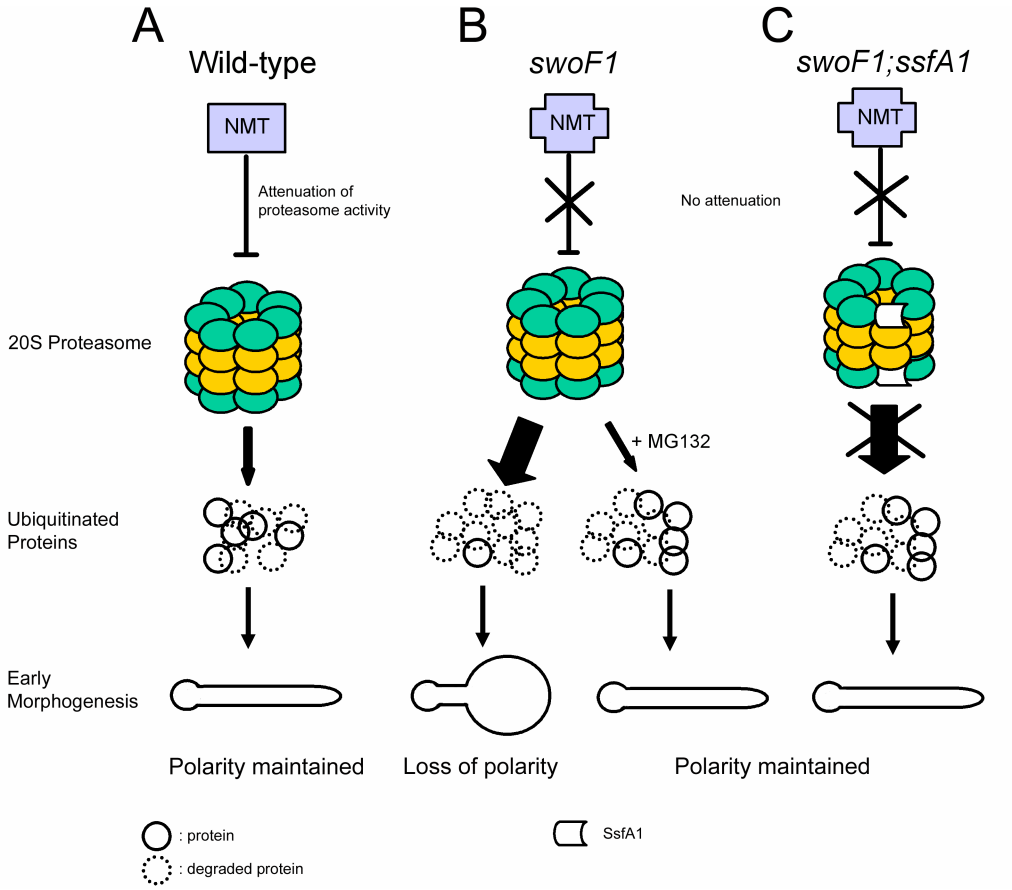

Figure 2.9 Model describing one possible role of N-myristoylation in cell morphogenesis of A. nidulans. (A) In wild-type, the activity of the proteasome is diminished by N-myristoylation of a protein or proteins. Regulation of ubiquitinated protein enables the wild-type cell to maintain growth along its long axis of polarity. (B) In the swoF1 myristoylation mutant, the activity of the proteasome is elevated so that the half-life of ubiquitinated proteins is shortened resulting in loss of polarity maintenance due to degradation of unidentified proteins. Proteasome inhibitor MG132 suppresses the polarity defect by inactivating the proteasome. (C) In swoF1;ssfA1, a mutation in the proteasome results in inactivation or depression of activity of the proteasome, which leads to suppression of the polarity defect.

EXPERIMENTAL PROCEDURES

Strains and growth condition, plasmids, media, and reagents

A. nidulans strains and plasmids used in this study are listed in Table 2.1 and 2.3, respectively. The plasmids were amplified and maintained in *E. coli* XL1-blue (Stratagene, La Jolla, CA, USA) as described (Sambrook *et al.*, 1989). Complete and minimal media for *A. nidulans* were prepared using standard recipes (Kaminskyj, 2001; Momany *et al.*, 1999). All reagents for media, buffer, and supplements were purchased from Sigma (St. Louis, MO, USA) unless otherwise indicated.

Generation of suppressor mutants of *swoF1*

To obtain *swoF1* suppressor mutants, secondary mutations were generated by irradiating AXL19 (*swoF1; pyrG89*) with ultraviolet light (wavelength = 253.7 nm) with a UV Stratalinker^{TM} 2400 (Stratagene, La Jolla, CA, USA). A killing curve was established by irradiating spores in deionized distilled H_2O 14 cm from the UV source with 0 to 300 µJ of energy. 225 µJ was chosen as the dose at which 70 % of the spores were killed. The UV-exposed conidia were spread onto minimal media containing 1.5 % agar (Difco, Sparks, MD, USA) and grown at restrictive temperature (42 ºC). After 4 days incubation, visible colonies were selected for further analysis since temperature sensitive *swoF1* mutant strains are not able to form mycelial colonies on solid media at restrictive temperature (42 ºC) (Shaw *et al.*, 2002).

Genetic analyses of suppressor mutants

Sexual crosses were performed for genetic analysis and to release single suppressor mutants from *swoF1* using standard procedures (Kaminskyj, 2001; Shaw and Upadhyay, 2005). To verify whether the mutations are dominant or recessive, diploid strains with heterozygous alleles of each *ssf* gene were generated as previously described (Kaminskyj, 2001).

Microscopic images

Germlings were prepared for observation using the 'coverslip method' previously described (Momany *et al.*, 1999). Microscopic observation and image processing were conducted using equipment outlined previously (Shaw and Upadhyay, 2005). For observation of cleistothecia during sexual development, an Olympus SZX9 stereo microscope connected to an Olympus DP70 digital camera (Olympus America Inc., Melville, NY, USA) was used.

Transformation of *A. nidulans* and complementation

Protoplasts of mutant strains were prepared for transformation (Shaw *et al.*, 2002) with a genomic library (Osherov *et al.*, 2000; Osherov and May, 2000) as previously described. Complementation was judged by the ability to establish a mycelial colony at 42 ºC.

Recovery of complementing plasmids, identification of *ssfA* gene, and cloning of AN1757.3 and AN8054.3

Complementing plasmids were recovered as outlined previously (Shaw and Upadhyay, 2005). Recovered plasmids were re-introduced into the mutants to re-confirm complementation. Transposon insertion using the GPS-1 Genome Priming System (New England Biolabs Inc., Ipswich, MA, USA) was used to identify the complementing gene using previously described methods (Shaw *et al.*, 2002; Shaw and Upadhyay, 2005). The AN1757.3 gene including 336 bp upstream of the start codon and 31 bp downstream of the stop codon was amplified by PCR using the Expand High Fidelity PCR System (Roche Diagnostics, Indianapolis, IN., USA) with the primers:

SDF 5'- **GGATCC**GGTATACGTAGACTTGAGCA -3' and

SDR 5' – **GCATGC**GCAGAGATCCGTAACTCTAT -3'. *Bam*HI and *Sph*I (in bold) recognition sites were inserted at the 5' end of SDF and SDR primer respectively. Wild-type *A. nidulans* A4 genomic DNA was used as template. Amplicons were gel-purified with the Qiagen gel extraction kit (Qiagen Inc., CA). After digestion with *Bam*HI and *Sph*I, the fragments were ligated into *Bam*HI-*Sph*I digested pRG3AMA1 vector (Osherov *et al.*, 2000) by using the Quick ligation kit (New England Biolabs Inc., Ipswich, MA, USA) to create pAN1757. To clone the AN8054.3 gene, the same cloning steps were conducted with primers:

SBR 5'-GGATCCTAGCGGATCATGTACAGCAT-3' and

8054F 5'- **GCATGC**GATGGTTCGTTTCTACAGAGCC-3'. The pRG3AMA1 with the AN8054.3 gene including 484 bp upstream of the start codon and 100 bp downstream of

the stop codon was named pAN8054. Plasmids pAN1757 and pAN8054 were transformed into ASL16 (*ssfsup1*), ASL21 (*ssfA1* (*ssfsup2*)), and ALS42 (*ssfsup3*) to confirm that these genes are responsible for complementation.

To find the mutant lesion, the AN1757.3 and AN8054.3 genes from the ASL16, ASL21, and ASL42 strains were amplified by PCR. For gene AN1757.3, we used MDF and MDR primers: 5'-AGCAGAGATCCGTAACTCTA-3' and 5'-CATTGCTACTTCACCTCTGA-3' and for the AN1757.3 gene we used the same primers used to clone the AN8054.3 gene as described above. The amplicons were cloned into pGEM-T easy vector (Promega, Madison, WI, USA) for sequencing. Three independent amplicons were cloned and sequenced.

Sequence analysis

DNA Blast algorhythms (Altschul *et al.*, 1997) were used to compare mutant sequence to the genomic DNA sequence of A4 strain at the Broad Institute Data for *A. nidulan*s (http:://www.broad.mit.edu/annotation/fungi/aspergillus/).. DNA sequencing was performed by the Gene Technologies Lab, Texas A&M University (http:://www.ibmb.tamu.edu/gtl/compute.htm).

Construction of vectors and tagging *swoF1* with 3xHA

We used the pMT-3xHA gateway cloning vector (Toews *et al.*, 2004) to tag SwoF1^{D369}. The mutant *swoF1* gene was amplified with the following primers:

swofF 5'-CACCATGTCAGACTCAAAAGACTC-3',

swofR 5'- GAGCATAACAACGCCCACA-3'. The amplicon was cloned into gateway entry vector, pENTR (Invitrogen, Carlsbad, CA, USA) to produce pmSwoF1-entry. The *ccdB* box was exchanged with the *swoF1* gene in pMT-3xHA to produce pmSwoF-3xHA as described previously (Toews *et al.*, 2004). This construct places the *swoF1::3xHA* under control of the inducible *alcA* promoter (Flipphi *et al.*, 2002). Plasmid pmSwoF-3xHA was transformed into ASL84, a *swoF1* mutant *A. nidulans* strain (Table 2.1) to recover ectopic insertions.

Protein extraction and western blotting

Total protein from mycelial growth was extracted as previously described (Osherov and May, 1998) with the following modifications. Conidia were incubated in liquid complete media (Kaminskyj, 2001) containing 50 µg/ml ampicillin and incubated at restrictive temperature (42 ºC). The mycelia were filtered through miracloth (Calbiochem, La Jolla, CA, USA) and washed with deionized distilled H_2O. The mycelial mass was then dried by blotting with filter papers. Dried mycelia (50 mg) was transferred into a clean microcentrifuge tube and ground with a pellet pestle in the presence of 100 µl of 9 M urea sample buffer (1 % SDS, 9 M urea, 25 mM Tris-HCl pH 6.8, 1 mM EDTA, 0.7 M beta mercapto-ethanol) with 1 µl of protease inhibitor cocktail (Catalog number P-8849, Sigma, St. Louis, MO, USA). The sample was boiled for 2 min, vortexed for 1 min, and boiled again for 1 min. An additional centrifugation for 1 min was carried out at 13,000 rpm. The supernatant was transferred to new microcentrifuge

tubes and loaded on precast 12 % sodium dodecyl sulfate- polyacrylamide gel electrophoresis (SDS-PAGE) gel (Life Gels, Clarkton, GA, USA) or stored at -20 ºC for later use. The concentration of the protein was determined by Bradford analysis as described previously (Bradford, 1976).

For western blotting, 5 µg of protein per lane was separated on a 12 % SDS-PAGE gel and transferred to nitrocellulose membrane (Amersham Biosciences, Piscataway, NJ, USA) using Mini-PROTEAN 3CELL and Mini Trans-Blot module (Bio-Rad, Hercules, CA. USA), following the manufacturer's protocol. The membrane was incubated in blocking solution (2 % bovine serum albumin, 20 mM Tris-HCl pH 8.0, 137 mM NaCl, 0.05 % Tween-20) for 1 hr followed by 1 hr additional incubation in the blocking solution with mouse anti-ubiquitin monoclonal or mouse anti-HA monoclonal antibody (1:2000) (both from Santa Cruz Biotechnology, Inc. Santa Cruz, CA). After washing with TBS-Tween buffer (20 mM Tris-HCl pH 8.0, 137 mM NaCl, 0.05 % Tween-20), the membrane was incubated in the blocking solution for 1 hr at room temperature (approximately 22 ºC) with bovine anti-mouse antibody conjugated with horse radish peroxidase (1:5000) (Santa Cruz Biotechnology, Inc., Santa Cruz, CA, USA). Protein was visualized by using ECL Western blotting substrate (Pierce Biotechnology, Inc., Rochford, IL, USA) following the manufacturer's protocol followed by 1 min exposure to X-Omat AR film (Kodak, Rochester, NY, USA). Equal loading was verified by protogold staining of the membrane following the manufacturer's protocol (BBInternational Ltd, Cardiff, UK) and by Coomassie blue staining (Sambrook *et al.*, 1989) of a replica gel.

CHAPTER III

Aspergillus nidulans ARFB IS LINKED TO ENDOCYTOSIS AND POLARIZED GROWTH

SUMMARY

Filamentous fungi undergo polarized growth during the majority of their life cycle. The spitzenkörper, an apical organelle composed of a cloud of vesicles that is unique to filamentous fungi, is thought to direct this growth by acting as a vesicle supply center. Vesicle assembly and trafficking are therefore, important for polarized hyphal growth. ADP-ribosylation factors (ARFs), a group of small GTPase proteins, play an important role in vesicle formation by nucleating their assembly. Little is known about the role of ARFs in filamentous hyphal growth. We found that *Aspergillus nidulans* is predicted to encode six Arf family proteins. Protein sequence alignments suggest that *A. nidulans* ArfB shares similarity with Arf6 of *Homo sapiens* and Arf3p of *Saccharomyces cerevisiae*. ScArf3p plays a role in bud site selection and actin cytoskeleton assembly. An *arfB* disrupted strain (*arfB::Tn*) is characterized by extended isotropic growth of germinating conidia followed by cell lysis and multiple, random germ-tube emergence, consistent with a failure to establish polarity. The mutant germ-tubes and hyphae that do form meander abnormally off of the axis of polarity and frequently exhibit dichotomous branching at cell apices, consistent with a defect in polarity maintenance. FM4-64 staining of the *arfB::Tn* strain revealed that another phenotypic characteristic of the *arfB::Tn* is a reduction and delay in endocytosis. ArfB::GFP localizes to the plasma

membrane and endomembranes and mutation ($ArfB^{G2A}$::GFP) of the N-terminal myristoylation motif disperses the protein to the cytoplasm rather than membranes. N-myristoylation of the protein is critical for localization and function. These results demonstrate that ArfB functions in endocytosis to play important roles in polarity establishment during isotropic growth and polarity maintenance during hyphal extension.

INTRODUCTION

Polarized growth is a biological process observed in many different eukaryotic cell systems including: pollen tube formation (Taylor and Hepler, 1997), neuronal cell development (Bradke and Dotti, 1997), and fungal hyphal growth (Bartnicki-Garcia and Lippman, 1969). Filamentous fungi are characterized by extensive polarized hyphal growth throughout most of their life cycles. This unique developmental pattern makes filamentous fungi an attractive system to study polarized growth. Invasive hyphal polarized growth is an important strategy for animal and plant pathogenic fungi to infect and penetrate their host. Therefore understanding the polarized hyphal growth will be critical to develop therapeutic or anti-fungal agents.

Girbardt reported the existence of the spitzenkörper (apical body) at growing hyphae and proposed that the spitzenkörper coincide with the polarized growing site (Girbardt, 1957). Electron microscopic analyses revealed the spitzenkörper consists of two populations of vesicles, apical vesicle (79 to 90 nm in diameter) and microvesicles (30 to 40 nm in diameter) according to their size. Microvesicles are found to have chitin synthesis activity and have been called ‘chitosomes’ (Bartnicki-Garcia, 2006; Bracker *et*

al., 1976). The spitzenkörper corresponds with a postulated vesicle supply center (VSC) thought to be necessary to explain hyphal tip growth (Grove and Bracker, 1970; Harris *et al.*, 2005). This has driven the hypothesis that vesicle assembly and trafficking play a key role in polarized growth in filamentous growth.

ADP-ribosylation factors (Arfs) are small GTPases that are involved in vesicle assembly and intracellular trafficking (Molendijk *et al.*, 2004; Moss and Vaughan, 1998). In *S. cerevisiae*, Arf3 is involved in polarity establishment during budding and an *arf3* mutant shows a random budding phenotype (Giaever *et al.*, 2002; Huang *et al.*, 2003). The Arf3 protein localizes to cell membranes and predominantly to polarized growing site (Huang *et al.*, 2003). Arf3 also genetically interacts with actin cable and actin patch components including profilin (Pfy1), Arp2/3 complex protein (Las17p and Vrp1), formins (Bni1 and Bnr1), Arf-GTP Exchange Factor (Gea1), and actin organizing proteins (Syp1, and Bud6) (Lambert *et al.*, 2007). Another function of Arf3p in yeast is in membrane trafficking during endocytosis (Costa and Ayscough, 2005; Costa *et al.*, 2005).

Shaw *et al*. reported that a temperature sensitive N-myristoyl transferase mutant displayed a phenotype characterized by a polarity maintenance defect in *Aspergillus nidulans* (Shaw *et al.*, 2002). Myristate from myristoyl Co-A is covalently attached to the secondary glycine of target proteins by NMT increasing hydrophobicity (Johnson *et al.*, 1994a). Myristoylated protein more readily associates with membranes or takes part in hydrophobic protein protein interactions (Johnson *et al.*, 1994a; Rudnick *et al.*, 1993). Many Arfs including ScArf3p are N-myristoylated (Balch *et al.*, 1992; Moss and

Vaughan, 1995). We hypothesized that Arf proteins may be the direct connection between N-myristoylation and polarized cell morphogenesis in filamentous fungi. Indeed, in *S. cerevisiae*, N-myristoylated Arfs, including Arf1p, Arf2p, Arf3p, and Arl1p are shown to be associated with polarized budding, in which Arf1p, Arf2p and Arl1p are involved in a secretion pathway through the Golgi network (Rosenwald *et al.*, 2002; Stearns *et al.*, 1990). These secretory vesicles may be destined for the spitzenkörper in filamentous fungi.

In this study we found six Arf family proteins in *A. nidulans.* Three of them, AN1126.3, AN5020.3, and AN5912.3 (ArfA, ArfB, and ArlA respectively), are predicted to be myristoylated (Lee and Shaw, 2007). We chose ArfB for further investigation since it is the putative ortholog of Arf3p in *S. cerevisiae* (Figure 3.1) which is associated with polarized bud site selection (Huang *et al.*, 2003) and action organization (D'Souza-Schorey and Chavrier, 2006; Lambert *et al.*, 2007). Here we show that ArfB is important for establishment and maintenance of hyphal polarity, possibly by directing endocytosis in *A. nidulans* and that this role requires N-myristoylation of the protein.

RESULTS

ADP-ribosylation factor B is an ARF6 family protein in *A. nidulans*

A. nidulans and *S. cerevisiae* encode six Arf family proteins (ArfA (AN1126.3), ArfB (AN5020.3), ArlA (AN5912.3), AN3934.3, AN0411.3, and AN0634.3 for *A.*

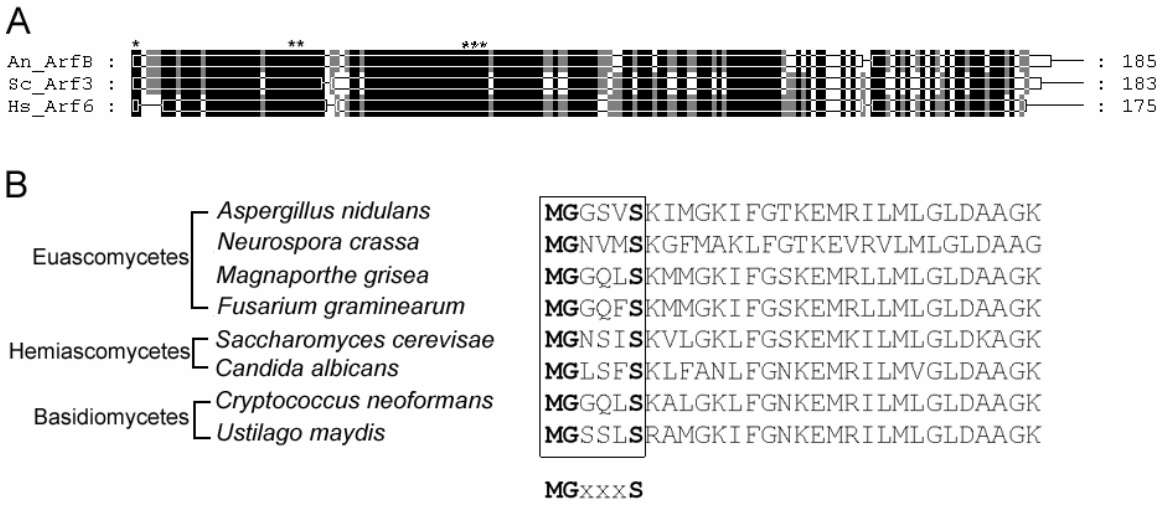

Figure 3.1 Similarity in amino acid sequence of ArfB (*A. nidulans*), Arf3p (*S. cerevisiae*), and Arf6 (*H. sapiens*) and the N-terminus of Arf6 family proteins of representative filamentous fungi. (A) Alignment of protein sequences of ArfB, Arf3p, and Arf6. Black boxes indicate all three sequences are identical. Grey boxes indicate amino acid identity in two of three sequences. An_ArfB: *A. nidulans*, Sc_Arf3: *S. cerevisiae*, Arf3p, Hs_Arf6: *Homo sapiens*. *: N-myristoylation motif, **: GTP binding site, ***: GFP hydrolysis site. (B) N-terminal 30 amino acid sequences of Arf6 family proteins of *A. nidulans* (AN5020.3), *N. crassa* (NCU07173.1), *M. grisea* (MGG10676), *F. graminearum* (FG04483.1), *S. cerevisiae* (Arf3p), *C. albicans* (CaO19.5964), *C. neoformans* (CNL06630), *U. maydis* (UM05580.1). All fungal Arf6 orthologs contain the consensus N-myristoylation motif (M-G-x-x-x-S-).

nidulans) and (Arf1p, Arf2p, Arf3p, Arl1p, Sar1p, and Arl3p for *S. cerevisiae*) (Figure 3.2). We found that ArfB (AN5020.3) is a putative ortholog of ScArf3p which was previously shown to be involved in selecting bud sites (Huang *et al.*, 2003) through interactions with proteins involved in actin assembly (Lambert *et al.*, 2007). The AnArfB and ScArf3p are further grouped into the ARF6 family (or Class III Arfs) of proteins, named after human ARF6 (Gillingham and Munro, 2007)**.** The AnArfB, ScArf3p, and HsARF6 protein sequences were aligned (Figure 3.1A). AnArfB shares 59 % amino acid sequence identity with ScArf3p and 72 % identity with HsARF6. ScArf3p shares 59% similarity with HsARF6. The AnArfB, ScArf3p, and HsARF6 proteins have a conserved N-terminal myristoylation site and conserved GTP binding and hydrolysis site for their GTPase activity (Figure 3.1A). The *arfB* gene is located on chromosome III from base pairs 507503 to 508272 on Contig 84 (of release 3 of the genome database http://www.broad.mit.edu/annotation/genome/aspergillus_group/ MultiHome.html). The *arfB* gene is 770 bp in length, and contains four introns at the positions 94-153 bp, 312-363 bp, 511-561 bp, and 674-725 bp. ARF6 family proteins were retrieved from filamentous fungal genome databases including *A. nidulans*, *N. crassa*, *Magnaporthe grisea*, *Fusarium graminearum*, *C. albicans*, *Cryptococcus neoformans*, and *Ustilago maydis* in addition to *S. cerevisiae*. All of these proteins contain the consensus Met-Gly-x-x-x-Ser/Thr motif at their N-terminus (Figure 3.1B) suggesting N-myristoylation of ARF6 family protein is important for function.

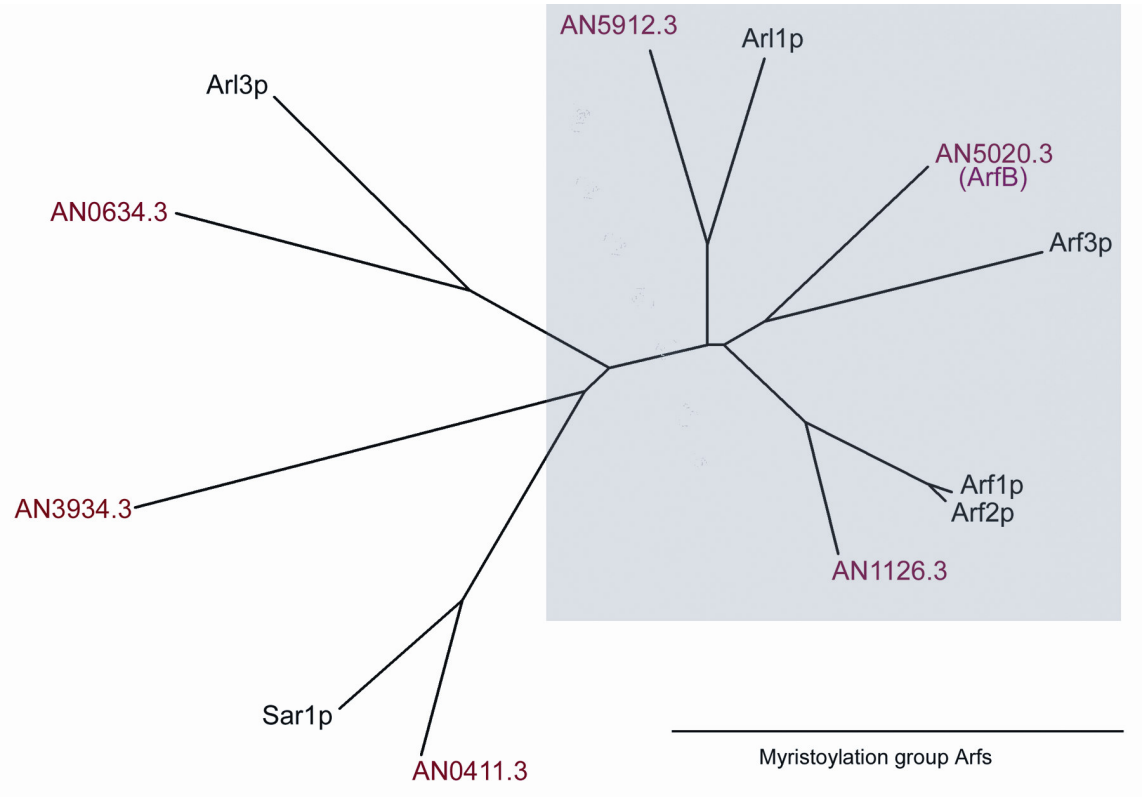

Figure 3.2 Unrooted NJ tree for Arfs of *A. nidulans* and *S. cerevisiae*. *A. nidulans* proteins indicated in Red. *S. cerevisiae* proteins indicated in black. Grey box indicates the myristoylation group Arfs.

Disruption of *arfB* by a transposon insertion

To investigate the role of *arfB* in *A. nidulans* we made a disruption construct. The *arfB* disruption cassette was constructed in pGEM-T Easy vector (See Experimental procedures), in which a transposon is inserted into the first intron of the *arfB* gene (Figure 3.3A). The transposon contains the *N. crassa pyr-4* gene as a nutritional selection marker. Sequencing verified the transposon insertion site in the first intron of the *arfB* gene (after 139 bp from start of the gene). The intact *arfB* gene was replaced by transformation in the *nkuA70* deletion strain (TN02A7) (Figure 3.3B). A single insertion was verified by PCR (data now shown). Southern blot analysis showed that the *arfB* disruptant (BTN1) has an 8.8 kb band that is up-shifted relative to the approximately 4.4 kb of the control strain. This indicates that the BTN1 strain contains a single copy of the *arfB::Tn* cassette (Figure 3.3C) within the *arfB* gene. We were unable to generate protoplasts from the disruption strain to complement it by transformation with the intact *arfB* gene. This is due to both its impaired growth and thickened cell walls (see below). Therefore, we confirmed that observed phenotypes were due to disruption of the *arfB* locus and not due to a second site mutation introduced by transformation by back-crossing BTN1 to the wild-type strain. In this back cross we obtained progeny with a segregation ratio of 1:1 (n=153, 74:79 = mutant: wild-type). We confirmed that four independent progeny displayed an identical phenotype to BTN1 and contained the *arfB::Tn* cassette at the *arfB* locus (data not shown). Therefore strain BTN1 and its progeny contains one homologous insertion of *arfB::Tn* and the disruption of the *arfB* gene resulted in the abnormal phenotype.

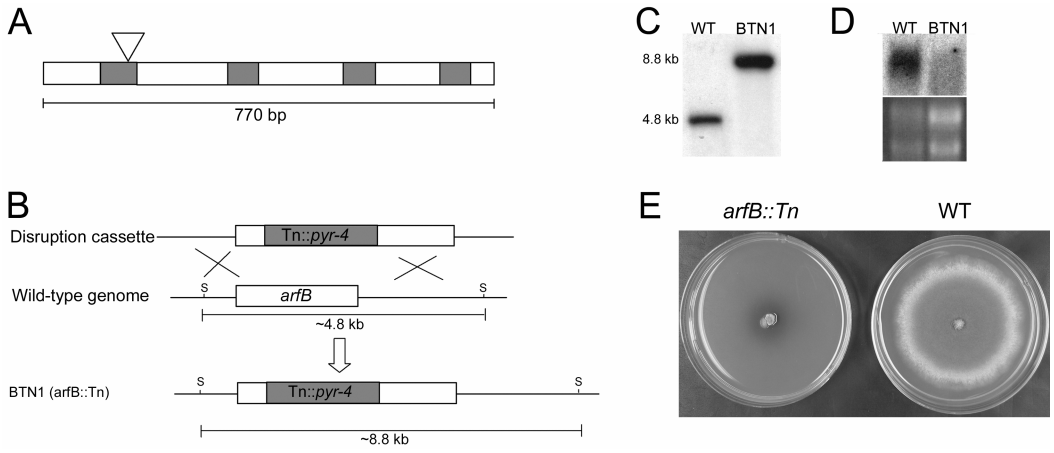

Figure 3.3 Disruption of *arfB* gene and colony phenotype. (A) Position of the transposon in the *arfB* disruption construct. Grey boxes are introns. The triangle indicates the transposon insertion site. (B) The disruption construct homologously replaced the native *arfB* locus to create the BTN1 (*arfB::Tn*) strain. S: *Sph*I recognition site. (C) Southern blot analysis of wild-type and BTN1 indicates a single copy of the *arfB::Tn* cassette replaced the native *arfB* locus in the BTN1 strain. (D) Northern blot analysis shows that the transposon insertion in the first intron disrupted expression of *arfB* gene. (E) BNT1 colonies develop markedly slower than those of wild-type.

Since the transposon is in the first intron, we examined the expression of the *arfB* gene in the control strain and the *arfB::Tn* strain. A northern blot (Figure 3.3D) shows that the control strain expressed intact mRNA of *arfB*, however the *arfB::Tn* was disrupted for mRNA expression of the *arfB* gene. These results indicate that the transposon insertion within the first intron disrupts the expression of the *arfB* gene.

Compared to the control strain, the *arfB::Tn* disrupted strain produced slow growing colonies that are aconidial (Figure 3.3E). Lack of conidiation is suppressed in the presence of an osmotic stabilizer (1.2M sorbitol) (data now shown). This characteristic allowed propagation of the *arfB::Tn* disrupted strain by conidia.

The *arfB::Tn* strain is defective in polarity establishment during spore germination and polarity maintenance during hyphal growth

The *arfB::Tn* strain displayed extended isotropic growth, multiple germ tube emergence, and dichotomous branching at hyphal apices (Figure 3.4). Under identical conditions, the wild type strain sent a primary germ tube following isotropic growth and a secondary germ-tube (Figure 3.4A). Using time lapsed image acquisition, we compared the *arfB::Tn* strain to wild type during spore germination and establishment of hyphal growth. Wild type grows isotropically and establishes a polarization site to send a germ tube (Figure 3.4B). After primary germ-tube formation, the secondary germ tube emerges approximately 180 degrees from the primary germ tube and then primary germ-tube becomes septated. The *arfB::Tn* strain shows extended isotropic growth to produce a germ tube up to approximately 20 μm in diameter (Figure 3.4B). After an extended

isotropic growth period, the *arfB::Tn* strain displays three different developmental phenotypic variations (Figure 3.4B): 1) Large isotropically swollen conidia lyse (35.3 ± 3.7 %; n=607.). 2) Large isotropically swollen conidia send a germ-tube, followed by loss of polarity of the germ-tube (17.2 ± 4.4 %). These apolar germ tubes can latter recover polarity to produce additional germ tubes. 3) Multiple germ-tubes emerge simultaneously from the swollen conidium (47.5 ± 3.7 %). Hyphae often dichotomously split at their apices. Multiple simultaneous septation events were observed in dichotomously branching hyphae (Black arrow in the Figure 3.4B). Initial hyphal growth is consistently irregular. Hyphae meandered and produce irregularly lobed cell compartments (Figure 3.4C). Interestingly, hyphae that emerge later (after 60-80 μm of initial hyphal growth) appear almost wild-type, suggesting that another gene may function to compensate for the absence of the *arfB*. The cell walls and nuclei of the reference and *arfB::Tn* strains were stained with calcofluor to visualize cell walls and Hoechst 33258 respectively to visualize nuclei (Figure 3.4D). Multiple nuclei in cell compartments of the *arfB::Tn* strain indicate no cell cycle associated phenotypes.

We next examined the spitzenkörper of wild-type strain (A4) and the *arfB::Tn* strain. The spitzenkörper is a filamentous fungal specific 'organelle' composed of a cloud of secretory vesicles, which is involved in polarized hyphal growth (Harris *et al.*, 2005). We visualized the spitzenkörper by staining with FM4-64 (Fischer-Parton *et al.*, 2000). The wild-type strain has an intact spitzenkörper at the hyphal apex (Figure 3.5A), however, the *arfB::Tn* strain displays a compromised spitzenkörper *e.g.* containing

Figure 3.4 Phenotype of the *arfB* disruptant. (A) Microscopic phenotype of wild-type and *arfB::Tn*. A site of dichotomous tip splitting is indicated by a white arrowhead. WT: Wild- type. (B) Time course images of the wild-type and BTN1 strains. The white arrows delineate septation sites, the black arrow head delineates a septum, the black arrows indicates simultaneous septation sites for *arfB::Tn*. (C) Hyphal polarized growth of the *arfB::Tn*. *: abnormal hyphal growth of the *arfB::Tn*. **: wild-type like hyphal growth of the *arfB::Tn*. (D) Combined Z-stack images from a spinning disc confocal microscope of the wild-type and *arfB::Tn* strain. Multiple nuclei in the isotropic, apolar conidium are observed in the *arfB::Tn* strain. N.A. = 1.4 with oil. Scale = 20 μm.

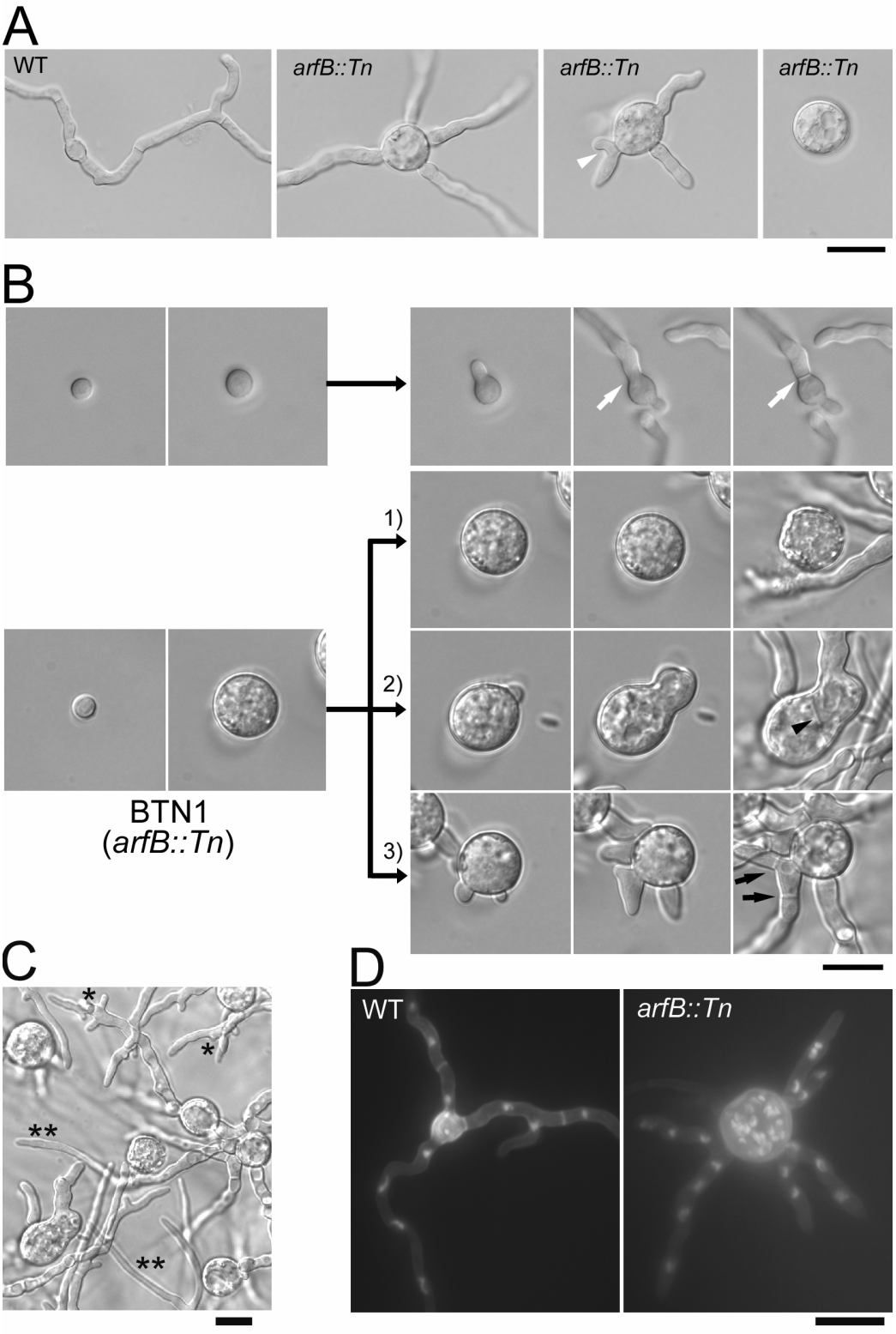
A
WT
arfB::Tn
arfB::Tn
arfB::Tn
B
1)
2)
3)
BTN1
(arfB::Tn)
C
*
*
**
**
D
WT
arfB::Tn

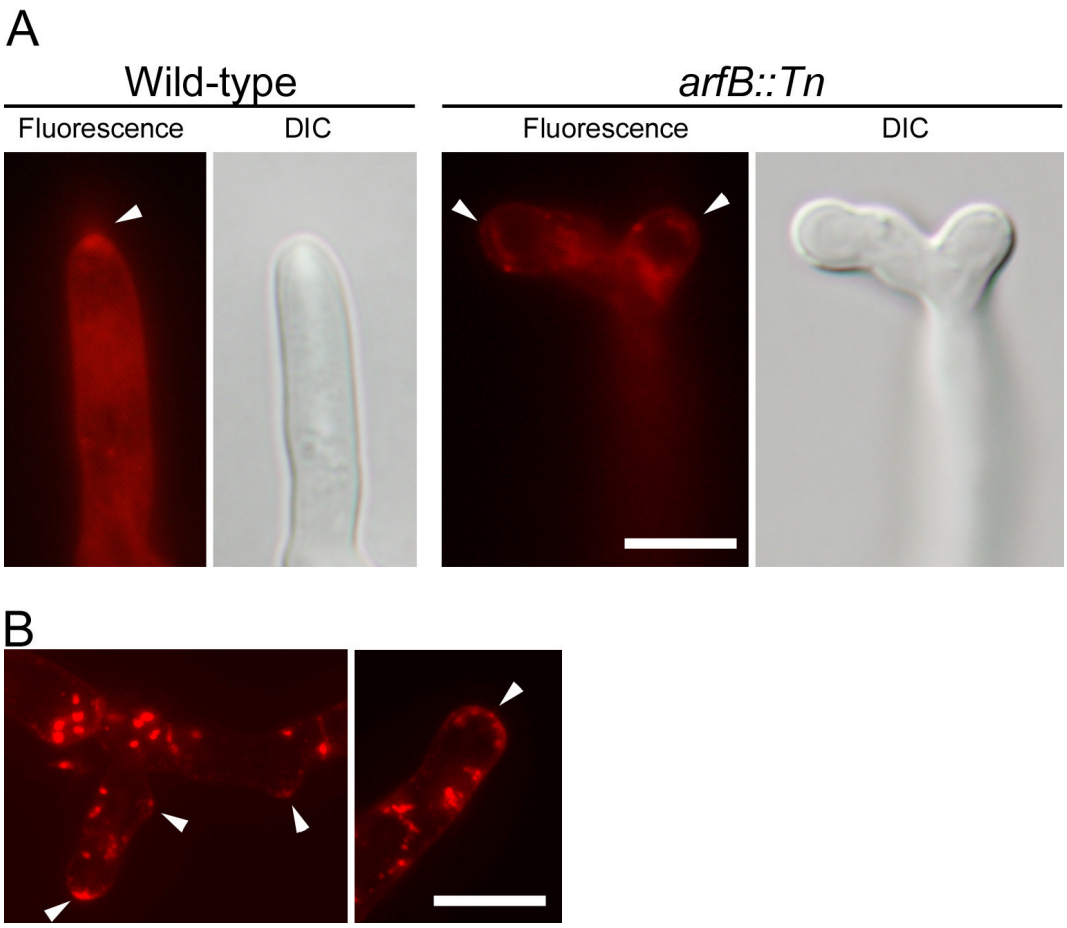

Figure 3.5 Spitzenkörper of wild-type and the *arfB::Tn* strain stained with FM4-64. (A) Wide field images of intact spitzenkörper in wild-type strains and diffuse and/ or multiple foci spitzenkörpers in hyphal apices undergoing tip splitting in the *arfB::Tn* strain. (B) Confocal microscopic images of compromised spitzenkörper in the *arfB::Tn*. The white arrow heads indicate the spitzenkörper. DIC: differential interference of contrast. N.A. = 1.4 with oil. Scale = 5 µm.

multiple foci, diffuse apical bodies or absence of a spitzenkörper at the dichotomously splitting tip (Figure 3.5B). Confocal microscopy revealed that irregular branches and hyphal tip also have a compromised spitzenkörper (Figure 3.5B). These results indicate that intact ArfB is required to assemble a wild type spitzenkörper.

ArfB protein is involved in endocytosis

To verify the function of ArfB in endocytosis in *A. nidulans*, we stained live cells of the reference and *arfB::Tn* strains with FM4-64 and tracked uptake of the dye over time. In the wild-type strain, similar to previous observations (Penalva, 2005), the dye appeared on the plasma membrane within 10 min after treatment. After 45 min, the dye was taken up by cells and localized to endomembranes (Figure 3.6A and B). In the *arfB::Tn* strain dye uptake was delayed. After 30 min treatment, the dye remained on the plasma membrane and moved to endomembrane only after 60 min or more of treatment. The fluorescent signals were, however, weak compared to that of the visualized cells in wild type. We also observed that the endomembrane structures were diffuse and irregular in the *arfB::Tn* strains (Figure 3.6B).

Actin patches are thought to be sites of endocytosis (Kaksonen *et al.*, 2003). Therefore, we also observed actin patches in the wi1d-type and *arfB::Tn* strains. Our lab has previously constructed ActA::GFP (actin) and FimA:GFP (fimbrin) strains (Upadhyay and Shaw, in preparation) in which actin and fimbrin localized to cortical patches. To obtain an *arfB::Tn* strain expressing ActA::GFP, we crossed ASUAGA4 (*actA::GFP*) to BTN1 (*arfB::Tn*). Progeny displaying the *arfB::Tn* phenotype were

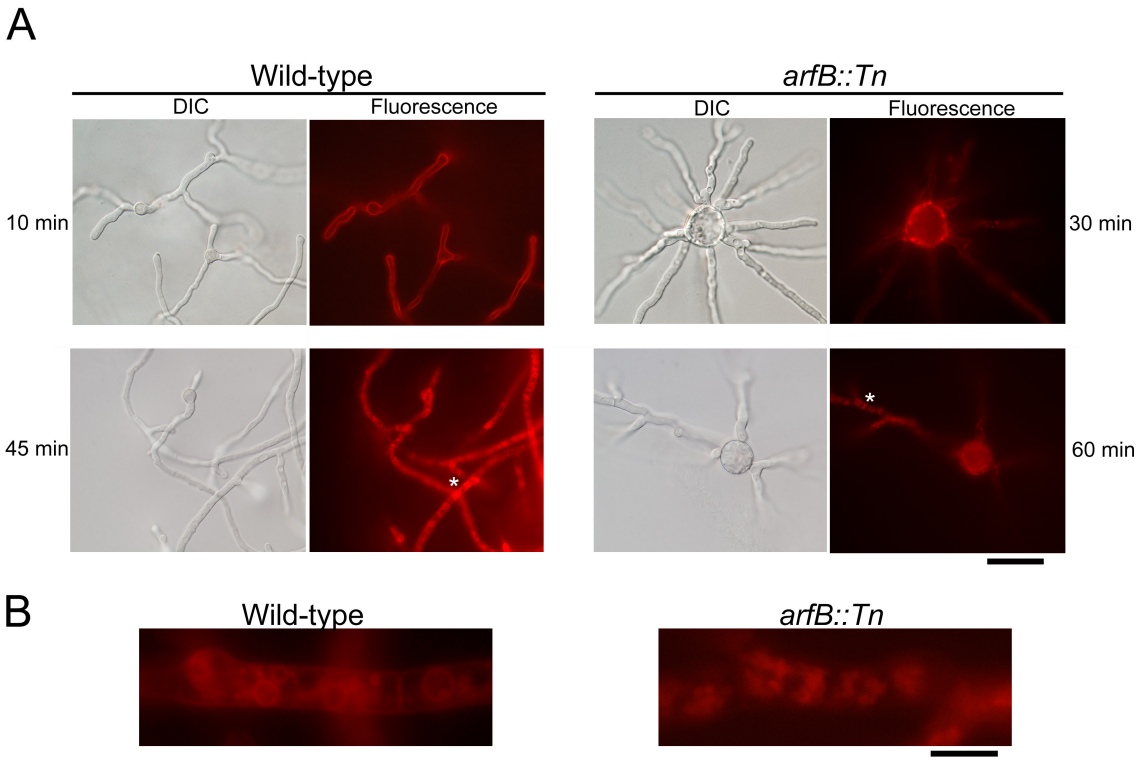

Figure 3.6 Monitoring of endocytosis with FM4-64 staining in the wild-type and *arfB::Tn* strain. (A) Movement of FM4-64 into the wild-type and *arfB::Tn* cells. Scale = 20 µm. N.A. = 1.4 with oil. (B) Hyphae of the wild-type and *arfB::Tn* in panel A after 45 min and 60 min treatment of FM4-64 respectively were enlarged. Scale = 5 µm. N.A. = 1.4 with oil.

examined for expression of ActA::GFP. In wild-type cells, actin patches are concentrated at growing hyphal apices (Figure 3.7A). In the *arfB::Tn* cells, however, the actin patches were dispersed randomly throughout apolar cell, while in polarized cells the actin patches were enriched at hyphal apices (Figure 3.7B).

ArfB::GFP localization

To observe the localization of ArfB, expression constructs driven by the alcohol inducible *alcA* promoter (Flipphi *et al.*, 2002) were assembled for ArfB::GFP and ArfB^{G2A}::GFP. These constructs were ectopically inserted in the wild-type A773 strain**.** Western blot with monoclonal GFP antibody showed a single band from total proteins of WB17 and MB13 (*arfB::sGFP* and *arfB^{G2A}::sGFP* respectively, see table 3.1) (data not shown) indicating that GFP localization reported below was not caused by free GFP. ArfB::GFP localized to the plasma membrane, to septa and endomembrane (Figure 3.7C and E). Plasmolysis of labeled cells indicated that ArfB::GFP is not on the septum but rather on the plasma membrane at the septum (Figure 3.7F). Because septa have plasma membrane on both sides of the wall, they were comparatively brighter than hyphal cell walls.

To elucidate the role of N-myristoylation in the localization of ArfB, we constructed a non-myristoylated form of ArfB by mutating the secondary glycine to alanine (G2A). ArfB^{G2A}::GFP localized to the cytoplasm (Figure 3.7C). We also expressed ArfB::GFP in the *swoF1*, N-myristoyl transferase mutant (Shaw *et al.*, 2002),

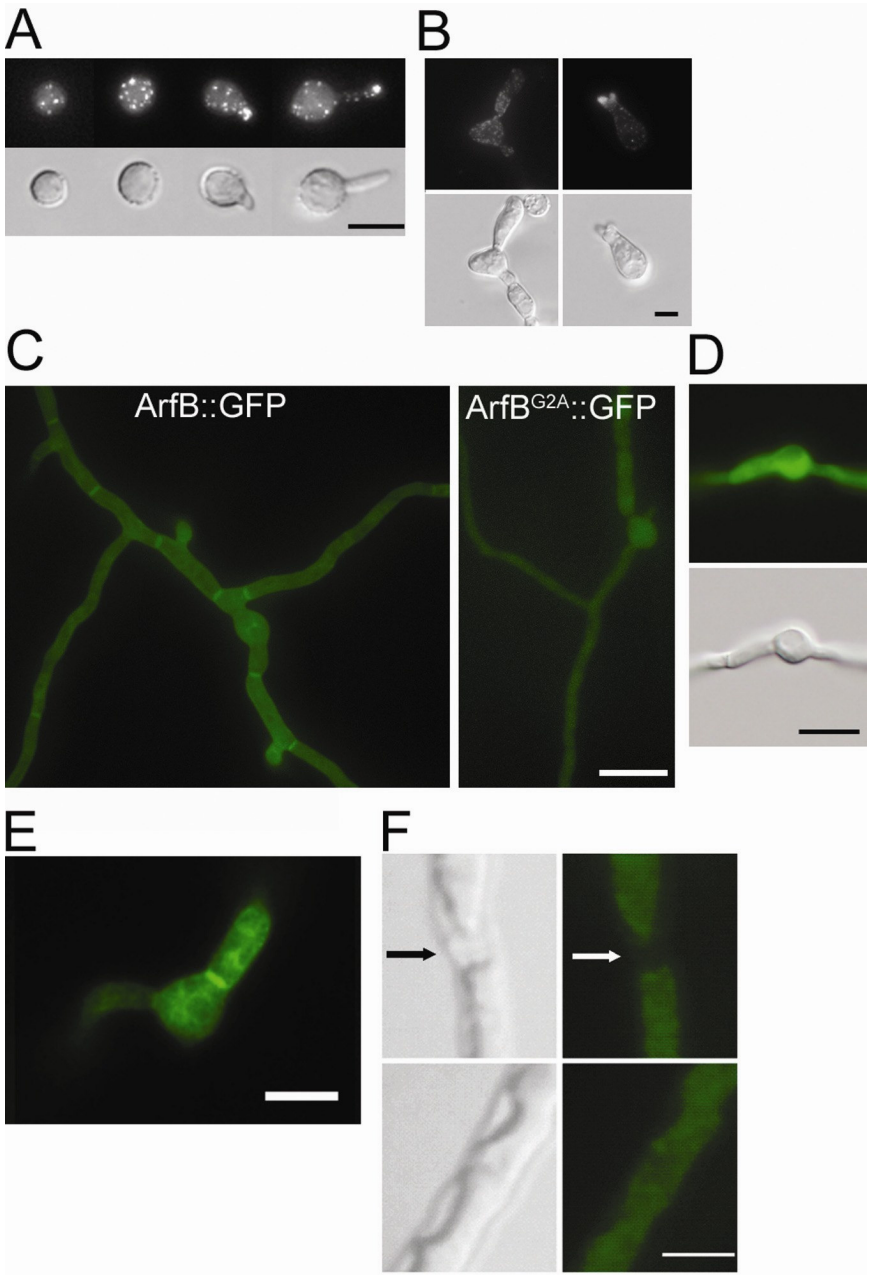

Figure 3.7 Localization of actin patches in the wild-type and *arfB::Tn* and localization of ArfB::GFP and Arf^{G2A}::GFP. (A and B) Combined Z-stack from wide field fluorescent microscope of Actin::GFP patches in the wild-type (A) and in the *arfB::Tn* strains (B) (upper) and bottom is DIC image. (C) Localization of ArfB::GFP and ArfB^{G2A}::GFP in the wild-type cells with combined Z-stack from a confocal microscopes. (D) Wild field fluorescent image of ArfB::GFP localization in the *swoF1* (N-myristoyl transferase mutant) (upper) and bottom is DIC image. (E) Wide field fluorescent image of ArfB::GFP on endomembranes. (F) DIC image (left) and wide field fluorescent image (right) of ArfB::GFP after plasmolysis. Arrows indicate a septum. Scale = 5 μm for (A), (B), (E), and (F). Scale = 10 μm for (C) and (D). N.A. = 1.4 with oil.

where its localization was cytoplasmic (Figure 3.7D). Multiple independent transformants with the *arfB::sGFP* (12 transformants) and *arfB*^{G2A}*::sGFP* (5 transformants) constructs displayed the same localization pattern (data not shown). Thus, the elimination of the myristoylation motif completely disrupts the localization of ArfB. This result demonstrates that N-myristoylation ArfB is required for proper localization of the protein.

ArfB is N-myristoylated

We over-expressed ArfB::GFP and ArfB^{G2A}::GFP from wild-type strains. After total protein extraction, the GFP tagged proteins were selectively purified by immunoprecipitation using monoclonal GFP antibody (Santa Cruz Biotechnology, Inc., Santa Cruz, CA, USA). The immunoprecipitated ArfB::GFP and ArfB^{G2A}::GFP protein were approximately 47 kDa (data not shown). These bands were differentiated from the heavy chain (50 kDa) of the GFP antibody. Bands were excised from Poly-acrylamide gel containing and subjected to trypsin digestion. We confirmed by MALDI TOF that IP purified ArfB::GFP was myristoylated, though a mixture of myristoylated and non-myristoylated forms co-exists in the cell (Lee, Dangott and Shaw, data in preparation). The ArfB^{G2A}::GFP protein lacked the myristoyl moiety, but instead existed in a non-myristoylated form, without the N-terminal methionine cleaved (data not shown).

DISCUSSION

One of the long-term goals of our lab is to better understand how N-myristoylation plays a role in polarized cell morphogenesis in *A. nidulans*. Indeed, the temperature sensitive *swoF1* mutant, containing a mutation in the N-myristoyl transferase (NMT), displayed an abnormal polarized growth at the restrictive temperature (Shaw *et al.*, 2002). When grown in submerged culture at restrictive temperature, the *swoF1* mutant first grows isotropically, then sends a germ tube similar to wild-type. Immediately after this germ tube emerges, hyphal growth ceases and the tip swells isotropically. Previously we found that NMT regulates 26S proteasome activity during early polarized morphogenesis and established the myristoylome of *A. nidulans* with 41 predicted myristoylated proteins (Lee and Shaw, 2007). The exact role of NMT in polarized growth in systems including *S. cerevisiae*, filamentous fungi, and mammalian cells remains to be elucidated.

In filamentous fungi, the spitzenkörper directs hyphal polarized growth (Girbardt, 1957). The spitzenkörper consists of a cloud of vesicles and has been considered a vesicle supply center (VSC) (Grove and Bracker, 1970; Harris *et al.*, 2005). Since ADP-ribosylation factors (Arfs) are involved in coated vesicle formation and trafficking and many Arfs are N-myristoylated (Balch *et al.*, 1992; Molendijk *et al.*, 2004; Moss and Vaughan, 1995, 1998), they could link N-myristoylation to the polarized growth in the filamentous fungi.

A comparative genome analysis of *A. nidulans* and *S. cerevisiae* revealed both organisms encode six Arf family proteins (Figure 3.1). In a previous study in yeast,

Arf3p has been shown to be involved in developing polarity during bud formation (Huang *et al.*, 2003) and in actin cytoskeleton organization (Lambert *et al.*, 2007). ArfB (AN5020.3) of *A. nidulans* shares close similarity with Arf3p (Figure 3.1A) and both proteins have a conserved N-myristoylation motif. ArfB and Arf3p are further classified to the ARF6 protein family (named for human ARF6) and many filamentous fungal ARF6 family proteins contain a conserved consensus N-myristoylation motif (Figure 3.1B). ArfB, therefore, may be one of the connections between N-myristoylation and polarized cell morphogenesis.

Disruption of the *arfB* gene resulted in defective phenotype during polarized development (Figure 3.4). The ArfB disruptant displayed extended isotropic growth upon spore germination leading to apolar cells of up to 20μm diameter. In contrast unlike wild-type conidia grow isotropically to no more than 5 μm of diameter before sending out a germ tube (Figure 3.4B). The loss of polarity did not coincide with an arrest of cell cycle (Figure 3.4D) similar to other polarity defective mutants examined in our lab (Shaw *et al.*, 2002; Shaw and Upadhyay, 2005; Upadhyay and Shaw, 2006). After the isotropic growth stage, approximately 48% of the *arfB* mutant germlings sent germ tubes (Figure 3.4A and B). Multiple germ tube emergence of the *arfB* mutant is similar to the random budding of *arf3* mutant in yeast (Huang *et al.*, 2003). Previously, it was observed that delivery of active Cdc42 to an artificial polar site triggers a spontaneous polarization without polarity determinants in *S. cerevisiae* (Wedlich-Soldner *et al.*, 2003). Arf3 function in actin organization in *S. cerevisiae* (Lambert *et al.*, 2007), so it is speculated that in the ArfB mutant, the actin cytoskeleton may not be

organized properly. Therefore random actin distribution could cause the random polarization resulting in multiple germ tube emergence sites. Our data also show that *A. nidulans* is likely to polarize spontaneously without the function of ArfB.

The *arfB* mutant also displayed abnormal hyphal morphologies in the early stages of hyphal growth (less than 100 μm length of the hyphae), in which the mutant often meandered off the long axis of polarity and branched dichotomously at hyphal apices, which may result from the loss of the ability to maintain polarity during hyphal growth (Figure 3.4C). Hyphal growth after 60 to 80 μm from conidia displayed almost wild-type like morphology suggesting that the cell may mobilize another mechanism to compensate for the loss of ArfB, perhaps by upregulating one of the other five Arfs encoded in *A. nidulans.*

It is evident that disruption of the *arfB* gene resulted in defects in endocytosis (Figure 3.6). The *arfB* mutant displayed a significant delay of FM4-64 uptake, and the efficiency of the dye uptake was lower than wild-type (Figure 3.6). In addition, actin patches, which are considered to be clathrin-mediated endocytosis sites (Kaksonen *et al.*, 2003), were disrupted in apolar *arfB* mutant cells (Figure 3.7A) suggesting ArfB is may be involved in the clathrin-mediated endocytosis in *A. nidulans*. The clathrins have been shown to be recruited by ADP-ribosylation factor (Kaksonen *et al.*, 2003). Therefore ArfB may play a role in recruiting the clathrins to the endocytosis site. One more phenotype of the *arfB* mutant includes perturbation of endo-membranes (Figure 3.6B). This phenomenon is similar to the perturbation of endo-membranes in the human ARF6 mutant (Peters *et al.*, 1995).

Polarization of exocytosis is thought to be a key mechanism in polarized hyphal growth (Bartnicki-Garcia, 2002; Virag and Harris, 2006). Our data suggest a role for endocytosis in polarized growth in filamentous fungi. Recently Steinberg has reviewed the growing evidence suggesting an important role for endocytosis in hyphal tip growth (Steinberg, 2007). Other recent data from our lab supports the hypothesis that endocytosis at hyphal tips plays a key role in growth. A fimbrin mutant displayed loss of polarity and endocytosis phenotypes very similar to the *arfB::Tn* phenotypes reported here (Upadhyay, Lee, and Shaw in preparation).

ArfB localized to endo-membranes and plasma membranes (Figure 3.7). This localization pattern was similar to that observed in human ARF6 (D'Souza-Schorey *et al.*, 1995; Peters *et al.*, 1995). In contrast, Arf3p in yeast is concentrated to the polarized budding site though it localizes to peripheral membranes (Huang *et al.*, 2003). The localization of ArfB to membranes depends on myristoylation of the proteins. We have shown that mutation of the N-myristoylation motif changes the ArfB localization pattern to be diffused throughout the cytoplasm (Figure 3.7). Similarly ArfB::GFP was diffuse in the *swoF* myristoylation mutant. Therefore, loss of myristoylation of ArfB may explain in part the polarity defect previously reported in the NMT mutant (Shaw *et al.*, 2002).

ArfB localized to the plasma membrane and to endomembranes but we did not observe it specifically concentrated to the hyphal apices. How then does the ArfB take part in the polarity establishment and maintenance? One possible explanation is that a protein which interacts with ArfB, such as its GDP/GTP exchange factor (GEF)

concentrates to growing hyphal apices, or its GTPase activation protein (GAP) concentrates at sites away from the growing apex. A similar pattern has been observed in the yeast where Bud1, a ras-like GTPase is required for bud site selection (Cabib *et al.*, 1998). The localization of Bud1p is cytosolic (Huh *et al.*, 2003). But its GAP, Bud2, localizes specifically to the bud sites (Huh *et al.*, 2003).

In this paper, we showed that ArfB plays a critical role in the polarity establishment and maintenance. At least one function of ArfB is in endocytosis, whether it does this through nucleating vesicle assembly or through participating in organization of the actin cytoskeleton remains to be fully elucidated. N-myristoylation of ArfB protein is critical for its proper localization. ArfB is only one of 41 proteins in the predicted myristoylome of *A. nidulans* (Lee and Shaw, 2007). Therefore, further investigation will continue to elucidate the role of myristoylation in regulating cell development in *A. nidulans*.

EXPERIMENTAL PROCEDURES

Strains, growth condition, plasmids, media, and reagents

A. nidulans strains and plasmids used in this study are listed in Table 3.1 and 3.2, respectively. The plasmids were maintained in *E. coli* XL1-blue (Stratagene, La Jolla, CA, USA) and manipulated as previously described (Sambrook *et al.*, 1989). *E. coli* DB3.1 was used for propagation of plasmids containing *ccdB* box. *E. coli* CC118 was used for propagation of the transposon donor plasmid containing the R6K replication

Table 3.1 Strains used in this study

Name	Description	Source
A773	*pyrG89; pyroA4; wA3; veA1*	FGSC
A4	Wild-type	FGSC
TN02A7	*pyrG89; pyroA4; nkuA::argB; riboB2*	(Nayak *et al.*, 2006)
BTN1	*pyrG89; pyroA4; nkuA::argB; riboB2; arfB::Tn::pyr-4*	This study
WB17	*pyrG89; pyroA4; arfB::sGFP::pyr-4; wA3; veA1*	This study
MB13	*pyrG89; pyroA4; arfB^{G2A}::sGFP::pyr-4; wA3; veA1*	This study
ASUAGA4	*pyrG89; pyroA4; argB1; riboB2; actA::GFP::argB*	
BAC1	*arfB::Tn::pyr-4; actA::GFP::argB*	This study

Table 3.2 Plasmids used in this study

Name	Description	Source
pGEM-T easy vector	TA cloning vector for PCR product cloning	Promega
pGEM-arfB	*arfB* in pGEM-T easy vector	This study
pENTR	entry vector for gateway cloning	Invitrogen
pArfB-entry	*arfB* in pENTR	This study
pArfB^{G2A}-entry	*arfB^{G2A}* in pENTR	This study
pGEM-pyr4	*pyr-4* in pGEM-T easy vector	This study
pMT-sGFP	Gateway destination vector with *argB* gene	(Toews *et al.*, 2004)
pSL-sGFP	Gateway destination vector with *pyr-4* gene	This study
pArfB::GFP-pyr4	pSL-sGFP with *arfB::sGFP* replacing the *ccdB* box	This study
pArfB^{G2A}::GFP-pyr4	pSL-sGFP with *arfB^{G2A}::sGFP* replacing the *ccdB* box	This study

origin. Complete and minimal media for *A. nidulans* were prepared as described (Momany *et al.*, 1999). All chemicals for media, buffer, and supplements were purchased from Sigma (St. Louis, MO, USA) unless otherwise indicated.

Disruption of *arfB* by a transposon

The *arfB* gene was PCR amplified from 500 bp upstream of the start codon and 451 bp downstream of the stop codon using the following primers: 5020F 5'- GGGGTACCCC GGCTCGTGGGCGCGCTGAGT-3' and AN5020TNR

5'- ACGGCATAACATGACGGAAT-3'. The amplicon was cloned into pGEM-T easy vector (Promega, Madison, WI, USA) to produce pGEM-*arfB*. We next used a transposon insertional mutagenesis strategy (Nayak *et al.*, 2006) to disrupt the *arfB* gene. This transposon contains the *Neurospora crassa pyr-4* gene as a selectable marker. In-frame insertion of the transposon was verified by PCR. The exact insertion site was determined by sequencing with primers N and S from the GPS-1 kit (New England Biolabs Inc., Ipswich, MA, USA). pArfBTn2 carrying the transposon in the first intron of the *arfB* (after 139 bp from start of the gene) in the vector pGEM-*arfB* was linearized with *Sph*I (New England Biolabs Inc., Ipswich, MA, USA) which cuts the plasmid outside of the *arfB* gene. The linearized plasmid was transformed using previously described methods (Shaw *et al.*, 2002) into *A. nidulans* strain TN02A7 (Table 3.1). This strain is disrupted at *nkuA* to enhance homologous recombination (Nayak *et al.*, 2006). We named the disrupted strain BTN1 (Table 3.1). GFP tagging of ArfB and ArfB^{G2A}. The intact *arfB* gene was amplified from wild-type strain A4 genomic DNA with the

following primers: GarfBF 5'-CACCATGGGCGGCTCAGTGTCGAA-3' and GarfBR 5'-TTTTTGGGGTTGTTGGACCT-3'. To generate non-myristoylated ArfB protein, a site-directed mutation was introduced by using a primer: mGarfBF 5'-CACCATGGCCGGCTCAGTGTCGAAGAT-3' instead of GarfBF, which changed the secondary glycine into alanine (G2A). The secondary glycine is critical for myristoylation (Maurer-Stroh *et al.*, 2002). The *arfB* and *arfB*^{G2A} amplicons were cloned into the gateway entry vector, pENTR (Invitrogen, Carlsbad, CA, USA) to produce pArfB-entry and pArfB^{G2A}-entry respectively.

To construct a GFP expression vector with the *pyr-4* marker gene, pMT-sGFP (Toews *et al.*, 2004) was partially digested with *Not*I (New England Biolabs Inc., Ipswich, MA, USA) and the vector fragment without the 1.8kb fragment containing the *argB* gene was ligated with a 1.6kb fragment containing the *pyr-4* gene from pGEM-pyr4 to produce pSL-sGFP (Table 3.2).

The *ccdB* box in pSL-sGFP was exchanged with *arfB* or *arfB*^{G2A} in the entry vectors above through a LRR clonase reaction following the manufacturers instructions (Invitrogen, Carlsbad, CA, USA) to generate pArfB::sGFP-pyr4 or pArfB^{G2A}::sGFP-pyr4 respectively. Each vector was transformed into A773 (Table 3.1) or TN02A7. pArfB::sGFP-pyr4 was also transformed into AXL18, an N-myristoyl transferase mutant (Shaw *et al.*, 2002), to observe the localization pattern of ArfB::GFP in the absence of N-myristoylation.

Southern, northern, and western blotting

The intact *arfB* gene amplified with primers GarfBF and GarfBR was used as probe for Southern and northern blotting. The probe was labeled by using the Prime-It II, a Random primer labeling kit (Stratagene, La Jolla, CA, USA) by using [γ-^{32}P]CTP. For Southern blotting, the reference strain (TN02A7) and BTN1 (table 1) genomic DNA was digested with *Sph*I and separated on 1% Agarose gel. For northern blotting, total RNA from the reference strain and BTN1 was extracted by using TRIzol reagent (Invitrogen, Carlsbad, CA, USA) as indicated by instruction for the manufacturers. The RNA was separated on 1% Agarose gel containing 2.2 M of formaldehyde. Standard procedures for Southern and northern blotting were followed (Sambrook *et al.*, 1989).

Monoclonal GFP antibody (Santa Cruz Biotechnology, Inc., Santa Cruz, CA, USA) was used for western blotting for GFP tagged proteins. Total proteins were extracted from WB17 and MB13 (*arfB*::GFP and *arfB*^{G2A}::GFP respectively, table 3.1) and separated on a precast 12% sodium dodecyl sulfate- polyacrylamide gel electrophoresis (SDS-PAGE) gel (BioRad, Hercules, CA. USA). Protein extraction and western blotting were performed as previously described (Lee and Shaw, 2007).

Matrix-assisted laser desorption/ionization-time of flight mass spectrometry (MALDI-TOF MS)

Proteins for MALDI-TOF MS analysis were prepared by immunoprecipitation (IP). From a total protein preparation prepared as previously described (Lee and Shaw, 2007)**,** ArfB::GFP and ArfB^{G2A}::GFP proteins were selectively bound to the monoclonal

GFP antibody (see above) and the antibody-protein complexes were precipitated with protein A in ImmunoPure Immobilized Protein A system (Pierce Biotechnology, Inc., Rochford, IL, USA) following the company's instructions. Bands corresponding to ArfB::GFP and ArfB^{G2A}::GFP proteins were excised and subjected to Trypsin digestion. Peptides were then assayed by MALDI-TOF. Observed mass/charge peaks were compared to the predicted *in silico* digestion products for each protein.

Microscopy

GFP protein and FM4-64 stained live cells were visualized in germlings grown in a custom made aluminum chambers designed for live cell imaging of fungal cells (Kuo and Hoch, 1996). For time-lapsed imaging an Olympus Microscope BX51 (Olympus America Inc., Melville, NY, USA) outfitted with a Prior shutter (www.prior.com) to limit phototoxicity to the cells. Simple PCI software (Version 5.3.1.081004) (Compix Inc., Imaging Systems, Cranberry Township, PA) was used to acquire images of growth at 30 second intervals. To observe the endocytosis process in cells, wild-type and BTN1 were grown on a coverslip submerged in liquid complete medium. After 24 hr incubation, fresh medium containing 12.5 μM of FM4-64 was replaced with the growing media lacking the dye. The coverslip with cells was overlaid on the aluminum chamber. A narrow band G-excitation filter with 530-550 nm of excitation and 590 nm of emission (Olympus America Inc., Melville, NY, USA) was used to obtain FM4-64 fluorescent images. Microscopic observation for GFP and all image processing were

conducted as previously described (Shaw and Upadhyay, 2005; Upadhyay and Shaw, 2006).

CHAPTER IV

CONCLUSION

Filamentous fungi have a unique polarized growth form, hypha, which is not shared with yeast and mammalian systems. This characteristic suggests great promise in the drive to develop pharmaceuticals which target fungal hyphal growth for a number of important pathogens. The genetics of polarized growth is well-studied in *Saccharomyces cerevisiae,* however the information from yeast has not fully explained the growth mode for filamentous fungi, for example the small GTPase protein Cdc42 is critical in bud site selection in yeast, yet it is now known to be non-essential for hyphal growth in filamentous fungi (see Chapter I). Therefore, my work to further elucidate mechanisms regulating hyphal growth is critical.

In a forward genetic screen for polarity determinants, N-myristoyl transferase (NMT) was found to be critical for the hyphal polarity. The NMT mediates protein N-myristoylation, in which 14 carbon myristate is covalently attached to the secondary glycine residue of target proteins. N-myristoylated proteins have an increased hydrophobicity so that they are able to be associated with membranes or take part in hydrophobic protein-protein interactions. The conditional NMT mutant (*swoF1*) of *Aspergillus nidulans* displayed abnormal swelling, resulting from a loss of polarity during germination. This observation drove my hypothesis: A **downstream target or targets of NMT are essential for polarized growth.** My research tested this hypothesis

using forward genetics in a suppressor screen and reverse genetics in a candidate gene approach.

N-MYRISTOYLATION LINKS PROTEASOME ACTIVITY TO POLARIZED GROWTH

Findings in this study

For the forward genetic approach, six suppressors of *swoF1* were generated. These second site mutations were introduced to the *swoF1* mutant by UV mutagenesis. The suppression phenotypes included restoration of polarity, mycelial colony formation, and rescue from conditional lethality. All six suppressor mutants were also found to be temperature sensitive for colony formation. Three of the suppressor mutants were complemented by two different proteasome subunits [SsfA (AN1757.3), AN8054.3]. I found a DNA sequence change in the *ssfA* gene only for one suppressor mutant. The mutation is predicted to cause a 71 amino acid truncation at the C-terminus. Further analyses found that the *swoF1* mutant accumulated a lower concentration of ubiquitinated proteins compared to wild-type. In contrast, the suppressor double mutants and single mutants accumulated more ubiquitinated proteins. Treatment with MG132, a proteasome inhibitor, rescued the polarity defect of the *swoF1* mutant. Therefore, it was confirmed that the *swoF1* mutant has an elevated proteasome activity resulting in loss of polarity and a mutation in a proteasome subunit decreases the proteolytic activity so that the polarity defect is partially corrected.

Future directions to verify the direct regulation of N-myristoylation in proteasome activity

This suppressor mutant analysis demonstrates a novel connection between N-myristoylation and the activity of 26S proteasome; NMT negatively regulates the activity of the proteasome (Figure 4.1). How does myristoylation affect the activity of the 26S proteasome? **I hypothesize that the connection may be mediated by N-myristoylation of a 19S proteasome subunit (AN2213.3).** A consensus myristoylation motif of the AN2213.3 protein and confirmed myristoylation of orthologs from other eukaryotic systems strengthen this possibility. The 26S proteasome is formed by the interaction between the 20S and 19S proteasome particles, therefore assembly of the two particles is critical for function of the 26S proteasome. The interior of the 20S particle is hydrophobic and therefore the N-myristoylation motif of the 19S subunit may be involved in hydrophobic interactions between the two particles. This hypothesis remains to be tested. Future work in this area could include protein interaction studies, through TAP tagging or yeast two hybrid analysis in backgrounds that are myristoylation positive and negative. Assembly of intact 26S proteasome could also be assessed by transmission electron microscopy.

Impact of studying the proteasome

Proteasome mediated protein degradation is an important biological process. This is demonstrated by the many human diseases known to involve malfunctioning proteasome including: several cancers (Hoeller *et al.*, 2006); neurodegenerative diseases

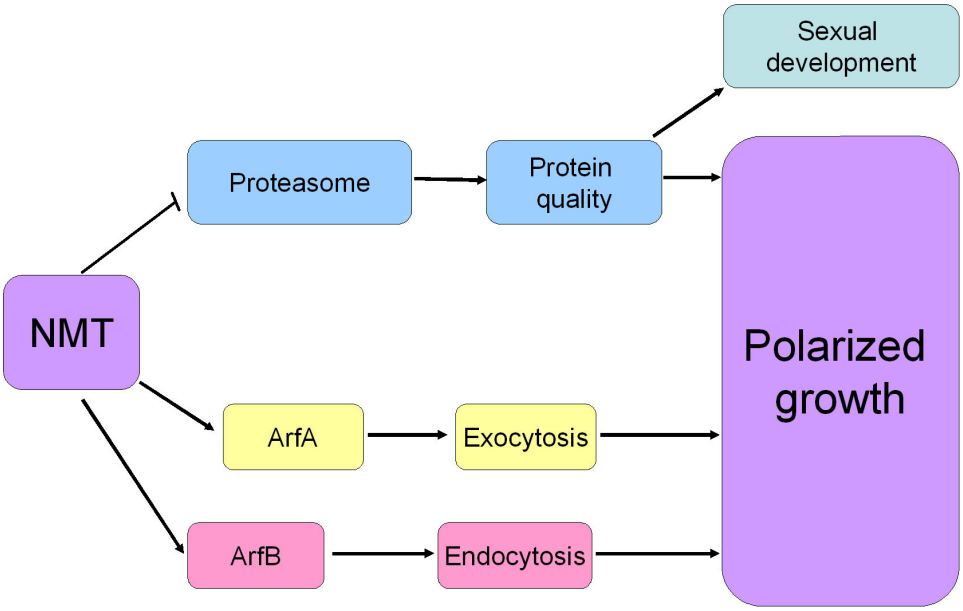

Figure 4.1 The role of N-myristoyl transferase (NMT) in polarized growth. NMT negatively regulates the activity of 26S proteasome which takes part in polarized growth and sexual development by controlling the half life of proteins. NMT also controls localization of ArfA and ArfB. ArfA is likely involved in polarized growth by participating exocytosis. ArfB mediates cell polarity through endocytosis.

such as Parkinson's disease and Huntington disease; cystic fibrosis, Angelman's syndrome; and Liddle syndrome (Schwartz and Ciechanover, 1999). The host proteasome may also be hijacked by in a variety of infectious disease processes by pathogenic bacteria and viruses (Butler *et al.*, 2006; Darwin *et al.*, 2003; Levitskaya *et al.*, 1997; Wiertz *et al.*, 1996). Therefore, further work to verify the exact role of N-myristoylation of the 19S subunit is needed to enhance our understanding of proteasome function in disease.

Further study of proteasome activity in polarized growth

In this study, I have shown that proteasome is associated with polarized growth of fungi (Figure 4.1). It is possible that the connection between the proteasome and polarized growth lies in the uncontrolled degradation of polarity proteins in the NMT mutant. Indeed, phenotypes associated with the NMT mutant are pleiotropic, and it is likely that a variety of cellular processes are affected by the malfunctioning proteasome. Regardless of this pleiotropy, I have shown that the polarity phenotype of the NMT mutant is bypassed in proteasome mutants, suggesting that a direct link may exist.

In filamentous fungi, the science of cataloging polarity proteins remains in its infancy. One possible future direction could include a comparison of protein populations form NMT mutant versus wild-type using 2D proteomics approaches. This could be helpful to find proteins required for the polarized growth of filamentous fungi.

Proteasome activity in sexual development

An additional phenotype of the proteasome mutants is abnormal sexual development. Previous work with the COP9 signalosome, showed that COP9 mutants also displayed the sexual sterility (Busch *et al.*, 2003). The COP9 signalosome can replace the 19S proteasome particle in interactions with the 20S proteasome particle forming yet another type of proteasome (Huang *et al.*, 2005; Serino and Deng, 2003). Interestingly, no COP9 subunits are predicted to be myristoylated. Therefore, it may be that the COP9/20S proteasome is fulfilling at least some of the functions of the proteasome in the NMT mutant.

ARFB LINKS ENDOCYTOSIS TO POLARIZED GROWTH

Findings in this study

Proteins with a predicted N-myristoylation motif were examined in the candidate gene approach. I established the predicted myristoylome for *A. nidulans* which includes 40 proteins with an N-terminal myristoylation motif and 1 protein with an internal N-myristoylation motif. This represents less than 0.4% of total proteins predicted to be encoded by *A. nidulans*. Among these proteins ArfB (AN5020.3) was selected due to its predicted role in vesicle assembly and actin cytoskeleton function. I disrupted the *arfB* gene by a transposon insertional strategy. Disruption and expression of the *arfB* gene were verified by Southern blot and northern blot analysis respectively. The *arfB* disruptant displayed significantly extended isotropic growth with large cells (up to 20 µm diameter) compared to that of wild-type (up to 5µm). This abnormal isotropic

growth is caused by a defect in polarity establishment. After isotropic growth, the *arfB* disruptant undergoes: 1) lysis, 2) germ tube swelling, or 3) random, multiple germ tube formation. There may be no polarity center for cells of lysis or premature polarity centers for cells of germ tube swelling and multiple germ tube emergences. During hyphal growth, the *arfB* disrupted strain forms multiple branches, undergoes dichotomous branching at its apex, and undergoes multiple septation events. The spitzenkörper, as visualized by FM4-64 staining, of the *arfB* disrupted strain is multiple-centered or diffused. FM4-64 staining also revealed that the *arfB* disrupted strain displays delayed endocytosis compared to wild-type. Moreover the endomembranes of the *arfB* mutant were perturbed, which is similar to observations made with human ARF6 (an ortholog of ArfB) mutant. ArfB localization was determined by observing GFP tagged protein. ArfB::GFP in wild-type cells localizes to cell and endomembranes, however, ArfB::GFP in the *swoF1* mutant cells diffuses to the cytosol. The non-myristoylated form of ArfB::GFP ($ArfB^{G2A}$::GFP) also mislocalizes in wild-type cells. Myristoylation of ArfB::GFP and lack of myristoylation in $ArfB^{G2A}$::GFP were verified by MALDI/TOF.

I also characterized ArfA during my studies (see appendix B). Overexpression of ArfA partially suppressed the temperature sensitive phenotype of the *swoF1* mutant. It is evident that ArfA is involved in the polarity of the fungus (Figure 4.1). ArfA::GFP localized to cellular compartments that are likely to be part of the exocytosis machinery. Like ArfB, the localization of ArfA is dependant on the N-terminal myristoylation of the protein.

Role of endocytosis in polarized growth

I am particularly interested in the role of endocytosis in regulating hyphal growth during polarity establishment and maintenance. Endocytosis functions to recycle plasma membrane and cell-surface components (Kaksonen *et al.*, 2003; Walther *et al.*, 2006). Although there is sporadic evidence for a role for endocytosis in polarized growth in *S. cerevisiae* (Marco *et al.*, 2007; Valdez-Taubas and Pelham, 2003), a connection to hyphal polarity in filamentous fungi has been largely ignored (for example (Harris, 2006)). The vesicle supply center (VSC) model has been widely accepted as an explanation for hyphal tip growth in filamentous fungi (Bartnicki-Garcia, 2002). This model predicts that exocytosis through a VSC (likely to be the spitzenkörper) can explain differences in growth rates and morphology of hyphal tips in various fungi. An infinite supply of new growth materials (e.g. cell wall assembly components, and membrane components) is required for the VSC to predict growth accurately. My results with ArfB (Chapter III) as well as unpublished work from my lab colleagues dealing with the actin binding protein fimbrin (Upadhyay, Lee and Shaw) suggest an important role for endocytosis in regulating cell shape. Additional work is needed to tie together the VSC model and a requirement for tip localized endocytosis. It is likely that the role for endocytosis at the tip is in recycling machinery required for active growth.

Future directions to study how endocytosis is involved in polarized growth of filamentous fungi

The question remains however; how does endocytosis control cell polarity in filamentous fungi? One possibility is that endocytosis may regulate the maintenance of polarity landmark proteins to the hyphal tip. In this model, polarity landmark proteins are delivered to the polarization site through exocytosis. As the cells grow and new membrane is added to the growth site, the markers mature backward away from the polarization site. Endocytotic machinery is located just subapical of the polarization site. Here the markers are taken up by endocytosis to be recycled or degraded. Therefore the role of endocytosis is to maintain a subpopulation of polarity markers at the growing hyphal tip. If the markers are not recycled through endocytosis, for example in the *arfB* mutant, the cell will grow isotropically and its hyphae will exhibit uncontrolled swelling, as observed in the *arfB* mutant.

This role for endocytosis in polarized growth in filamentous fungi is yet to be confirmed. Future work in the area could include: 1) Investigation of the role of other orthologous endocytosis proteins from other eukaryotic systems in filamentous fungi; 2) identification of proteins that are taken up through endocytosis or components. In this approach I hypothesize that tip localized proteins would be enriched for the polarity marker and for proteins that take part in endocytotic recycling. Therefore I would construct a GFP tagged expression library to screen for proteins which localize to the hyphal tip. Then characterization of their GFP localization characteristics during growth would give a clue as to if they are taking part in endocytosis, exocytosis and or other

growth processes. Co-localization studies of these hyphal tip proteins with endocytosis markers such as FM4-64 or Lucifer yellow could be used to find possible endocytosed proteins. Alternatively endocytotic vesicle proteins such as actin or fimbrin or Arp2/3 protein complex could be applied for co-localization study to find possible endocytosed proteins. Additionally systematic disruption of the genes encoding these tip localized proteins would also give insight into their function.

Study of other myristoylated proteins in polarized growth

Other future work could involve the characterization of other proteins predicted to be myristoylated in *A. nidulans*. Systemic disruption of all of the genes and verification of the myristoylation status of each would enhance the understanding of the role of N-myristoylation in polarized growth of *A. nidulans*. In addition, double or multiple knock-out strain constructions would be useful in constructing a genetic interaction network between them. This is an exciting area of research in which much work remains to be initiated.

REFERENCES

Adams, A.E., Johnson, D.I., Longnecker, R.M., Sloat, B.F., and Pringle, J.R. (1990) CDC42 and CDC43, two additional genes involved in budding and the establishment of cell polarity in the yeast *Saccharomyces cerevisiae*. *J Cell Biol* **111**: 131-142.

Altschul, S.F., Madden, T.L., Schaffer, A.A., Zhang, J., Zhang, Z., Miller, W., and Lipman, D.J. (1997) Gapped BLAST and PSI-BLAST: a new generation of protein database search programs. *Nucleic Acids Res* **25**: 3389-3402.

Balch, W.E., Kahn, R.A., and Schwaninger, R. (1992) ADP-ribosylation factor is required for vesicular trafficking between the endoplasmic reticulum and the *cis*-Golgi compartment. *J Biol Chem* **267**: 13053-13061.

Bartnicki-Garcia, S., and Lippman, E. (1969) Fungal morphogenesis: cell wall construction in *Mucor rouxii*. *Science* **165**: 302-304.

Bartnicki-Garcia, S. (2002) Hyphal tip growth: Outstanding questions. In *Molecular Biology of Fungal Development*. Osiewacz, H.D. (ed). New York: Marcel Dekker, pp. 29-58.

Bartnicki-Garcia, S. (2006) Chitosomes: past, present and future. *FEMS Yeast Res* **6**: 957-965.

Bhatnagar, R., and Gordon, J. (1997) Understanding covalent modifications of proteins by lipids: where cell biology and biophysics mingle. *Trends Cell Biol* **7**: 14-20.

Bolen, J.B., Veillette, A., Schwartz, A.M., DeSeau, V., and Rosen, N. (1987) Activation of pp60c-src protein kinase activity in human colon carcinoma. *Proc Natl Acad Sci USA* **84**: 2251-2255.

Bourett, T.M., and Howard, R.J. (1991) Ultrastructural immunolocalization of actin in a fungus. *Protoplasma* **163**: 199-202.

Boyce, K.J., Hynes, M.J., and Andrianopoulos, A. (2001) The CDC42 homolog of the dimorphic fungus *Penicillium marneffei* is required for correct cell polarization during growth but not development. *J Bacteriol* **183**: 3447-3457.

Bracker, C.E., Ruiz-Herrera, J., and Bartnicki-Garcia, S. (1976) Structure and transformation of chitin synthetase particles (chitosomes) during microfibril synthesis *in vitro*. *Proc Natl Acad Sci USA* **73**: 4570-4574.

Bradford, M.M. (1976) A rapid and sensitive method for the quantitation of microgram quantities of protein utilizing the principle of prorein-dye binding. *Anal Biochem* **72**: 248-254.

Bradke, F., and Dotti, C.G. (1997) Neuronal polarity: vectorial cytoplasmic flow frecedes axon formation. *Neuron* **19**: 1175-1186.

Bruno, K.S., Aramayo, R., Minke, P.F., Metzenberg, R.L., and Plamann, M. (1996) Loss of growth polarity and mislocalization of septa in a *Neurospora* mutant altered in the regulatory subunit of cAMP-dependent protein kinase. *EMBO J* **15**: 5772-5782.

Bryant, M., and Ratner, L. (1990) Myristoylation-dependent replication and assembly of *Human Immunodeficiency Virus* 1. *Proc Natl Acad Sci USA* **87**: 523-527.

Busch, S., Eckert, S.E., Krappmann, S., and Braus, G.H. (2003) The COP9 signalosome is an essential regulator of development in the filamentous fungus *Aspergillus nidulans*. *Mol Microbiol* **49**: 717-730.

Butler, S.M., Festa, R.A., Pearce, M.J., and Darwin, K.H. (2006) Self-compartmentalized bacterial proteases and pathogenesis. *Mol Microbiol* **60**: 553-562.

Cabib, E., Drgonova, J., and Drgon, T. (1998) Role of small G proteins in yeast cell polarization and wall biosynthesis. *Annu Rev Biochem* **67**: 307-333.

Casey, P. (1995) Protein lipidation in cell signaling. *Science* **268**: 221-225.

Castiglioni Pasgon, R., Pizzirani-Kleiner, A.A., and Miller, B.L. (2001) The *Aspergillus nidulans bncA1* mutation causes defects in the cell division cycle, nuclear movement and developmental morphogenesis. *Mol Genet Genomics* **264**: 546-554.

Chenevert, J., Valtz, N., and Herskowitz, I. (1994) Identification of genes required for normal pheromone-induced cell polarization in *Saccharomyces cerevisiae*. *Genetics* **136**: 1287-1297.

Chow, M., Newman, J.F.E., Filman, D., Hogle, J.M., Rowlands, D.J., and Brown, F. (1987) Myristoylation of picornavirus capsid protein VP4 and its structural significance. *Nature* **327**: 482-486.

Chuang, J.S., and Schekman, R.W. (1996) Differential trafficking and timed localization of two chitin synthase proteins, Chs2p and Chs3p *J Cell Biol* **135**: 597-610.

Clutterbuck, J., and Arst, H. (1995) *TIG* Genetic nomenclature guide: *Aspergillus nidulans Trends Genet* **11 Supplement**: 13-14.

Costa, R., and Ayscough, K.R. (2005) Interactions between Sla1p, Lsb5p and Arf3p in yeast endocytosis. *Biochem Soc Trans* **33**: 1273-1275.

Costa, R., Warren, D.T., and Ayscough, K.R. (2005) Lsb5p interacts with actin regulators Sla1p and Las17p, ubiquitin and Arf3p to couple actin dynamics to membrane trafficking processes. *Biochem J* **387**: 649-658.

Crampin, H., Finley, K., Gerami-Nejad, M., Court, H., Gale, C., Berman, J., and Sudbery, P. (2005) *Candida albicans* hyphae have a spitzenkorper that is distinct from the polarisome found in yeast and pseudohyphae. *J Cell Sci* **118**: 2935-2947.

D'Souza-Schorey, C., Li, G., Colombo, M.I., and Stahl, P.D. (1995) A regulatory role for ARF6 in receptor-mediated endocytosis. *Science* **267**: 1175-1178.

D'Souza-Schorey, C., and Chavrier, P. (2006) ARF proteins: roles in membrane traffic and beyond. *Nat Rev Mol Cell Biol* **7**: 347-358.

Darwin, K.H., Ehrt, S., Gutierrez-Ramos, J.-C., Weich, N., and Nathan, C.F. (2003) The proteasome of *Mycobacterium tuberculosis* is required for resistance to nitric oxide. *Science* **302**: 1963-1966.

Driscoll, J., and Goldberg, A.L. (1990) The proteasome (multicatalytic protease) is a component of the 1500-kDa proteolytic complex which degrades ubiquitin-conjugated proteins. *J Biol Chem* **265**: 4789-4792.

Duronio, R.J., Towler, D.A., Heuckeroth, R.O., and Gordon, J.I. (1989) Disruption of the yeast N-myristoyl transferase gene causes recessive lethality. *Science* **243**: 796-800.

Eisenhaber, F., Eisenhaber, B., Kubina, W., Maurer-Stroh, S., Neuberger, G., Schneider, G., and Wildpaner, M. (2003) Prediction of lipid posttranslational modifications and localization signals from protein sequences: big-Pi, NMT and PTS1. *Nucleic Acids Res* **31**: 3631-3634.

Felsted, R., Glover, C., and Hartman, K. (1995) Protein N-myristoylation as a chemotherapeutic target for cancer. *J Natl Cancer Inst* **87**: 1571-1573.

Finley, D., Tanaka, K., Mann, C., Feldmann, H., Hochstrasser, M., Vierstra, R., Johnston, S., Hampton, R., Haber, J., and McCusker, J. (1998) Unified nomenclature for subunits of the *Saccharomyces cerevisiae* proteasome regulatory particle. *Trends Biochem Sci* **23**: 244-245.

Fischer-Parton, S., Parton, R.M., Hickey, P.C., Dijksterhuis, J., Atkinson, H.A., and Read, N.D. (2000) Confocal microscopy of FM4-64 as a tool for analysing endocytosis and vesicle trafficking in living fungal hyphae. *J Microsc* **198**: 246-259.

Flipphi, M., Kocialkowska, J., and Felenbok, B. (2002) Characteristics of physiological inducers of the ethanol utilization (*alc*) pathway in *Aspergillus nidulans*. *Biochem J* **364**: 25-31.

Fujita, A., Oka, C., Arikawa, Y., Katagai, T., Tonouchi, A., Kuhara, S., and Misumi, Y. (1994) A yeast gene necessary for bud-site selection encodes a protein similar to insulin-degrading enzymes. *Nature* **372**: 567-570.

Fujiwara, T., Tanaka, K., Mino, A., Kikyo, M., Takahashi, K., Shimizu, K., and Takai, Y. (1998) Rho1p-Bni1p-Spa2p interactions: implication in localization of Bni1p at the bud site and regulation of the actin cytoskeleton in *Saccharomyces cerevisiae*. *Mol Biol Cell* **9**: 1221-1233.

Gems, D., Johnstone, I.L., and Clutterbuck, A.J. (1991) An autonomously replicating plasmid transforms *Aspergillus nidulans* at high frequency. *Gene* **98**: 61-67.

Giaever, G., Chu, A.M., Ni, L., Connelly, C., Riles, L., Veronneau, S., Dow, S., Lucau-Danila, A., Anderson, K., Andre, B., Arkin, A.P., Astromoff, A., El Bakkoury, M., Bangham, R., Benito, R., Brachat, S., Campanaro, S., Curtiss, M., Davis, K., Deutschbauer, A., Entian, K.-D., Flaherty, P., Foury, F., Garfinkel, D.J., Gerstein, M., Gotte, D., Guldener, U., Hegemann, J.H., Hempel, S., Herman, Z., Jaramillo, D.F., Kelly, D.E., Kelly, S.L., Kotter, P., LaBonte, D., Lamb, D.C., Lan, N., Liang, H., Liao, H., Liu, L., Luo, C., Lussier, M., Mao, R., Menard, P., Ooi, S.L., Revuelta, J.L., Roberts, C.J., Rose, M., Ross-Macdonald, P., Scherens, B., Schimmack, G., Shafer, B., Shoemaker, D.D., Sookhai-Mahadeo, S., Storms, R.K., Strathern, J.N., Valle, G., Voet, M., Volckaert, G., Wang, C.-y., Ward, T.R., Wilhelmy, J., Winzeler, E.A., Yang, Y., Yen, G., Youngman, E., Yu, K., Bussey, H., Boeke, J.D., Snyder, M., Philippsen, P., Davis, R.W., and Johnston, M.

(2002) Functional profiling of the *Saccharomyces cerevisiae* genome. *Nature* **418**: 387-391.

Gillingham, A.K., and Munro, S. (2007) The small G proteins of the Arf family and their regulators. *Annu Rev Cell Dev Biol* **23**.

Girbardt, M. (1957) Der spitzenkörper von *Polystictus versicolor*. *Planta* **50**: 47-59.

Glotzer, M., Murray, A.W., and Kirschner, M.W. (1991) Cyclin is degraded by the ubiquitin pathway. *Nature* **349**: 132-138.

Göttlinger, G., Sodroski, J., and Haseltine, W. (1989) Role of capsid precursor processing and myristoylation in morphogenesis and infectivity of *Human Immunodeficiency Virus* type 1. *Proc Natl Acad Sci USA* **86**: 5781-5785.

Govindan, B., Bowser, R., and Novick, P. (1995) The role of Myo2, a yeast class V myosin, in vesicular transport. *J Cell Biol* **128**: 1055-1068.

Groll, M., Bajorek, M., Kohler, A., Moroder, L., Rubin, D.M., Huber, R., Glickman, M.H., and Finley, D. (2000) A gated channel into the proteasome core particle. *Nat Struct Mol Biol* **7**: 1062-1067.

Grove, S.N., and Bracker, C.E. (1970) Protoplasmic organization of hyphal tips among fungi: vesicles and spitzenkorper. *J Bacteriol* **104**: 989-1009.

Harris, S.D., Morrell, J.L., and Hammer, J.E. (1994) Identification and characterization of *Aspergillus nidulans* mutants defective in cytokinesis. *Genetics* **136**: 517-532.

Harris, S.D., and Momany, M. (2004) Polarity in filamentous fungi: moving beyond the yeast paradigm. *Fungal Genet Biol* **41**: 391-400.

Harris, S.D., Read, N.D., Roberson, R.W., Shaw, B., Seiler, S., Plamann, M., and Momany, M. (2005) Polarisome meets spitzenkorper: Microscopy, genetics, and genomics converge. *Eukaryot Cell* **4**: 225-229.

Harris, S.D. (2006) Cell polarity in filamentous fungi: shaping the mold. *Int Rev Cytol* **251**: 41-77.

Hiller, M.M., Finger, A., Schweiger, M., and Wolf, D.H. (1996) ER degradation of a misfolded luminal protein by the cytosolic ubiquitin-proteasome pathway. *Science* **273**: 1725-1728.

Hoch, H.C., and Staples, R.C. (1983) Ultrastructural organization of non-differentiated uredospore germlings of *Uromyces phaseoli* variety typical. *Mycologia* **75**: 795-824.

Hochstrasser, M. (1996) Ubiquitin-dependent protein degradation. *Annu Rev Genet* **30**: 405-439.

Hoeller, D., Hecker, C.-M., and Dikic, I. (2006) Ubiquitin and ubiquitin-like proteins in cancer pathogenesis. *Nat Rev Cancer* **6**: 776-788.

Howard, R.J. (1981) Ultrastructural analysis of hyphal tip cell growth in fungi: Spitzenkorper, cytoskeleton and endomembranes after freeze-substitution. *J Cell Sci* **48**: 89-103.

Huang, C.-F., Liu, Y.-W., Tung, L., Lin, C.-H., and Lee, F.-J.S. (2003) Role for Arf3p in development of polarity, but not endocytosis, in *Saccharomyces cerevisiae*. *Mol Biol Cell* **14**: 3834-3847.

Huang, X., Hetfeld, B.K.J., Seifert, U., Kahne, T., Kloetzel, P.-M., Naumann, M., Bech-Otschir, D., and Dubiel, W. (2005) Consequences of COP9 signalosome and 26S proteasome interaction. *FEBS J* **272**: 3909-3917.

Huh, W.-K., Falvo, J.V., Gerke, L.C., Carroll, A.S., Howson, R.W., Weissman, J.S., and O'Shea, E.K. (2003) Global analysis of protein localization in budding yeast. *Nature* **425**: 686-691.

Jaquenoud, M., and Peter, M. (2000) Gic2p may link activated Cdc42p to components involved in actin polarization, including Bni1p and Bud6p (Aip3p). *Mol Cell Biol* **20**: 6244-6258.

Johnson, D.R., Bhatnagar, R.S., Knoll, L.J., and Gordon, J.I. (1994a) Genetic and biochemical studies of protein N-myristoylation. *Annu Rev Biochem* **63**: 869-914.

Johnson, D.R., Cok, S.J., Feldmann, H., and Gordon, J.I. (1994b) Suppressors of nmt1-181, a conditional lethal allele of the *Saccharomyces cerevisiae* myristoyl-CoA:protein N-Myristoyltransferase gene, reveal proteins involved in regulating protein N-myristoylation. *Proc Natl Acad Sci USA* **91**: 10158-10162.

Käfer, E. (1965) Origins of translocations in *Aspergillus nidulans*. *Genetics* **52**: 217-232.

Kaksonen, M., Sun, Y., and Drubin, D.G. (2003) A pathway for association of receptors, adaptors, and actin during endocytic internalization. *Cell* **115**: 475-487.

Kaminskyj, S.G.W. (2001) Fundamentals of growth, storage, genetics and microscopy of *Aspergillus nidulans*. *Fungal Genet Newsl* **48**: 25-31.

Kennedy, M.T., Brockman, H., and Rusnak, F. (1996) Contributions of myristoylation to calcineurin structure/function. *J Biol Chem* **271**: 26517-26521.

Kimura, Y., Saeki, Y., Yokosawa, H., Polevoda, B., Sherman, F., and Hirano, H. (2003) N-Terminal modifications of the 19S regulatory particle subunits of the yeast proteasome. *Arch Biochem Biophys* **409**: 341-348.

Kohler, A., Cascio, P., Leggett, D.S., Woo, K.M., Goldberg, A.L., and Finley, D. (2001) The axial channel of the proteasome core particle is gated by the Rpt2 ATPase and controls both substrate entry and product release. *Mol Cell* **7**: 1143-1152.

Konzack, S., Rischitor, P.E., Enke, C., and Fischer, R. (2005) The role of the kinesin motor KipA in microtubule organization and polarized growth of *Aspergillus nidulans*. *Mol Biol Cell* **16**: 497-506.

Krappmann, S., Jung, N., Medic, B., Busch, S., Prade, R.A., and Braus, G.H. (2006) The *Aspergillus nidulans* F-box protein GrrA links SCF activity to meiosis. *Mol Microbiol* **61**: 76-88.

Kuo, K., and Hoch, H.C. (1996) Germination of *Phyllosticta ampelicida* pycnidiospores: Prerequisite of adhesion to the substratum and the relationship of substratum wettability. *Fungal Genet Biol* **20**: 18-29.

Lambert, A.A., Perron, M.P., Lavoie, E., and Pallotta, D. (2007) The *Saccharomyces cerevisiae* Arf3 protein is involved in actin cable and cortical patch formation. *FEMS Yeast Res* **7**: 782-795.

Lee, D.H., and Goldberg, A.L. (1996) Selective inhibitors of the proteasome-dependent and vacuolar pathways of protein degradation in *Saccharomyces cerevisiae*. *J Biol Chem* **271**: 27280-27284.

Lee, S.C., and Shaw, B.D. (2007) A novel interaction between N-myristoylation and the 26S proteasome during cell morphogenesis. *Mol Microbiol* **63**: 1039-1053.

Levitskaya, J., Sharipo, A., Leonchiks, A., Ciechanover, A., and Masucci, M.G. (1997) Inhibition of ubiquitin/proteasome-dependent protein degradation by the Gly-Ala repeat domain of the Epstein-Barr virus nuclear antigen 1. *Proc Natl Acad Sci USA* **94**: 12616-12621.

Li, L., Xue, C., Bruno, K., Nishimura, M., and Xu, J.-R. (2004) Two PAK kinase genes, CHM1 and MST20, have distinct functions in *Magnaporthe grisea*. *Mol Plant Microbe Interact* **17**: 547-556.

Lodge, J.K., Jackson-Machelski, E., Toffaletti, D.L., Perfect, J.R., and Gordon, J.I. (1994) Targeted gene replacement demonstrates that myristoyl-CoA:protein N-myristoyltransferase is essential for viability of *Cryptococcus neoformans*. *Proc Natl Acad Sci USA* **91**: 12008-12012.

Lucero, H.A., Chojnicki, E.W.T., Mandiyan, S., Nelson, H., and Nelson, N. (1995) Cloning and expression of a yeast gene encoding a protein with ATPase activity and high identity to the subunit 4 of the human 26S protease. *J Biol Chem* **270**: 9178-9184.

Ma, H.-H., Yang, L., Yang, X.-Y., Xu, Z.-P., and Li, B.-L. (2003) Bacterial expression, purification, and *in vitro* N-myristoylation of fusion hepatitis B virus preS1 with the native-type N-terminus. *Protein Expr Purif* **27**: 49-54.

Malloch, D. (1985) The Trichocomaceae: relationships with other Ascomycetes. In *Advances in Penicillium and Aspergillus Systematics.* Samson, R.A.and Pitt, J.I. (eds). New York: Plenum, pp. 365-382.

Marc, D., Drugeon, G., Haenni, A.-L., Girard, M., and van der Werf, S. (1989) Role of myristoylation of poliovirus capsid protein VP4 as determined by site-directed mutagenesis of its N-terminal sequence. *EMBO J* **8**: 2661-2668.

Marco, E., Wedlich-Soldner, R., Li, R., Altschuler, S.J., and Wu, L.F. (2007) Endocytosis optimizes the dynamic localization of membrane proteins that regulate cortical polarity. *Cell* **129**: 411-422.

Maurer-Stroh, S., Eisenhaber, B., and Eisenhaber, F. (2002) N-terminal N-myristoylation of proteins: prediction of substrate proteins from amino acid sequence. *J Mol Biol* **317**: 541-557.

McGoldrick, C.A., Gruver, C., and May, G.S. (1995) *myoA* of *Aspergillus nidulans* encodes an essential myosin I required for secretion and polarized growth. *J Cell Biol* **128**: 577-587.

Miller, W.J., and Hollander, W.F. (1995) Three neglected advances in classical genetics. *Bioscience* **45**: 98-104.

Miller, W.J. (1997) Dominance, codominance and epistasis. *Braz J Genet* **20**: 663-665.

Molendijk, A.J., Ruperti, B., and Palme, K. (2004) Small GTPases in vesicle trafficking. *Curr Opin Plant Biol* **7**: 694-700.

Momany, M., Westfall, P.J., and Abramowsky, G. (1999) *Aspergillus nidulans swo* mutants show defects in polarity establishment, polarity maintenance and hyphal morphogenesis. *Genetics* **151**: 557-567.

Moss, J., and Vaughan, M. (1995) Structure and function of ARF proteins: activators of cholera toxin and critical components of intracellular vesicular transport processes. *J Biol Chem* **270**: 12327-12330.

Moss, J., and Vaughan, M. (1998) Molecules in the ARF orbit. *J Biol Chem* **273**: 21431-21434.

Mumby, S.M., Heukeroth, R.O., Gordon, J.I., and Gilman, A.G. (1990) G-Protein alpha subunit expression, myristoylation, and membrane association in COS cells. *Proc Natl Acad Sci USA* **87**: 728-732.

Nayak, T., Szewczyk, E., Oakley, C.E., Osmani, A., Ukil, L., Murray, S.L., Hynes, M.J., Osmani, S.A., and Oakley, B.R. (2006) A versatile and efficient gene-targeting system for *Aspergillus nidulans*. *Genetics* **172**: 1557-1566.

Nimchuk, Z., Marois, E., Kjemtrup, S., Leister, R.T., Katagiri, F., and Dangl, J.L. (2000) Eukaryotic fatty acylation drives plasma membrane targeting and enhances function of several Type III effector proteins from *Pseudomonas syringae*. *Cell* **101**: 353-363.

Oberholzer, U., Marcil, A., Leberer, E., Thomas, D.Y., and Whiteway, M. (2002) Myosin I is required for hypha formation in *Candida albicans*. *Eukaryot Cell* **1**: 213-228.

Osherov, N., and May, G. (1998) Optimization of protein extraction from *Aspergillus nidulans* for gel electrophoresis. *Fungal Genet Newsl* **45**: 38-40.

Osherov, N., Mathew, J., and May, G.S. (2000) Polarity-defective mutants of *Aspergillus nidulans*. *Fungal Genet Biol* **31**: 181-188.

Osherov, N., and May, G. (2000) Conidial germination in *Aspergillus nidulans* requires RAS signaling and protein synthesis. *Genetics* **155**: 647-656.

Penalva, M.A. (2005) Tracing the endocytic pathway of *Aspergillus nidulans* with FM4-64. *Fungal Genet Biol* **42**: 963-975.

Peters, P.J., Hsu, V.W., Ooi, C.E., Finazzi, D., Teal, S.B., Oorschot, V., Donaldson, J.G., and Klausner, R.D. (1995) Overexpression of wild-type and mutant ARF1 and ARF6: distinct perturbations of nonoverlapping membrane compartments. *J Cell Biol* **128**: 1003-1017.

Pines, J., and Lindon, C. (2005) Proteolysis: anytime, any place, anywhere? *Nat Cell Biol* **7**: 731-735.

Pruyne, D., and Bretscher, A. (2000a) Polarization of cell growth in yeast. I. Establishment and maintenance of polarity states. *J Cell Sci* **113**: 365-375.

Pruyne, D., and Bretscher, A. (2000b) Polarization of cell growth in yeast. *J Cell Sci* **113**: 571-585.

Pruyne, D., Legesse-Miller, A., Gao, L., Dong, Y., and Bretscher, A. (2004) Mechanisms of polarized growth and organelle segregation in yeast. *Annu Rev Cell Dev Biol* **20**: 559-591.

Riquelme, M., Gierz, G., and Bartnicki-Garcia, S. (2000) Dynein and dynactin deficiencies affect the formation and function of the spitzenkorper and distort hyphal morphogenesis of *Neurospora crassa*. *Microbiology* **146**: 1743-1752.

Rosenwald, A.G., Rhodes, M.A., Van Valkenburgh, H., Palanivel, V., Chapman, G., Boman, A., Zhang, C., and Kahn, R.A. (2002) *ARL1* and membrane traffic in *Saccharomyces cerevisiae*. *Yeast* **19**: 1039-1056.

Rubin, D., Glickman, M., Larsen, C., Dhruvakumar, S., and Finley, D. (1998) Active site mutants in the six regulatory particle ATPases reveal multiple roles for ATP in the proteasome. *EMBO J* **17**: 4909-4919.

Rudnick, D.A., McWherter, C.A., Gokel, G.W., and Gordon, J.I. (1993) MyristoylCoA:protein N-myristoyltransferase. *Adv Enzymol Relat Areas Mol Biol* **67**: 375-430.

Sagot, I., Klee, S.K., and Pellman, D. (2002) Yeast formins regulate cell polarity by controlling the assembly of actin cables. *Nat Cell Biol* **4**: 42-50.

Sambrook, J., Fritsch, E.F., and Maniatis, T (1989) *Molecular Cloning: A Laboratory Manual.* New York: Cold Spring Harbor Laboratory Press.

Scheffer, J., Chen, C., Heidrich, P., Dickman, M.B., and Tudzynski, P. (2005) A CDC42 homologue in *Claviceps purpurea* is involved in vegetative differentiation and is essential for pathogenicity. *Eukaryot Cell* **4**: 1228-1238.

Schmid, J., and Harold, F.M. (1988) Dual roles for calcium ions in apical growth of *Neurospora crassa*. *J Gen Microbiol* **134**: 2623-2631.

Schott, D., Ho, J., Pruyne, D., and Bretscher, A. (1999) The COOH-terminal domain of Myo2p, a yeast myosin V, has a direct role in secretory vesicle targeting. *J Cell Biol* **147**: 791-808.

Schwartz, A.L., and Ciechanover, A. (1999) The ubiquitin-proteasome pathway and pathogenesis of human diseases. *Annu Rev Med* **50**: 57-74.

Schwechheimer, C. (2004) The COP9 signalosome (CSN): an evolutionary conserved proteolysis regulator in eukaryotic development. *Biochim Biophys Acta* **1695**: 45-54.

Seiler, S., and Plamann, M. (2003) The genetic basis of cellular morphogenesis in the filamentous fungus *Neurospora crassa*. *Mol Biol Cell* **14**: 4352-4364.

Serino, G., and Deng, X.-W. (2003) The COP9 signalosome: regulating plant development through the control of proteolysis. *Annu Rev Plant Biol* **54**: 165-182.

Sharpless, K.E., and Harris, S.D. (2002) Functional characterization and localization of the *Aspergillus nidulans* formin SEPA. *Mol Biol Cell* **13**: 469-479.

Shaw, B.D., and Hoch, H.C. (2001) Ions as regulators of growth and development. In *The Mycota*. Vol. VIII. Howard, R.J. and Gow, N.A.R. (eds.) Berlin: Springer-Verlag, pp. 73-89.

Shaw, B.D., Momany, C., and Momany, M. (2002) *Aspergillus nidulans swoF* encodes an N-myristoyl transferase. *Eukaryot Cell* **1**: 241-248.

Shaw, B.D., and Momany, M. (2002) *Aspergillus nidulans* polarity mutant *swoA* is complemented by protein O-mannosyltransferase *pmtA*. *Fungal Genet Biol* **37**: 263-270.

Shaw, B.D., and Upadhyay, S. (2005) *Aspergillus nidulans swoK* encodes an RNA binding protein that is important for cell polarity. *Fungal Genet Biol* **42**: 862-872.

Sheu, Y.-J., Santos, B., Fortin, N., Costigan, C., and Snyder, M. (1998) Spa2p interacts with cell polarity proteins and signaling components involved in yeast cell morphogenesis. *Mol Cell Biol* **18**: 4053-4069.

Silverman-Gavrila, L.B., and Lew, R.R. (2003) Calcium gradient dependence of *Neurospora crassa* hyphal growth. *Microbiology* **149**: 2475-2485.

Smalle, J., and Vierstra, R.D. (2004) The ubiquitin 26S proteasome proteolytic pathway. *Annu Rev Plant Biol* **55**: 555-590.

Stearns, T., Kahn, R.A., Botstein, D., and Hoyt, M.A. (1990) ADP ribosylation factor is an essential protein in *Saccharomyces cerevisiae* and is encoded by two genes. *Mol Cell Biol* **10**: 6690-6699.

Steinberg, G. (2007) On the move: endosomes in fungal growth and pathogenicity. *Nat Rev Microbiol* **5**: 309-316.

Taylor, L.P., and Hepler, P.K. (1997) Pollen germination and tube growth. *Annu Rev Plant Physiol Plant Mol Biol* **48**: 461-491.

Taylor, T.C., Kahn, R.A., and Melancon, P. (1992) Two distinct members of the ADP-ribosylation factor family of GTP-binding proteins regulate cell-free intra-golgi transport. *Cell* **70**: 69-79.

Toews, M., Warmbold, J., Konzack, S., Rischitor, P., Veith, D., Vienken, K., Vinuesa, C., Wei, H., and Fischer, R. (2004) Establishment of mRFP1 as a fluorescent marker in *Aspergillus nidulans* and construction of expression vectors for high-

throughput protein tagging using recombination in vitro (GATEWAY). *Curr Genet* **45**: 383-389.

Torralba, S., Raudaskoski, M., Pedregosa, A.M., and Laborda, F. (1998) Effect of cytochalasin A on apical growth, actin cytoskeleton organization and enzyme secretion in *Aspergillus nidulans*. *Microbiology* **144**: 45-53.

Upadhyay, S., and Shaw, B.D. (2006) A phosphoglucose isomerase mutant in *Aspergillus nidulans* is defective in hyphal polarity and conidiation. *Fungal Genet Biol* **43**: 739-751.

Valdez-Taubas, J., and Pelham, H.R.B. (2003) Slow diffusion of proteins in the yeast plasma membrane allows polarity to be maintained by endocytic cycling. *Curr Biol* **13**: 1636-1640.

Velichutina, I., Connerly, P, Arendt, C.S., Li, X., and Hochstrasser, M (2004) Plasticity in eucaryotic 20S proteasome ring assembly revealed by a subunit deletion in yeast. *EMBO J* **11**: 500-510.

Veronese, F., Copeland, T., Oroszlan, S., Gallo, R., and Sarngadharan, M. (1988) Biochemical and immunological analysis of human immunodeficiency virus gag gene products p17 and p24. *J Virol* **62**: 795-801.

Virag, A., and Griffiths, A.J.F. (2004) A mutation in the *Neurospora crassa* actin gene results in multiple defects in tip growth and branching. *Fungal Genet Biol* **41**: 213-225.

Virag, A., and Harris, S.D. (2006) The spitzenkorper: a molecular perspective. *Mycol Res* **110**: 4-13.

Walch-Solimena, C., Collins, R.N., and Novick, P.J. (1997) Sec2p mediates nucleotide exchange on Sec4p and is involved in polarized delivery of post-Golgi vesicles. *J Cell Biol* **137**: 1495-1509.

Walther, T.C., Brickner, J.H., Aguilar, P.S., Bernales, S., Pantoja, C., and Walter, P. (2006) Eisosomes mark static sites of endocytosis. *Nature* **439**: 998-1003.

Wedlich-Soldner, R., Altschuler, S., Wu, L., and Li, R. (2003) Spontaneous cell polarization through actomyosin-based delivery of the Cdc42 GTPase. *Science* **299**: 1231-1235.

Wiertz, E.J.H.J., Tortorella, D., Bogyo, M., Yu, J., Mothes, W., Jones, T.R., Rapoport, T.A., and Ploegh, H.L. (1996) Sec6l-mediated transfer of a membrane protein from the endoplasmic reticulum to the proteasome for destruction. *Nature* **384**: 432-438.

Wilkinson, C.R.M., Wallace, M., Morphew, M., Perry, P., Allshire, R., Javerzat, J.-P., McIntosh, J.R., and Gordon, C. (1998) Localization of the 26S proteasome during mitosis and meiosis in fission yeast. *EMBO J* **17**: 6465-6478.

Yarden, O., Plamann, M., Ebbole, D.J., and Yanofsky, C. (1992) *cot-1*, a gene required for hyphal elongation in *Neurospora crassa*, encodes a protein kinase. *EMBO J* **11**: 2159-2166.

Zahner, J.E., Harkins, H.A., and Pringle, J.R. (1996) Genetic analysis of the bipolar pattern of bud site selection in the yeast *Saccharomyces cerevisiae*. *Mol Cell Biol* **16**: 1857-1870.

Zarrin, M., Leeder, A.C., and Turner, G. (2005) A rapid method for promoter exchange in *Aspergillus nidulans* using recombinant PCR. *Fungal Genet Biol* **42**: 1-8.

Ziman, M., Chuang, J.S., and Schekman, R.W. (1996) Chs1p and Chs3p, two proteins involved in chitin synthesis, populate a compartment of the *Saccharomyces cerevisiae* endocytic pathway. *Mol Biol Cell* **7**: 1909-1919.

APPENDIX A

OTHER SUPPRESSORS OF *swoF1*

COMPLEMENTATION OF THE *ssfB1* AND *ssfB2*

In chapter II, I described that the *ssfB1* and *ssfB2* suppressor of *swoF1* mutants were grouped together since no wild-type progeny were recovered from the cross between them (data not shown). As described in chapter II, the *ssfB* mutation suppresses polarity defects of the *swoF1* mutant (Figure A.1). The single *ssfB* mutant displays small colonies and also secretes an unknown pigment into the media (Figure A.2). The *ssfB* mutant also displays abnormal hyphal growth, including fewer lateral branches and a less complex mycelial network in agar (Figure A1). To determine if the *ssfB* mutation was dominant or recessive, synthetic diploid strains $ssfB^{+}/ssfB^{-}$ were constructed as described in chapter II. Interestingly both diploids of $ssfB1^{+}/ssfB^{-}$ and $ssfB2^{+}/ssfB2^{-}$ have develop mycelial colonies on nutrient agar that appear wild-type in size, however, the diploids continued to secrete the red pigment into the media at restrictive temperature (Figure A.2A). These characteristics of the diploids lead me to declare that the *ssfB* mutations are co-dominant (see chapter II).

The *ssfB* group was partially complemented by using a genomic library using methods described in chapter II (Figure A.2B). Complementing plasmids (pF1 and pF2 respectively) were rescued from the strains (see chapter II). I exchanged the two plasmids between *ssfB1* and *ssfB2* and confirmed that *ssfB1* and *ssfB2* are in the same complementation group (data not shown).

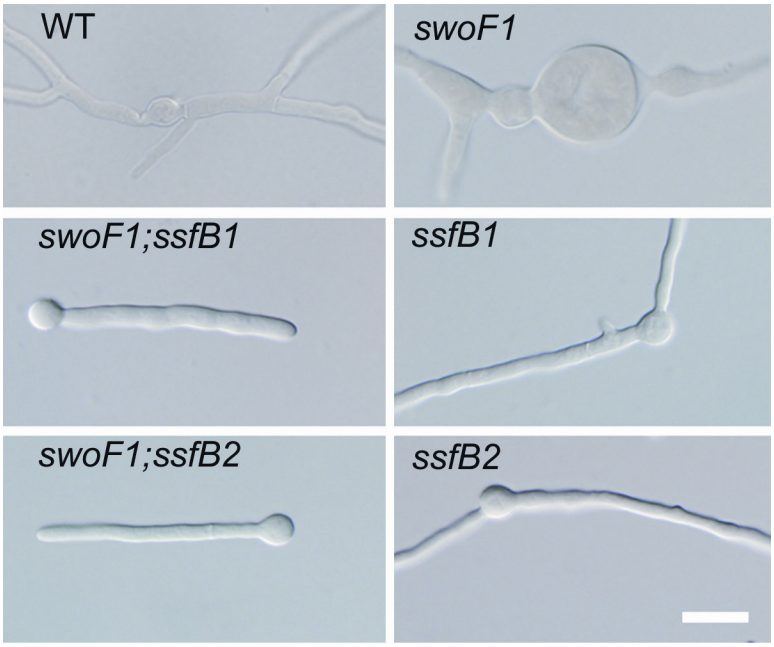

Figure A.1 DIC image of wild-type, *swoF1*, the *ssfB;swoF1* alleles, and the two alleles of *ssfB* at restrictive temperature.

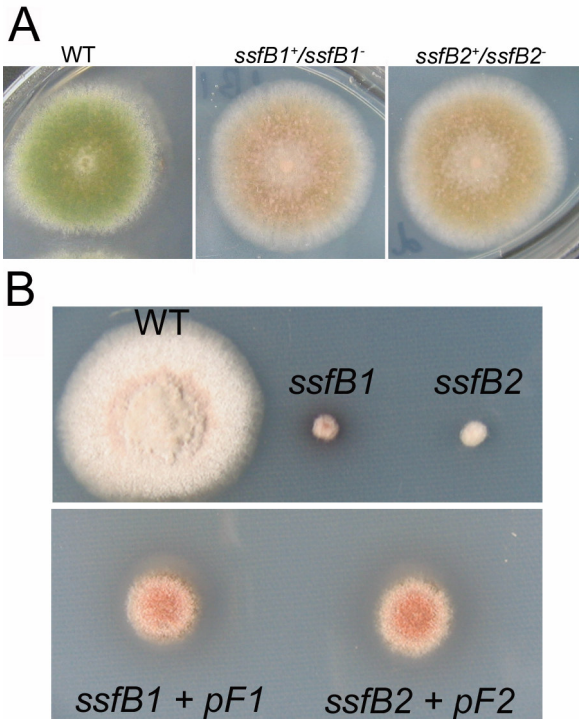

Figure A.2 Colony phenotypes of *ssfB* mutants, diploid cells, and complemented cells.

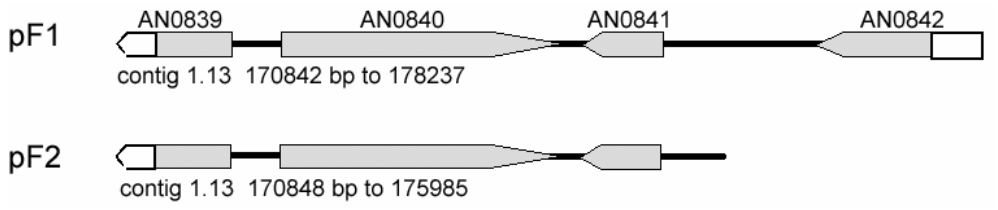

Figure A.3 Schematic diagram of genomic fragments in pF1 and pF2 plasmid.

The 5' and 3' ends of genomic the DNA fragments contained in the plasmids were sequenced and compared to the *A. nidulans* genomic database. The sequences were compared to the genome database using blast algorhythms (see chapter II). Plasmid pF1 contains sequence from 170842 bp to 178237 bp of contig 1.13 of the version 3 assembly of the genome. The genomic DNA fragment contained in plasmid pF2 overlaps with pF1 (170848 bp to 175985 bp at the same contig 1.13) (Figure A.2B). The overlapped ORFs include AN0840.3 and AN0841.3 and the truncated 3' end of AN0839.3. BlastP comparisons to NCBI protein database, nr, revealed that AN0839.3 is a protein similar to keiviton hydralase, a phytoalexin detoxification enzyme. The AN0840.3 protein contains an HMGL-like domain which is found in various metabolic enzymes. Finally AN0841.3 hit no protein in the database suggesting that it may be an *A. nidulans* specific protein. Further work is needed to determine which of these genes is responsible for the partial complementation of *ssfB1* and *ssfB2*. None of these three proteins are predicted to be myristoylated.

COMPLEMENTATION OF *ssfC*

The *ssfC* suppressor mutant group has only one strain (see chapter II). The *ssfC1* mutation also suppresses the polarity defect of the *swoF1* mutant. The single *ssfC1* mutant was generated by back-crossing the *ssfC1;swoF1* to wild-type (see experimental procedures in chapter II). The single *ssfC1* mutant shows limited hyphal growth as seen in the other suppressor single mutant (Figure A.4A) and produces an unknown red pigment at restrictive temperature (Figure A.4C). The synthetic diploid, $ssfC1^{+}/ssfC1^{-}$

produces a wild-type sized colony but continues to secrete the pigment (Figure A. 4B), suggesting that the *ssfC1* mutation is also co-dominant (see chapter II).

I transformed *ssfC1* using the genomic library and judged complementation based on the size of the colony, I found four complemented strains. Four unique plasmids were rescued from these complemented strains. The plasmid pC1 fully complements the *ssfC1* mutant in colony size and the complemented strain secretes less pigment compared to wild-type and the diploid cells. The plasmid pC2 also fully complements the *ssfC1* mutant for colony size but the strain continues to produce the red pigment. pC3 partially complements for colony size and pC4 eliminates the red pigment production of the *ssfC* mutant. All four plasmids were reintroduced into the *ssfC1* mutant to verify that I had recovered complementing plasmids. The 5' and 3' ends of the genomic DNA inserts from the four plasmids were sequenced and compared by blast to the genomic database (see chapter II). Plasmid pC1 contains about 8.1 kb of genomic DNA from 333420 bp to 341578 bp of contig 1.78 of the version 3 assembly of the database (Figure A.5). The fragment includes three complete ORFs and two truncated genes. AN4582.3 is an *A. nidulans* specific protein. AN4583.3 contains two domains including a cyclophilin D type peptidyl-prolyl *cis-trans* isomerase domain and a tetratricopeptide repeat (TPR) domain. AN4584.3 is predicted to encode a D-Tyr-tRNA deacylase functioning in protein translation. AN4585.3 contains an N-terminal region similar to the Not family protein forming a transcription complex in *S. cerevisiae*. Plasmid pC2 has two complete ORFs and the 5'

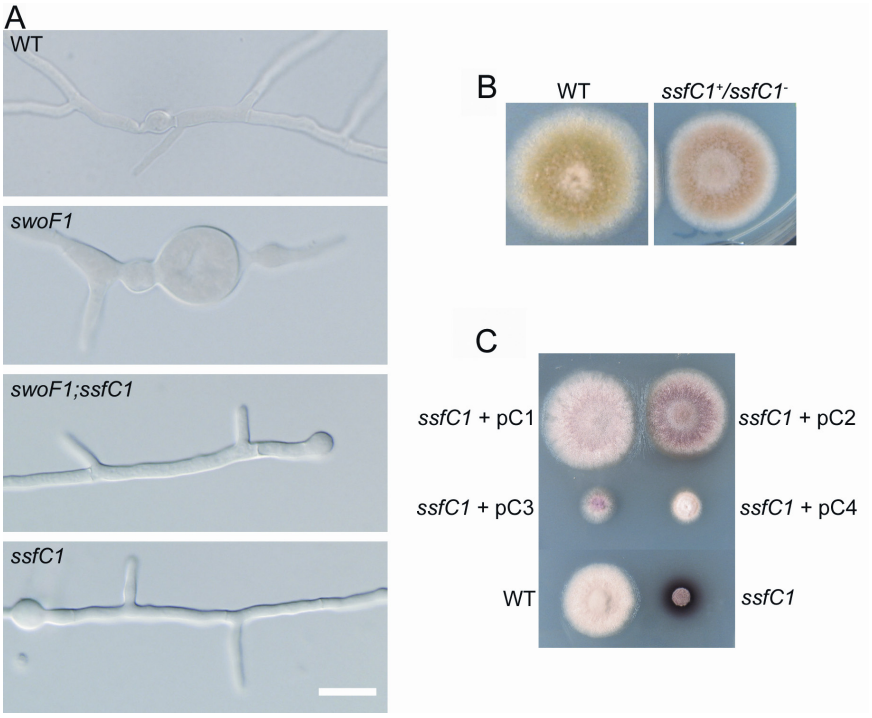

Figure A.4 Microscopic and colonial phenotype of *ssfC1* mutants. (A) DIC image of wild-type, *swoF1* mutant, *swoF1;ssfC1*, and *ssfC1* at restrictive temperature. Scale = 10μm. N.A. = 1.4 with oil. (B) Diploid phenotype of wild-type and *ssfC1*$^{+}$*/ssfC1*$^{-}$. (C) The *ssfC1* strains complemented with four different plasmids.

end of one truncated gene (Figure A.5) from 173520 bp to 179818 bp of contig 1.94. AN5437.3 is a hypothetical protein with no identifiable motifs and AN5438.3 is contains a TPR domain. Plasmid pC3 has a genomic fragment ranging from 280161 bp to 34973 bp of contig 1.35, which contains two complete ORFs and two truncated genes (Figure A.5). AN2201.3 is predicted to encode a proline specific permease and AN2202.3 is a hypothetical protein with no identifiable motifs. Finally pC4 harbors two truncated genes and contains DNA from 487177 bp to 494755 bp of contig 1.129. AN7517.3 is predicted to encode a filamentous fungal specific mechanosensitive ion channel protein. The other protein is AN7572.3 which contains a protein kinase domain. Interestingly plasmids pC1 and pC2, which fully restore the *ssfC1* mutant to wild-type growth of the colony, each contain coding sequence for proteins predicted to contain a TPR domain. This domain is involved in protein proteins interaction and assembly of multiprotein complex. Further work is needed to determine which of the genes from each plasmid is responsible for complementation of *ssfC1*. None of these three proteins are predicted to be myristoylated.

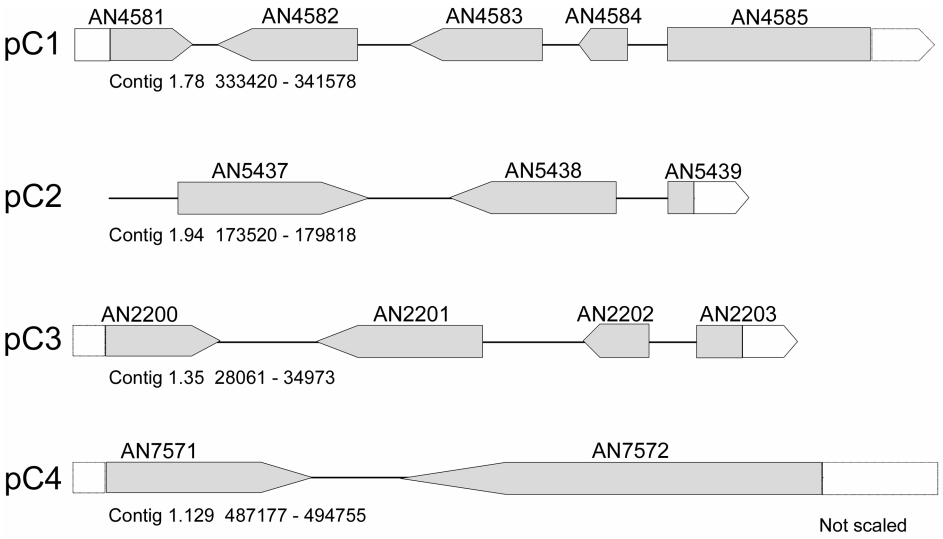

Figure A.5 *A. nidulans* genomic DNA fragments from four plasmids complementing the *ssfC1* mutant.

APPENDIX B

ADP RIBOSYLATION FACTOR A (ARFA)

OVEREXPRESSION OF ARFA SUPPRESSES PHENOTYPIC DEFECTS OF THE *SWOF1* MUTANT

I designated *A. nidulans gene* AN1126.3 *arfA*. The *arfA* gene including 442 bp upstream of start was amplified with primers:

1126F 5'- GGGGTACCCCCGCCGGCGGCTGAATTTCTC-3' and 1126R 5'-GGGATCCCGTTAGTGATGGTGATGGTGATGGTCGCGGCCAGTCTTCC-3'.

The forward primer contains the sequence GGTACC to introduce a *Kpn*I recognition site and the reverse primer contains GGATCC to introduce a *Bam*HI site. The reverse primer also contains coding sequence for six Histidine (6xHis) residues before the stop codon, to be used as an affinity tag. The amplicon was digested with *Kpn*I and *Bam*HI and cloned into the multi-copy plasmid, pRG3AMA1, to generate pRG-arfA. pRG-arfA was transformed into strains A773 (*pyrG89, pyroA4, veA1, wA3*) and AXL18 (*swoF1, pyrG89, pyroA4, veA1, wA3*). Interestingly, wild-type A773 overexpressing ArfA-6xHis shows reduced hyphal growth compared to wild-type (Figure B.1a and b), whereas the *swoF1* mutant overexpressing ArfA-6xHis was partially restored for growth (Figure B.1d). With myristate medium amendment overexpression of ArfA-6xHis fully suppresses hyphal growth defects of the *swoF1* mutant (Figure B.1e). These results suggest that the ArfA protein is a link between N-myristoylation and hyphal polarity.

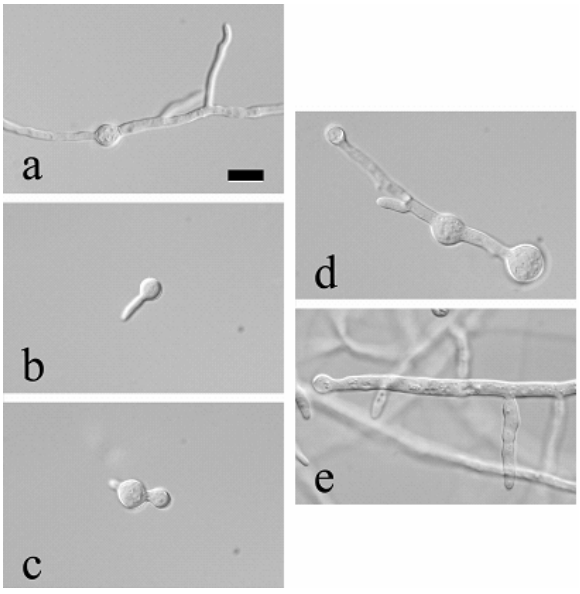

Figure B.1 DIC images of wild-type and the *swoF1* mutant with or without overexpression of ArfA:6xHis. (a) wild-type, (b) wild-type overexpressing ArfA::6xHis, (c) *swoF1*, (d) *swoF1* overexpressing ArfA::6xHis, (e) *swoF1* overexpressing ArfA::6xHis in the presence of myristate.

The *arfA* gene was also amplified with the primers: GarfAF 5' CACCATGGGTCTCGCCATCTCGAA-3' and GarfAR 5'-GTCGCGGCCAGTCTTCC-3'. The amplicon was cloned into the TOPO cloning vector, pENTR (Invitrogen, Carlbad, CA, USA) to produce pArfA-entry. Using the primer mGrarfAF 5'CACCATGGCTCTCGCCATCTCGAAGTT-3', an *arfA* point mutant containing cytosine instead of guanine at the 4th base pair position was amplified. This primer changes the coding sequence of the secondary glycine into alanine, which produces a non-myristoylated form of ArfA. This amplicon was cloned into pENTR to generate pmArfA-entry. Plasmids pArfA-entry and pmArfA-entry underwent a clonase reaction with the destination vector, pSL-sGFP vector (see Chapter III), for GFP tagging by gateway cloning. The *ccdB* box was exchanged with the *swoF1* gene in pSL-sGFP to produce pArfA::sGFP and pArfA^{G2A}::sGFP respectively (see chapter II and III). The pArfA::sGFP and pArfA^{G2A}::sGFP plasmids were transformed into wild-type A773 and *swoF1* strain AXL18. WA11 (wild-type with pArfA::sGFP) and MA (wild-type with pArfA^{G2A}::GFP) were visualized under the fluorescent microscope with GFP filter described in chapter 3. ArfA::sGFP localizes to cellular compartments which are likely to be endoplasmic reticulum or Golgi equivalent (Figure B.2a). The ArfA^{G2A}::sGFP construct disperses throughout the cytosol nonspecifically (Figure B.2b). In the *swoF1* myristoylation mutant ArfA::sGFP localization is also dispersed to the cytosol (Figure B.2c). For further confirmation of ArfA localization, immunofluorescence staining was performed by using monoclonal GFP antibody as primary antibody and FITC conjugated secondary antibody. As shown in Figure B.2, ArfA::sGFP displays the same localization

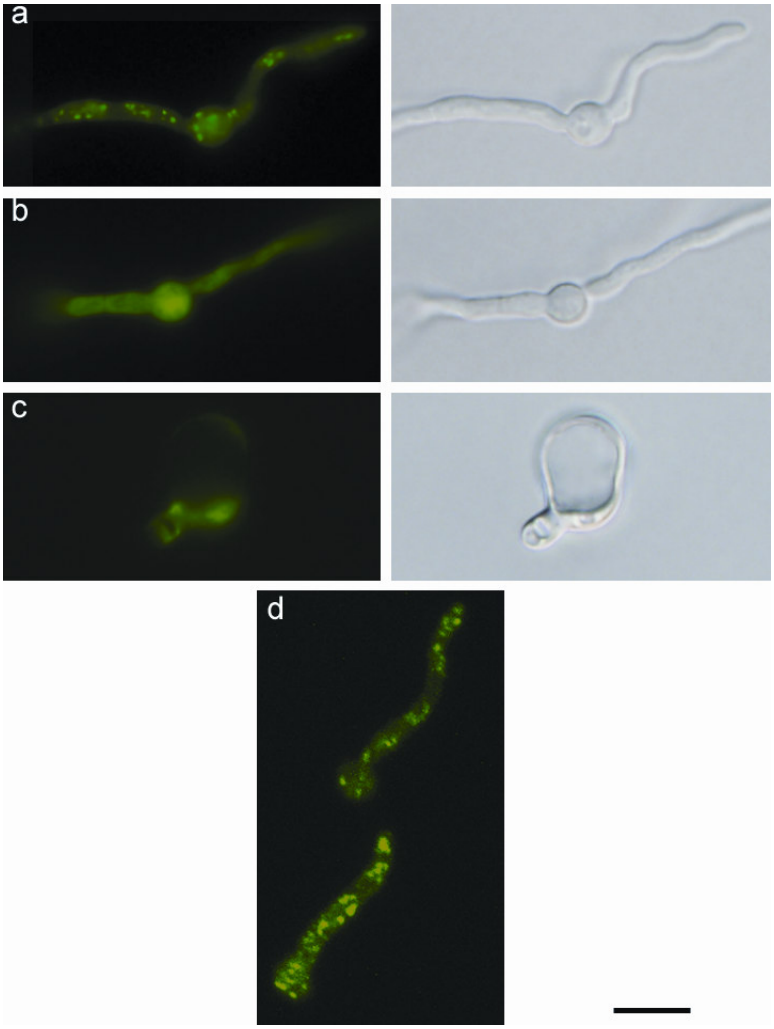

Figure B.2 Localization of ArfA::GFP and ArfA^{G2A}::GFP. (a) Wide field fluorescent image of ArfA::GFP in wild-type cells (left) and DIC image of germination (right), (b) wide field fluorescent image of ArfA^{G2A}::GFP in wild-type cells (left) and DIC image of germination (right), (c) wide field fluorescent image of ArfA::GFP in the *swoF1* mutant, (d) Immunofluorescent image of ArfA::GFP with combined Z-stack of confocal images. Scale = 10μm. N.A. 1.4 with oil.

pattern as GFP signal observed in live cell imaging. These results lead me to conclude that N-myristoylation is critical for ArfA to localize to its cellular compartment. More than one transformant was observed and shown to have same localization pattern (data not shown). In western blotting analysis using monoclonal GFP antibody, one band of GFP tagged ArfA or $ArfA^{G2A}$ was detected suggesting that no free GFP is present in the cell to complicate localization interpretation (data not shown).

To examine whether ArfA::GFP co-localizes with endocytosis machinery, the WA11 strain was treated with FM4-64 as previously described (see chapter II). After 20 min treatment with FM4-64, the endosomes are labeled with FM4-64. These endosomes do not co-localize with ArfA::GFP punctate spots (Figure B.3A) suggesting that ArfA does not localize to the early endocytosis machinery. Next, co-localization of ArfA::GFP with exocytosis machinery was tested. After 120 min treatment of FM4-64, ArfA::GFP co-localized with some of the FM4-64 stained bodies, indicating that a cellular compartment associated with late FM4-64 uptake is the body containing ArfA::GFP. (Figure B.3B). This compartment may be the endoplasmic reticulum or Golgi equivalents. More work is required to differentiate between the two bodies. The fluorescent images were taken with combined Z-stack as described in chapter III.

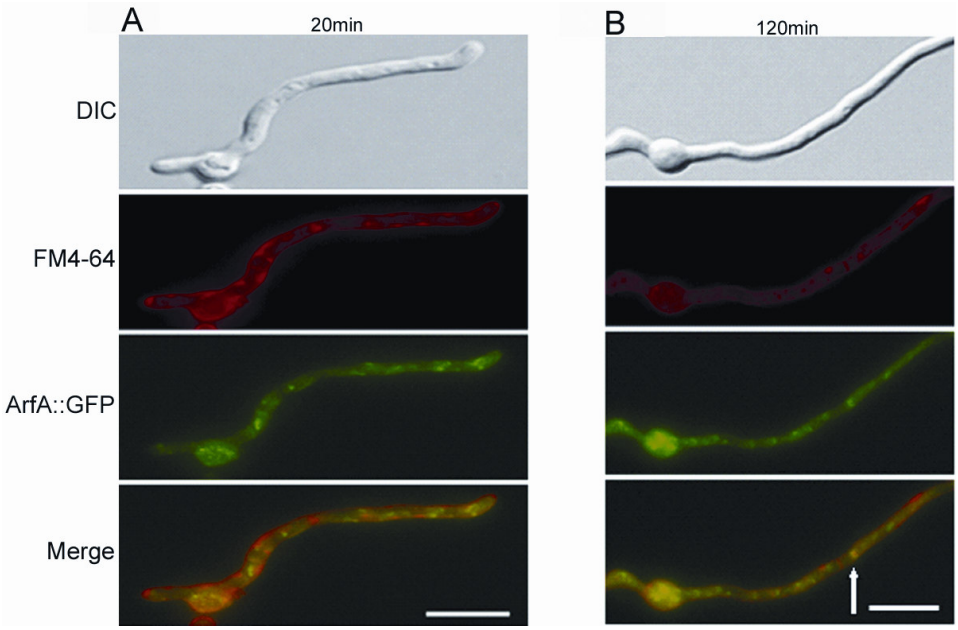

Figure B.3 Co-localization of ArfA::GFP with FM4-64. (A) Wide field images of FM4-64, ArfA::GFP, and overlay with combined Z-stack after 20 min treatment of FM4-64, (B) wide field images of FM4-64, ArfA::GFP, and overlay with combined Z-stack after 120 min treatment of FM4-64.

APPENDIX C

TEMPERATURE SENSITIVE MUTANT LIBRARY

MUTAGENESIS OF A773

A temperature sensitive mutant library was generated by irradiating *A. nidulans strain*, A773 (see chapter II and III) with UV light (wavelength = 253.7 nm) with a UV Stratalinker^{TM} 2400 (Stratagene, La Jolla, CA, USA). A killing curve was established by irradiating spores in deionized distilled H_2O 14 cm from the UV source with 0 to 1000 µJ of energy (Figure C.1). 200 µJ was chosen as the dose at which 70 % of the spores were killed. The UV-exposed conidia were spread onto minimal media containing 1.5 % agar (Difco, Sparks, MD, USA) and grown at restrictive temperature (42 ºC). After 4 days incubation, surviving colonies were replica-plated at permisive temperature (28 ºC) and restrictive temperature. Strains showing defective colony formation at restrictive temperature were selected and further analyzed and/or stored for future use (See table C.1).

tsB-15 was further analyzed. The phenotype of the mutant includes periodic intercalary swellings within the hyphae (Figure C.2). After genetic analysis (Long and Shaw, unpublished), the mutant was designated *swoN1*. The *swoN1* mutant was found to have a mutation in GDP mannose pyrophosphorylase (Rebello, Upadhyay, Lee and Shaw, unpublished).

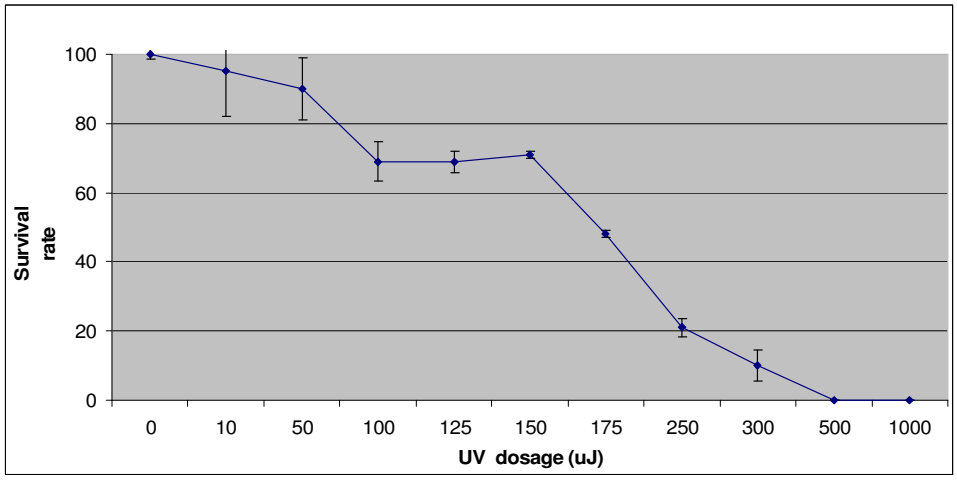

Figure C.1 Survival curve of A773 subjected to UV (wavelength = 253.7 nm) exposure.

Table C.1 Microscopic phenotype of temperature sensitive mutants

	Microscopic Phenotype			Microscopic Phenotype	
	28℃	42℃		28℃	42℃
tsA-1			tsB-19		
tsA-2			tsB-20		
tsA-3			tsB-21		swollen
tsA-4			tsB-22	no growth	no growth
tsA-5		short germ tube	tsB-23	short germ tube	very short germ tube or none
tsA-6		short germ tube	tsB-24		
tsA-11		no germ tube	tsB-25		
tsA-13		no germ tube	tsB-26		
tsA-15			tsB-27	no growth	no growth
tsA-17			tsB-28		
tsA-32			tsB-29		
tsA-35			tsB-30		
tsA-41			tsB-31		slightly short germ tube
tsA-42			tsB-32		
tsA-48			tsB-33		
tsA-64			tsB-34		
tsA-70			tsB-35		
tsA-71			tsB-36		
tsA-73			tsB-37		
tsA-76			tsB-38		
tsA-78			tsB-39		
tsA-94			tsB-40		
tsA-103			tsB-41		
tsB-1		slightly short germ tube	tsB-42		short germ tube
tsB-2		no germ tube	tsB-43		
tsB-3		short germ tube	tsB-44		
tsB-4	slightly short germ tube	no germ tube	tsB-45		
tsB-5		short germ tube	tsB-46		
tsB-6			tsB-47		
tsB-7			tsB-48		
tsB-8		slightly short germ tube	tsB-49		
tsB-9		short germ tube	tsB-50		

Table C.1 continued

	Microscopic Phenotype			Microscopic Phenotype	
	28℃	42℃		28℃	42℃
tsB-11			tsB-52		
tsB-12		short germ tube	tsB-53		
tsB-13			tsB-54		
tsB-14	slightly short germ tube	Swollen	tsB-55		
tsB-15		Swollen	tsB-56		
tsB-16		swollen	tsB-57		
tsB-17			tsB-58		
tsB-18		slightly short germ tube	tsB-59		
tsB-60			tsC-43		
tsB-61			tsC-44		
tsB-62			tsC-45		
tsB-63			tsC-46		
tsB-64			tsC-47		swollen and hyperbranch
tsB-65			tsC-48		swollen and reduced growth
tsB-66			tsC-49		
tsB-67			tsC-50		
tsB-68			tsC-51		
tsB-69			tsD-1		
tsC-1			tsD-2		
tsC-2			tsD-3		
tsC-3			tsD-4		
tsC-4			tsD-5		
tsC-5			tsD-6		
tsC-6			tsD-7		
tsC-7			tsD-8		
tsC-8			tsD-9		
tsC-9			tsD-10		
tsC-10			tsD-11		
tsC-11		hyperbranch	tsD-12		
tsC-12			tsE-1		
tsC-13			tsE-2		
tsC-14			tsE-3		
tsC-15			tsE-4		

Table C.1 continued

	Microscopic Phenotype			Microscopic Phenotype	
	28℃	42℃		28℃	42℃
tsC-17			tsE-6		
tsC-18			tsE-7		
tsC-19			tsE-8		
tsC-20			tsE-9		
tsC-21			tsE-10		
tsC-22			tsE-11		
tsC-23			tsE-12		
tsC-24			tsE-13		
tsC-25		swollen and hyperbranch	tsE-14		
tsC-26			tsE-15		
tsC-27			tsE-16		
tsC-28			tsE-17		
tsC-29			tsE-18		
tsC-30			tsE-19		
tsC-31			tsE-20		reduced growth
tsC-32			tsE-21		
tsC-33			tsE-22		
tsC-34			tsF-1		
tsC-35			tsF-2		
tsC-36			tsF-3		
tsC-37			tsF-4		
tsC-38			tsF-5		
tsC-39		hyperbranch	tsF-6		reduced growth
tsC-40			tsF-7		
tsC-41			tsF-8		
tsC-42			tsF-9		hyperbranch
tsF-10			tsF-23		
tsF-11			tsF-24		
tsF-12			tsF-25		
tsF-13			tsF-26		
tsF-14			tsF-27		
tsF-15			tsF-28		
tsF-16		swollen and reduced grwoth	tsF-29		
tsF-17		swollen and reduced grwoth	tsF-30		
tsF-18		swollen and reduced grwoth	tsF-31		
tsF-19			tsF-32		hyperbranch and reduced growth
tsF-20		swollen and reduced grwoth	tsF-33		swollen
tsF-21			tsF-34		
tsF-22					

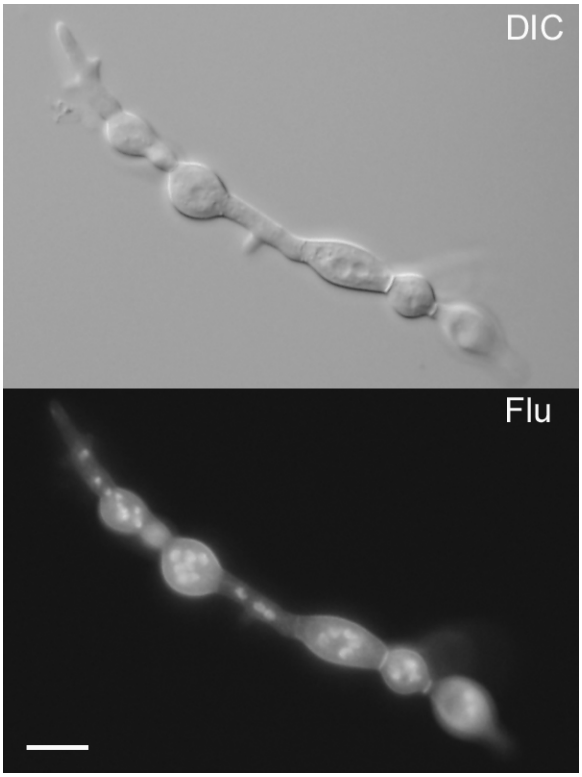

Figure C.2 DIC and fluorescent image of tsB-15 (*swoN1*) mutant. Calcofluor and Hoechst 33258 were used to stain cell wall and nuclei respectively. Scale = 5 μm. N. A. = 1.4 with oil.

VITA

Name: Soo Chan Lee

Address: Department of Plant Pathology and Microbiology,
c/o Dr. Brian Shaw
Texas A&M University
College Station, TX77843-2132

Email Address: sclee@tamu.edu

Education:

B.S. Biology, Kyung Hee University, Seoul, South Korea, 1999
M.S. Microbiology, Kyung Hee University, Seoul, Korea, 2001
Ph.D. Plant Pathology, Texas A&M University, College Station, TX, USA, 2007

Selected awards and honors:

- Robert Nicholson Endowed Fellowship, 2007
- American Society of Microbiology Graduate Student poster Award at Fungal Genetics Conference, 2007
- Graduate Student Excellence Award, 2007, Plant Pathology and Microbiology, TAMU
- Travel Award for 24th Fungal Genetics Conference of Genetic Society of America, Asilomar, 2007
- Mentor Travel Award for Mycological Society of America at Hilo, Hawaii, 2005
- 2nd place winner in the life science section at Student Research Week, Texas A&M University, 2005

Selected publications:

- Lee, Soo Chan and Shaw, B.D. 2007. A novel interaction between N-myristoylation and the 26S proteasome during cell morphogenesis. Mol. Microbiol. 2007 63(4), 1054-1068.
- Lee, Soo Chan and B. D. Shaw. The role of myristoylation of ADP ribosylation factors, small GTPases in early developmental stage of Aspergillus nidulans. 2007. In Preparation.
- S. Upadhyay, Lee, Soo Chan and B. D. Shaw. The actin cytoskeleton controls hyphal growth in fungal cells. 2007. In Preparation.
- B. D. Shaw, G. Rebello, Lee, Soo Chan, S. Upadhyay, and M. Long. A GDP mannose pyrophosphorylase regulates hyphal growth. 2007. In Preparation.